A NUMERICAL SOLUTION OF THE SHOCK-LAMINAR BOUNDARY

LAYER INTERACTION PHENOMENON NEAR THE SHARP

LEADING-EDGE OF A FLAT PLATE

By

KENNETH RAY ROYER

Bachelor of Science
Southwestern Louisiana Institute
Lafayette, Louisiana
1951

Bachelor of Science
Louisiana Polytechnic Institute
Ruston, Louisiana
1957

Master of Science
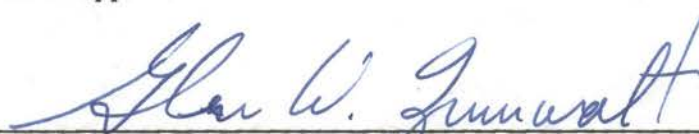Louisiana Polytechnic Institute
Ruston, Louisiana
1960

Submitted to the faculty of the Graduate College
of the Oklahoma State University
in partial fulfillment of the requirements
for the degree of
DOCTOR OF PHILOSOPHY
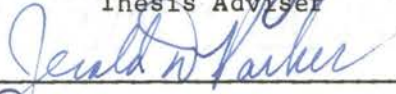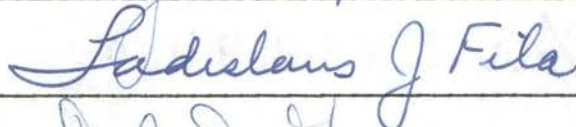May, 1967

A NUMERICAL SOLUTION OF THE SHOCK-LAMINAR BOUNDARY

LAYER INTERACTION PHENOMENON NEAR THE SHARP

LEADING-EDGE OF A FLAT PLATE

Thesis Approved:

Thesis Adviser

Dean of the Graduate College

660251

PREFACE

This document contains a description of the fluid flow properties near the leading-edge of a sharp flat plate. The work was undertaken on the basis of determining the characteristics of the fluid flow properties by use of a time-dependent, explicit finite-difference approximation of the momentum, energy, and continuity partial differential equations. The complete study included a numerical analysis of the leading-edge shock interaction with the viscous boundary layer and the interaction associated with an oblique shock wave incident on a laminar boundary layer a short distance downstream from the plate leading edge.

TABLE OF CONTENTS

LIST OF TABLES

LIST OF FIGURES

NOMENCLATURE

A (x, y, t)	Blurring term coefficient
B (x, y, t)	Blurring term coefficient
c	Local acoustic velocity
c_p	Specific heat at constant pressure
c_v	Specific heat at constant volume
e	Fluid energy
F	Function used in Equation 1
F^x	Defined on page 27
F^y	Defined on page 27
f	Defined on page 27
G	Function used in Equation 1
h	Diagonal of finite-difference net, altitude
h_1	Finite-difference net spacing in x-direction
h_2	Finite-difference net spacing in y-direction
K	Time parameter defined on page 32
K_1	Time parameter defined on page 32
K_2	Time parameter defined on page 32
k	Coefficient of thermal conductivity
L	Characteristic length
ℓ	Mesh number in y-direction
M	Mach number
m	Mesh number in x-direction

n	Time plane number
p	Static pressure
Pr	Prandtl number
R	Gas constant
Re	Reynolds number
S	Defined on page 27
S_1	Defined on page 28
S_2	Defined on page 28
S_3	Defined on page 28
t	Time
T_w	Wall temperature
T_{ad}	Adiabatic temperature
u	x component of velocity
v	y component of velocity
w	Velocity modulus $\sqrt{u^2 + v^2}$
x,y	Cartesian coordinates
α	Blurring term defined on page 34
β	Blurring term defined on page 34
δ	Boundary layer thickness
δ^*	Boundary layer displacement thickness
γ	Ratio of specific heats
η	Similarity parameter $\frac{y}{x}\sqrt{Re_{x,o}}$
λ	Coefficient defined on page 27
μ	Coefficient of viscosity
ρ	Density
σ	Courant number

σ_o	Maximum allowable Courant number
τ	Time increment; also shear stress
Φ	Blurring terms in difference form
χ	Finite-difference net angle (Figure 3)
Ω	Coefficient defined on page 27
ω	Damping term due to blurring technique

Superscripts

$-$	Dimensional quantity
	Nondimensional quantity
n	Time plane number
ℓ	Mesh number in y-direction
m	Mesh number in x-direction
o	Conditions in freestream

CHAPTER I

INTRODUCTION

One of the most fundamental problems encountered in the investigation of supersonic flow over a solid boundary is the phenomenon produced by the interaction of shock waves and boundary layers. This phenomenon normally results from the interaction of an externally produced, oblique shock wave and a viscous boundary layer. Of equal importance is the phenomenon observed in hypersonic fluid flow when the leading-edge shock wave and the viscous layer interact.

In either case, the distribution of static pressure along the body surface is not a given datum of the problem but is determined by the interaction between the external fluid and the viscous layer. As the fluid flows through the shock wave, the increase in the static pressure in the external supersonic flow can be communicated upstream through the boundary layer, and the translation of this increase in pressure enhances the possibility of boundary layer separation. Consequently, there is always a probability that such a shock wave will cause boundary layer separation. Continuing analytical and experimental efforts are being made to provide a better understanding of the mechanisms associated with shock-induced flow separation and to establish the required criteria necessary for accurately predicting such a phenomenon.

In spite of the long-time interest in the phenomenon of an interaction which is produced by introducing an oblique shock which is

incident on the boundary layer, a satisfactory theoretical analysis does not yet exist. In some theoretical studies, a modified Kármán-Pohlhausen method is used as the basis of the analysis; in others, the two-moment method is often used, but difficulty is often encountered in patching together the preseparation and postseparation regions. Still other studies are based on the semiempirical approach in which a mixing or mass entrainment rate is used between the inviscid and viscid regions [1].[1] The use of any of these methods is undesirable when it is necessary to analyze a complete flow field which contains shock waves and boundary layers. This undesirability becomes obvious when it is remembered that use must be made of an iteration process involving the usual Prandtl boundary layer equations, the inviscid method of characteristics, and the analysis of the interaction which is produced by introducing an oblique shock which is incident on the boundary layer. This iteration becomes tedious and often complicated because the process must be continued until complete compatibility is obtained between the inviscid fluid properties and the fluid properties at the outer edge of the boundary layer.

The interaction between the leading-edge shock and the boundary layer has only recently become relatively important since it is normally associated with hypersonic flow and low-density gases. However, at high supersonic Mach numbers and low densities, a weak interaction is present in the stagnation point region. In this region, it is physically impossible to obtain experimental test data. Consequently, analytical

----

[1]Numbers in small brackets refer to references in the bibliography.

methods must be devised to analyze the flow field of interest, and in the creation of these methods, major consideration must be given to the solution of such problems as slip flow, temperature jump, and, at hypersonic speeds, the possibility of free molecule flow in this region.

The primary objective set for this investigation was the development of a method for analyzing the complete flow field by using only one set of general equations. The region of primary interest was near the leading edge of a sharp flat plate where a weak interaction can exist between the bow shock and the laminar boundary layer. The conditions of primary interest were the stated weak interaction between the leading-edge shock and the boundary layer, the interaction between an externally produced incident oblique shock and the leading-edge shock, and the interaction between the externally produced incident oblique shock and the laminar boundary layer.

The steady-state nature of the flow field under investigation is such that the solution seems possible by use of the governing steady-state equations. However, as Crocco [2] states, there exists a fundamental difference between the usual interpretation of the solution of such steady-state problems and the way nature establishes such a solution. What is generally considered as a steady-state phenomenon exists only as the asymptotic form of a time-dependent phenomenon, and the customary steady-state solution is obtained without consideration of the transient phenomenon. Therefore, a logical solution of the general problem would be the determination of the asymptotic form of a time-dependent initial value problem.

This investigation, as well as the recent investigation of other steady-state problems which have been solved by various scholars, has

been based on an examination of the transient problem suggested by
Crocco [2], and a time-dependent solution of a general set of governing
equations has been sought. These equations are easier to solve than
the steady-state equations since the differential equations applicable
to the time-dependent problem are of a parabolic-hyperbolic nature. A
forward integration in time is allowed so that the solution of the
initial boundary value problem can be obtained when the initial con-
ditions are known. The method of analysis was formulated by using the
recent advances in explicit, time-dependent, numerical techniques where-
by the nonlinear equations of motion and the conservation of mass and
energy are solved by the application of the method of finite differences.
A basic requirement for the governing equations was that they be valid
in the inviscid flow field and the laminar boundary layer. Of equal
importance was the method used for solving the governing equations;
this method was particularly important in the region of shock discon-
tinuities where good resolution of the shock was required.

Two cases were considered in order to evaluate the method of attack
and the feasibility of using such a method in future studies. In the
first case, consideration was given only to the leading-edge shock
problem. In this case, the following flow conditions were assumed:

$$M_o = 3.0$$

$$h = 100,000 \text{ ft}$$

$$T_o = 418^\circ R$$

$$P_o = 23,603 \text{ lb}_f/\text{ft}^2$$

$$\rho_o = 3.2114 \ (10^{-5}) \text{ lb}_f\text{-sec}^2/\text{ft}^4$$

$$\mu_o = 3.1501 \ (10^{-7}) \text{ lb}_f\text{-sec}/\text{ft}^2$$

$$k_o = 3.3475 \ (10^{-6}) \text{ Btu/ft-sec-}^\circ R$$

$$Pr \quad = \quad 0.72$$

$$Re/L \quad = \quad 3.06 \; (10^5) \; ft^{-1}$$

$$T_w \quad = \quad T_{ad} \; (adiabatic \; wall)$$

In the second part of the study, consideration was given to the addition of an incident oblique shock to the flow field used in case 1. The combination of the two cases were considered sufficient for attaining the objective of analyzing the complete flow field by using only one set of equations.

CHAPTER II

PHYSICAL DESCRIPTION OF THE REGIONS OF INTERACTION

Interaction Induced by the Boundary Layer

The usual analytical approach to the treatment of transport effects in fluid flow problems involves the use of the thin boundary layer and thin shock approximations. In low-speed aerodynamics involving flow of air at normal densities around a body, the viscous dissipation and heat conduction are restricted to the thin boundary layer near the surface of the body. This boundary layer may be in a laminar, turbulent, or transitional state, and it can be considered separately from the outer or external inviscid flow. At hypersonic speeds, the leading-edge shock wave can be considered infinitesimally thin only as long as the boundary layer thickness is small in comparison to the shock layer thickness [3].

The deceleration of the fluid by a shock wave or by viscous processes in a boundary layer generally produces very high temperatures. One result of these high temperatures is an increase in the thickness of the boundary layer. This increased thickness of the boundary layer results in an interaction between the boundary layer and the inviscid flow field which Hayes and Probstein [3] call the "boundary layer induced" interaction or "pressure" interaction.

6

A schematic representation of the boundary-layer-induced interaction phenomenon is shown in Figure 1. In this type of flow, the growth of the boundary layer produces an outward deflection of a streamline (Figure 1) which amounts to a significant change in the "effective" shape of the body. Large induced pressures are transmitted into the external inviscid field along Mach lines, and the boundary layer generates an inviscid shock layer from the leading edge of the flat plate. The pressures govern the growth of the boundary layer; thus another term given for this type of interaction is "Mach wave" interaction. This type of interaction is entirely due to the displacement effect of the boundary layer. Without the viscous effects, the flow field would remain undisturbed.

The shock layer must contain an inviscid region of relatively cool, high-density flow outside the boundary layer. If the classical concept of the displacement thickness is used, the body boundary layer can be replaced by an equivalent or "effective" body in an inviscid flow field. This "effective" body is the original body thickened by the displacement thickness distribution $\delta^*(x)$. Hayes and Probstein [3] point out that, in hypersonic boundary layers, the density is very low and the approximation $\delta(x) = \delta^*(x)$ can be used.

The "pressure" interaction can be divided into two distinct regions called the strong and weak interaction zones [3] in those cases where the flow would be uniform if the boundary layer were absent. The concept of weak and strong interaction regions has become popular in theory related to hypersonic flow. In this view, the weak interaction region is characterized as the region where the effects produced by the self-induced pressure gradient are perturbations superposed on an already
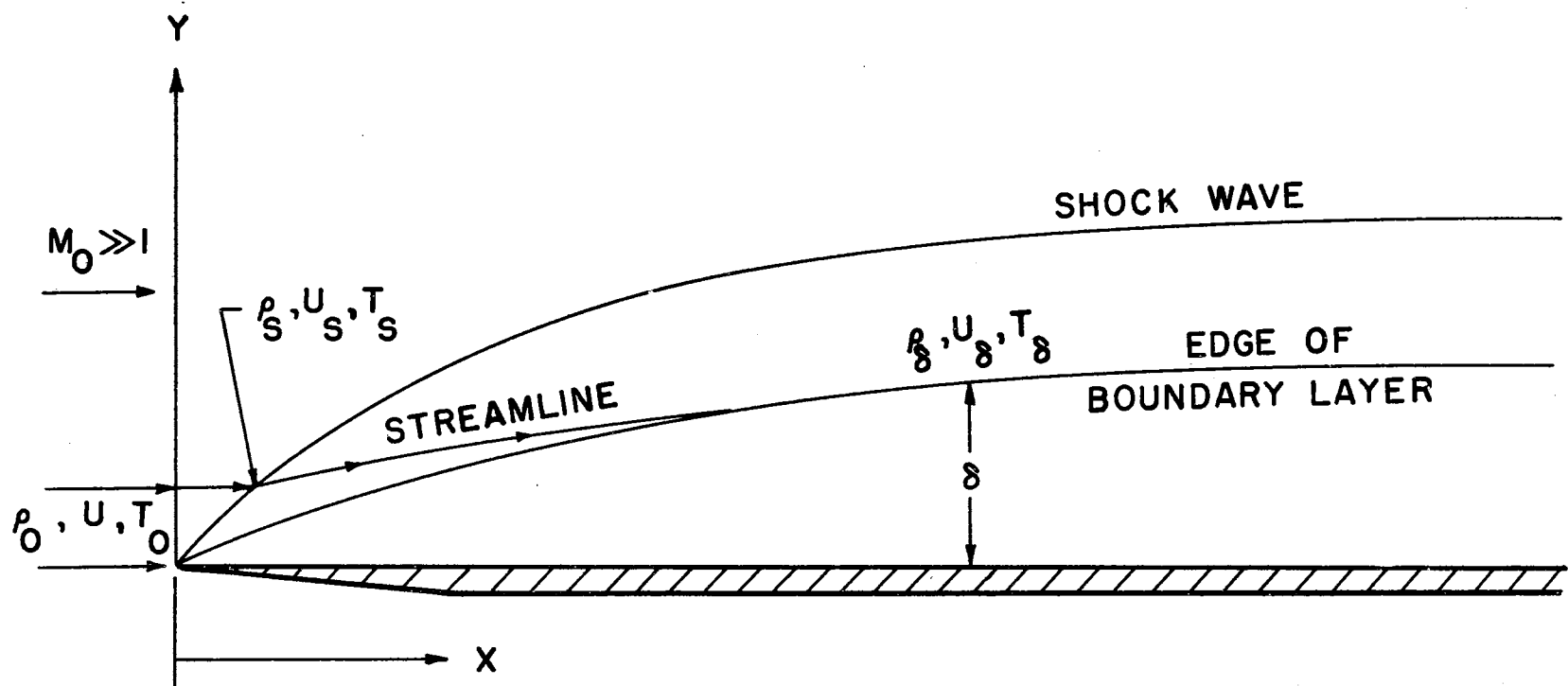
Figure 1. Schematic Representation of Boundary-Layer-Induced Flow Field Over
a Flat Plate

existing uniform flow. The strong interaction is characterized by the streamline inclination induced by the viscous layer. In this type of flow, the pressure gradient and viscous stress gradient terms are of the same order of magnitude. In the flat plate case, the strong inter-action zone is close to the leading edge while the weak interaction zone is farther downstream.

<div align="center">Interaction Between the Incident Shock
and the Laminar Boundary Layer</div>

Lees and Reeves [1] have presented a typical flow model of "subcritical" adiabatic flow in which the laminar boundary layer is separated and reattached. A schematic representation of the inter-action region is shown in Figure 2. The viscous flow is considered "subcritical" in the sense that the pressure rise generated by the incident shock is communicated smoothly all the way upstream to the "initial" flat plate flow. Lees [4] has shown that the overpressure existing on the plate surface (Figure 2) decays exponentially as a function of the distance upstream from the separation point. Therefore, upstream of the interaction region, initial conditions exist, and the positive pressure gradient produces no appreciable effect on the boundary layer.

When flow is separated, the concept of a "dividing streamline" is used. This streamline originates at the point of separation and ends at the reattachment point (Figure 2). The viscous flow above this "dividing streamline" includes all the fluid in the boundary layer just upstream of the separation point. Below this streamline, a steady,
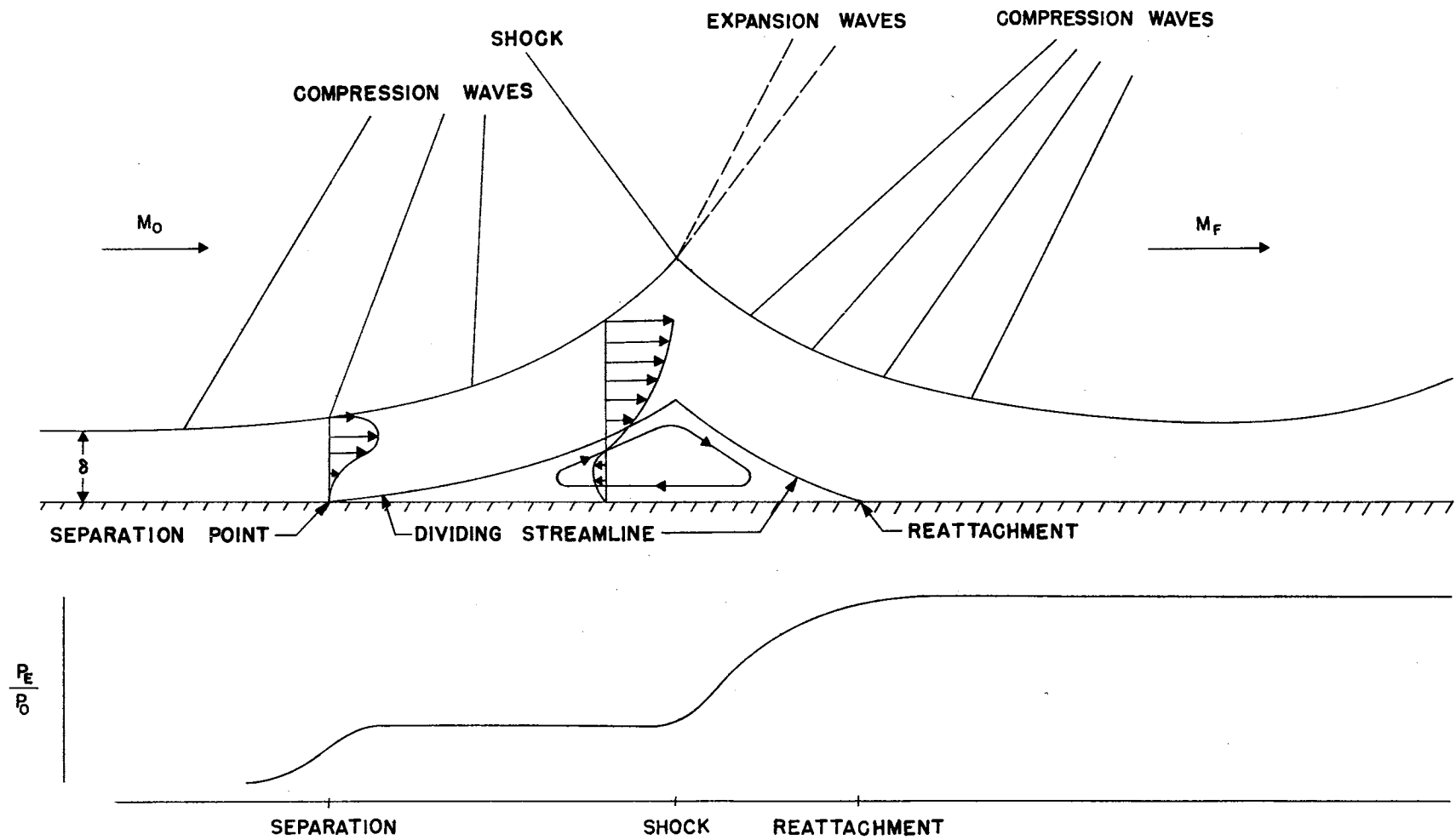
Figure 2. Schematic Representation of Shock-Wave-Laminar Boundary Layer
Interaction

recirculatory flow is trapped and forms a "separation bubble" between the separation and reattachment points (Figure 2).

Chapman, Kuehn, and Larson [5] and Glick [6] indicate that there exists a transfer of momentum from the external inviscid stream to the viscous flow above the dividing streamline. This increase in the fluid momentum allows the velocity of the fluid along the dividing streamline to increase continuously in the downstream direction. Consequently, the increase in fluid momentum will result in reattachment since the flow is sufficient to overcome the additional pressure rise that will be experienced during the reattachment process. As the viscous layer thickens downstream from the separation point, the positive pressure gradient steadily decreases until the "pressure plateau" is reached just upstream of the shock impingement point (Figure 2). In many instances, this is considered as a separated region in which the pressure is approximately constant.

The subsonic portion of the viscous boundary layer cannot support a sudden pressure rise; therefore, the incident shock is reflected as an expansion fan that exactly cancels the pressure jump across the shock. This reflection causes the flow at the outer edge of the viscous layer to be suddenly deflected toward the plate surface. The viscous layer is thereby squeezed against the plate surface and is forced to turn as it flows downstream. Thus the thickness of the viscous layer decreases, a deceleration of the viscous layer is realized, and a pressure increase is produced.

As the flow proceeds downstream, more and more fluid is turned back until the velocity along the dividing streamline is brought to rest

at the reattachment point (Figure 2). Downstream from the reattachment

point, the fluid above the dividing streamline forms a new boundary

layer. Once the new boundary layer is formed, the boundary layer

growth produces an interaction between the supersonic inviscid flow and

the viscous boundary layer.

Two facts have proved useful in analyzing the interaction region:

1. Both upstream and downstream from the shock impingement

    point, there is a constant-pressure, undisturbed region

    which can be used to make a "localized" study of the inter-

    action region.

2. The ultimate pressure rise on the plate resulting from an

    incident oblique shock-boundary layer interaction is

    approximately the same as that obtained in the inviscid

    case.

The above description of the two phenomena of interest is considered

sufficient for clarifying the following mathematical description of

these phenomena.

CHAPTER III

LITERATURE REVIEW

In deriving analytical methods for predicting the flow phenomenon associated with the incident shock-laminar boundary layer interaction, previous investigators have relied heavily on boundary layer theories developed in the past. Lees and Reeves [1] and Mitwally [7] have presented a thorough review of these analytical methods and of the ways in which the various boundary layer theories are used in obtaining the final result. It is therefore not necessary to review the material presented in references [1] and [7] since these publications are readily available. The various boundary layer theories are presented in textbooks written by Schlichting [8] and Meksyn [9].

The method of finite-differences has received wide-spread attention in recent years and has become a major tool in solving complicated inviscid fluid flow problems that involved shock dynamics which have previously remained unsolved. Tyler [10], Walker [11], and Walker and Tyler [12] have presented good reviews of the available literature on this subject.

Investigators have only recently shown interest in the application of the finite-difference numerical techniques to the viscous flow problem. One of the earliest pioneers in this particular phase of boundary layer analysis was Flügge-Lotz who, incidently, is still actively engaged in these studies.

13

Unfortunately, the various numerical techniques now used in solving the boundary layer equations are not applicable when shock waves are present in the flow field. Therefore, numerical techniques used in the study of shock dynamics must also be considered when the incident shock-boundary layer interaction problem is to be analyzed by means of the finite-difference method. For this reason the remaining portion of this chapter will be devoted to a discussion of the numerical techniques used in boundary layer analysis and the shock-dynamic studies not discussed in references [10], [11], and [12].

The boundary layer equations (conservation of mass, momentum, and energy) are normally expressed so that the dependent variables are the physical space coordinates and the independent variables are the velocity components, enthalpy, density, and viscosity. Flügge-Lotz and Baxter [13] present an explicit finite-difference technique based on an earlier work by Flügge-Lotz [14]. The two-dimensional boundary layer equations were reduced by using Crocco's transformation so that the shear stress (τ) and enthalpy (h) become the dependent variables while the coordinate x and the tangential velocity (u) form the independent variables. In reference [14], the numerical solutions of the cases studied were obtained by using the desk calculator. The apparent incentive for the work presented in reference [13] was the new popularity of the digital computer and the numerical stability difficulties observed near the wall of the flat plate. Thus reference [13] was devoted to the development of the finite-difference technique, a stability analysis of the finite-difference solution of parabolic equations in general, and an analysis of the imposed restrictions. Some aspects of

the programming for the IBM 650 digital computer were also discussed.
It should be noted that this type of finite-difference technique is not
time dependent. Application of the method involves the use of initial
boundary layer profiles as initial and boundary conditions. Finite-
difference methods are then used to establish boundary layer profiles
at succeeding x locations downstream from the initial boundary. This
method is commonly known as a marching technique.

In the follow-on work of reference [13], Baxter and Flügge-Lotz
[15] present the results obtained from some sixty examples which were
computed by using the finite difference method of reference [13].
Numerous problems, involving variable pressure gradients and wall
temperatures, were investigated. The wall conditions could not be de-
fined in a direct manner. A method of extrapolation from the computed
interior points (above the wall) had to be used to obtain the wall
conditions. Under certain conditions of favorable pressure gradient
and heated walls, velocity overshoots occurred in the boundary layer.
When a velocity overshoot was evident, a solution could not be obtained.
In view of this difficulty of velocity overshoot and the resultant in-
stability in the numerical solution, the authors suggested that the
difficulty could be overcome by solving the equations in their original
form, i.e., in the physical plane. However, the profiles required for
establishing starting conditions had to be initiated at some distance
downstream from the leading edge.

The influence of suction or blowing on a laminar boundary layer
has been of interest to aerodynamicists for more than half a century.
Flügge-Lotz and Howe [16] have used the finite-difference technique

described in references [14] and [15] to study the case of a transverse velocity at the wall. Emphasis was placed on the formulation and application of the new boundary conditions at the wall. The results obtained from a number of computed examples are presented in this study. These results include those obtained from examples of subsonic and supersonic flow over both hot and cold walls with and without pressure gradients.

Flügge-Lotz and Yu [17] first attempted the use of the finite-difference method presented in reference [15] to study the problem of the interaction which occurs between the exterior inviscid flow and the laminar boundary layer. They found that the boundary layer equations written in Crocco's form are unusable for the interaction problem because of the velocity overshoot problem. The equations were used in their original form in the analysis of two-dimensional boundary layer flow over a flat plate subjected to a constant wall temperature with and without pressure variations. An explicit finite-difference scheme was used, and in one case, which involved a high Mach number and a heated wall, instabilities occurred in the region from the wall to a height (normal to the wall) of approximately one-fourth of the boundary layer thickness. In a majority of the cases studied in reference [17], use of the difference scheme resulted in encountering instability in a narrow region next to the wall. The authors used simple approximation formulas to evaluate the properties in this region of instability.

Kramer and Lieberstein [18] have solve essentially the same equations as Baxter and Flügge-Lotz [15] by using an implicit finite-difference scheme. By using the implicit method, the stability problem

was eliminated; however, the step-size had to be sufficiently small to ensure convergence of the numerical solution to the exact solution. No comparison with known results is presented.

Flügge-Lotz and Blottner [19] present the development of two implicit finite-difference schemes and the results obtained from use of these schemes in the analysis of compressible laminar boundary layer flow, including displacement thickness interactions. Results of their study indicated that perhaps the best finite-difference scheme to use is the Crank-Nicolson method [20]. The authors found it necessary to "stretch" the coordinate normal to the wall to obtain smooth profiles across the boundary layer. The Howarth-Dorodnitsyn transformation was used to stretch this coordinate. Again, as in the case of all the previously discussed methods, the stagnation region could not be considered. Instead, starting profiles were used. In the case of supersonic flow, starting profiles were developed by using Low's method [21] while the method of Li and Nagamatsu [22] was used to obtain starting profiles in the analysis of hypersonic flow.

Wu [23] used an explicit finite-difference scheme to solve the boundary layer equations in the physical plane. Wu [23] used the Howarth-Dorodnitsyn transformation to stretch the normal coordinate in order to improve the stability of the equations. Flügge-Lotz and Blottner [19] state that Wu's transformed equations cannot be used to calculate the boundary layer in the presence of pressure gradients.

Fannelöp and Flügge-Lotz [24] use the finite-difference technique of reference [19] to predict the laminar boundary layer growth along a flat plate near the leading edge followed by a semi-infinite wavy wall.

An initial profile was given near the leading edge of the flat plate, and the step-wise finite-difference method was used to determine the behavior of the boundary layer. The method could not be used to obtain data at the separation point, and no attempt was made to analyze the separated region.

Clutter and Smith [25] present an accurate and rapid method for the solution of the general compressible, steady, laminar boundary layer equations for plane or axisymmetric flow, including transverse curvature effects. The method of solution consists of replacing the partial derivatives, with respect to the flow direction, by finite differences while retaining the derivatives in a direction normal to the boundary so that the partial differential equations can be approximated by the use of ordinary differential equations. Calculated results obtained from a number of specific problems are presented and these results are compared to the results obtained by using other analytical methods.

Smith and Clutter [26] extended the method described in reference [25] to include a compressible real gas subject to equilibrium dissociation. Smith and Jaffe [27] extended the method of references [25] and [26] for solving the non-equilibrium laminar boundary layer equations of a binary dissociating gas for two-dimensional or axisymmetric flow.

Thommen [28] considered the time-dependent solution of the full Navier-Stokes equations for the particular case of low Reynolds number (250 per foot) flow to demonstrate the applicability of a two-step technique for solution of the leading-edge shock-viscous interaction problem. For simplicity, he assumed a constant viscosity (μ) so that the numerical calculations were somewhat simplified. Use of the

numerical technique involved the calculation of the fluid properties at the half-step, i.e., the properties had to be evaluated at $(x + \frac{\Delta x}{2}$, $y + \frac{\Delta y}{2}$, $t + \frac{\Delta t}{2})$. These half-step properties were then used in the original equations to evaluate the fluid properties $(x + \Delta x, y + \Delta y, t + \Delta t)$.

A time-dependent, explicit finite-difference technique was recently reported by Kurzrock and Mates [29]. The complete Navier-Stokes equations were considered in the physical plane, and solutions were sought for viscous shock tube flow and the interaction phenomenon occurring in hypersonic low-density flow over a flat plate. In the latter study, free-stream Mach numbers of 6, 8 and 20 were considered. A cooled plate surface was enforced and the origin of the coordinate system was located at the leading edge of the plate. Free-stream conditions were specified as initial and boundary conditions along the column passing through the leading edge. No slip conditions were considered, and continuum flow conditions near the leading edge were assumed.

Cole [30] used the time-dependent, explicit finite-difference method developed by Rusanov [31] to solve the problem of the incident shock-laminar boundary layer interaction on an adiabatic flat plate. He was interested in working in the region far downstream from the leading-edge of the flat plate. His analysis was dependent on knowing boundary layer initial profiles at the starting point. Since the initial profiles are usually determined by use of approximate methods, they cannot be expected to satisfy the Navier-Stokes equations used. Consequently, in order to obtain suitable initial profiles, Cole was

forced to make repeated computer runs and constantly refine the initial profiles (while he retained the same boundary layer thickness) until the proper boundary layer growth rate was obtained. It is to be expected that no true similarity can be found between the assumed initial profile and the final profile obtained. The subsequent introduction of an external oblique shock incident on the boundary layer clearly produced flow separation, as was expected. It is not known if a comparison was made with experimental test data.

Filler and Ludloff [32] developed techniques for the numerical solution of the time-dependent, one-dimensional equations of motion of a viscous, heat conducting fluid. Both explicit and implicit finite-difference schemes were studied. The von Neumann stability analysis was used to predict the stability requirements. The formation of shock waves (by use of the explicit technique) was the same as that used by Lax [33]. In the case of the implicit method, an isentropic initial field was prescribed; this field consisted of two homogeneous states of different velocity, pressure, and density connected by a simple compression wave. The development of the flow field in time was then governed by the equations of motion. The authors were interested in the time required for the shock to form, the shock's final shape, and the entropy profiles developed. Results were presented for the case of both viscous and nonviscous flows.

Gary [34] considered two finite-difference schemes for the solution of the inviscid Navier-Stokes equation in one space dimension. The first method was that used by Lax and Wendroff [35]. The second method was based on an approximate solution of the centered, implicit difference

equations; this is an iterative method in which successive substitutions are used. The stability which resulted from the use of the implicit method depended on the number of iterations per time-step, i.e., stability is obtained if 3, 4, 7, 8, ... iterations are used per time-step, and instability is obtained if 1, 2, 5, 6, ... iterations are used per time-step. Unfortunately, the computation of flow fields containing shock discontinuities could not be achieved by using the implicit method, even for the case of the weak shock.

Thommen and D'Attores [36] considered the application of the Lax-Wendroff conservation difference scheme [35] to steady, two- and three-dimensional supersonic flow fields. They found that use of the Lax-Wendroff scheme resulted in obtaining large oscillations near the tail end of shock waves so that it was impossible to interpret the results with any degree of accuracy. The authors modified the scheme slightly and obtained excellent damping throughout the shock region. Use of the modified scheme produced larger truncation errors than those produced through use of the original Lax-Wendroff scheme, and the mesh size had to be made slightly smaller to obtain numerical stability.

An interesting report has recently been published by Welch, et al, [37]. This study contains a detailed description of a finite-difference technique called the Marker-and-Cell (MAC) technique. The complete incompressible Navier-Stokes equations are solved for the case of low-velocity, viscous flow involving free surfaces and with large-amplitude contortions in the field. The major features of the technique are the method by which the free-surface boundary conditions are satisfied and the fact that viscosity is not required as a stabilizer. This method

appears promising for studying the fluid behavior in fluid amplifiers and possibly as a new method in the study of supersonic viscous flow problems.

The above review of the literature indicates that no known investigation has previously used the approach adopted in the present study for problems involving large Reynolds numbers. Kurzrock and Mates [29] used a time-dependent, finite-difference method in an analysis in which the boundary conditions were enforced at the plate leading edge. They did not approach the problem from the standpoint of allowing the conditions and the equations to converge to a solution at the leading edge.

CHAPTER IV

MATHEMATICAL ANALYSIS

Governing Equations

The partial differential equations which describe the flow of a
viscous, compressible fluid include the basic laws of conservation of
mass, momentum, and energy. These conservation equations can be written
in various forms, and numerous approximations are often applied so that
simplified conservation equations usually result. When a direct solu-
tion is sought by use of these equations, the particular form of the
equations is relatively unimportant since, in the case of a particular
flow and given boundary conditions, the solution is usually unique.
However, when the conservation equations are to be solved by using
a finite-difference technique, the numerical solution will depend on
the particular form of the conservation equations and the finite-
difference approximations which are used.

The choice of the best form of the differential equations is
usually determined by knowing the physical behavior of the system under
study. As an example, when a normal shock discontinuity is present in
the flow field, it is known that the product of density and velocity
remains constant through the shock while the gradients of density and
velocity are very large. If the product of density and velocity, ρu,
is considered as a dependent variable, then the derivative $\frac{d}{dx} (\rho u)$

obtained by using the method of finite differences will, in general, be smaller than the derivatives of the individual fluid properties obtained by use of the same method. Large gradients are eliminated by using the equations in a "conservative" form, such as

$$\frac{\partial f}{\partial t} + \frac{\partial F}{\partial x} + \frac{\partial G}{\partial y} = 0. \tag{1}$$

This equation contains coefficients of unity; consequently, the space derivatives (in finite-difference form) produce only moderate gradients. It can usually be expected that the finite-difference approximations can be used to obtain more accurate results (and reduces the stability difficulties) when the equations are solved in the conservative form of Equation (1).

The development of the general two-dimensional ideal gas equations for the conservation of mass, momentum, and energy is well documented. These equations can be written in the aforementioned conservative form in terms of continuity,

$$\frac{\partial \bar{\rho}}{\partial t} + \frac{\partial}{\partial x} (\bar{\rho}\bar{u}) + \frac{\partial}{\partial y} (\bar{\rho}\bar{v}) = 0; \tag{2}$$

x-momentum,

$$\frac{\partial}{\partial t} (\bar{\rho}\bar{u}) + \frac{\partial}{\partial x} (\bar{\rho}\bar{u}^2 + \bar{p} + \bar{\tau}_{xx}) + \frac{\partial}{\partial y} (\bar{\rho}\bar{u}\bar{v} + \bar{\tau}_{xy}) = 0; \tag{3}$$

y-momentum,

$$\frac{\partial}{\partial t} (\bar{\rho}\bar{v}) + \frac{\partial}{\partial x} (\bar{\rho}\bar{u}\bar{v} + \bar{\tau}_{xy}) + \frac{\partial}{\partial y} (\bar{\rho}\bar{v}^2 + \bar{p} + \bar{\tau}_{yy}) = 0; \tag{4}$$

energy,

$$\frac{\partial \bar{e}}{\partial t} + \frac{\partial}{\partial x} \left[(\bar{e} + \bar{p})\bar{u} - \bar{k} \frac{\partial \bar{T}}{\partial x} + \bar{u}\bar{\tau}_{xx} + \bar{v}\bar{\tau}_{xy} \right] \tag{5}$$

$$+ \frac{\partial}{\partial y} \left[(\bar{e} + \bar{p})\bar{v} - \bar{k} \frac{\partial \bar{T}}{\partial y} + \bar{u}\bar{\tau}_{xy} + \bar{v}\bar{\tau}_{yy} \right] = 0;$$

where the sum of the internal and kinetic energy per unit volume is

$$\bar{e} = \bar{\rho}\left[\bar{c}_v \bar{T} + \frac{1}{2}(\bar{u}^2 + \bar{v}^2)\right] .$$

The shear stresses are defined as

$$\bar{\tau}_{xx} = -\bar{\mu}\left(\frac{4}{3}\frac{\partial \bar{u}}{\partial \bar{x}} - \frac{2}{3}\frac{\partial \bar{v}}{\partial \bar{y}}\right) , \tag{6}$$

$$\bar{\tau}_{yy} = -\bar{\mu}\left(\frac{4}{3}\frac{\partial \bar{v}}{\partial \bar{y}} - \frac{2}{3}\frac{\partial \bar{u}}{\partial \bar{x}}\right) ,$$

and

$$\bar{\tau}_{xy} = -\bar{\mu}\left(\frac{\partial \bar{u}}{\partial \bar{y}} + \frac{\partial \bar{v}}{\partial \bar{x}}\right) .$$

Equations (2), (3), (4), and (5) have to be supplemented by use of the usual ideal gas equation of state

$$\bar{p} = \bar{\rho}\bar{R}\bar{T} .$$

The method of nondimensionalizing the conservation equations differs somewhat from the method normally used in boundary layer theory. The nondimensionalizing technique is described in Appendix B. Use of this technique produces the equations for continuity,

$$\frac{\partial \rho}{\partial t} + \frac{\partial}{\partial x}(\rho u) + \frac{\partial}{\partial y}(\rho v) = 0; \tag{7}$$

x-momentum,

$$\frac{\partial}{\partial t}(\rho u) + \frac{\partial}{\partial x}(\rho u^2 + p + \lambda \tau_{xx}) + \frac{\partial}{\partial y}(\rho uv + \lambda \tau_{xy}) = 0; \tag{8}$$

y-momentum,

$$\frac{\partial}{\partial t}(\rho v) + \frac{\partial}{\partial x}(\rho uv + \lambda \tau_{xy}) + \frac{\partial}{\partial y}(\rho v^2 + p + \lambda \tau_{yy}) = 0; \tag{9}$$

energy,

$$\frac{\partial e}{\partial t} + \frac{\partial}{\partial x}\left[(e + p)u - \Omega\frac{\partial T}{\partial x} + \lambda\ (u\tau_{xx} + v\tau_{xy})\right]$$

$$+ \frac{\partial}{\partial y}\left[(e + p)v - \Omega\frac{\partial T}{\partial y} + \lambda\ (u\tau_{xy} + v\tau_{yy})\right] = 0. \tag{10}$$

The equation of state and the equation of shear stress become

$$p = \rho T, \tag{11}$$

$$\tau_{xx} = -\mu\left(\frac{4}{3}\frac{\partial u}{\partial x} - \frac{2}{3}\frac{\partial v}{\partial y}\right),$$

$$\tau_{yy} = -\mu\left(\frac{4}{3}\frac{\partial v}{\partial y} - \frac{2}{3}\frac{\partial u}{\partial x}\right),$$

$$\tau_{xy} = -\mu\left(\frac{\partial u}{\partial y} + \frac{\partial v}{\partial x}\right).$$

If a central finite-difference technique is applied to the spatial derivatives of Equations (8), (9), and (10), a 13-point network is required because of the presence of the second-order terms. It is interesting to note that Kurzrock and Mates [29] report that the most accurate numerical results are always obtained by differencing the equations in the completely conservative form. If the second-order terms are isolated, Equations (7) through (10) become

continuity,

$$\frac{\partial \rho}{\partial t} + \frac{\partial}{\partial x}(\rho u) + \frac{\partial}{\partial y}(\rho v) = 0 ; \tag{12}$$

x-momentum,

$$\frac{\partial}{\partial t}(\rho u) + \frac{\partial}{\partial x}(\rho u^2 + p) + \frac{\partial}{\partial y}(\rho uv) = -\lambda\left(\frac{\partial \tau_{xx}}{\partial x} + \frac{\partial \tau_{xy}}{\partial y}\right) ; \tag{13}$$

y-momentum,

$$\frac{\partial}{\partial t}(\rho v) + \frac{\partial}{\partial x}(\rho uv) + \frac{\partial}{\partial y}(\rho v^2 + p) = -\lambda(\frac{\partial \tau_{xy}}{\partial x} + \frac{\partial \tau_{yy}}{\partial y}) ; \qquad (14)$$

energy,

$$\frac{\partial e}{\partial t} + \frac{\partial}{\partial x}\left[(e + p)u\right] + \frac{\partial}{\partial y}\left[(e + p)v\right] = \Omega\left[\frac{\partial}{\partial x}(\frac{\partial T}{\partial x}) + \frac{\partial}{\partial y}(\frac{\partial T}{\partial y})\right]$$

$$- \lambda\left[\frac{\partial}{\partial x}(u\tau_{xx} + v\tau_{xy}) + \frac{\partial}{\partial y}(u\tau_{xy} + v\tau_{yy})\right] ; \qquad (15)$$

where

$$\lambda = \frac{M_o \sqrt{\gamma}}{Re} \quad \text{and} \quad \Omega = \frac{\gamma\lambda}{Pr(\gamma - 1)} .$$

It is observed that only a nine-point network is required in the use of the central finite-difference technique if the required differentiation is carried out on the molecular transport terms. The use of this simplification reduces the numerical accuracy somewhat; however, as reported by Kurzrock and Mates [29], the computation time can be reduced by as much as 45 percent.

Equations (12) through (15) can be represented as a single equation of the form

$$\frac{\partial f}{\partial t} + \frac{\partial F^x}{\partial x} + \frac{\partial F^y}{\partial y} = S , \qquad (16)$$

where f, F^x, F^y, and S are considered to be four component vectors. These can be represented as

$$f = \begin{bmatrix} \rho \\ \rho u \\ \rho v \\ e \end{bmatrix} , \qquad F^x = \begin{bmatrix} \rho u \\ \rho u^2 + p \\ \rho uv \\ (e + p)u \end{bmatrix} ,$$

$$F^y = \begin{bmatrix} \rho v \\ \rho u v \\ \rho v^2 + p \\ (e + p)v \end{bmatrix} \quad , \quad S = \begin{bmatrix} 0 \\ S_1 \\ S_2 \\ S_3 \end{bmatrix} .$$

The vector **S** will be referred to as the source vector which is used to describe the decrease in momentum caused by the viscous shear forces and the change in energy caused by heat conduction and dissipation. The components of the source vector, **S**, are

$$S_1 = \lambda \left[\mu \left(\frac{4}{3} \frac{\partial^2 u}{\partial x^2} + \frac{\partial^2 u}{\partial y^2} + \frac{1}{3} \frac{\partial^2 v}{\partial x \partial y} \right) + \frac{\partial \mu}{\partial x} \left(\frac{4}{3} \frac{\partial u}{\partial x} - \frac{2}{3} \frac{\partial v}{\partial y} \right) \right.$$
$$\left. + \frac{\partial \mu}{\partial y} \left(\frac{\partial u}{\partial y} + \frac{\partial v}{\partial x} \right) \right] ,$$

$$S_2 = \lambda \left[\mu \left(\frac{4}{3} \frac{\partial^2 v}{\partial y^2} + \frac{\partial^2 v}{\partial x^2} + \frac{1}{3} \frac{\partial^2 u}{\partial x \partial y} \right) + \frac{\partial u}{\partial x} \left(\frac{\partial u}{\partial y} + \frac{\partial v}{\partial x} \right) \right.$$
$$\left. + \frac{\partial \mu}{\partial y} \left(\frac{4}{3} \frac{\partial v}{\partial y} - \frac{2}{3} \frac{\partial u}{\partial x} \right) \right] ,$$

$$S_3 = \Omega \left[\frac{\partial^2 T}{\partial x^2} + \frac{\partial^2 T}{\partial y^2} \right] + \lambda \left\{ \mu \left[\frac{2}{3} \left(\frac{\partial^2 u^2}{\partial x^2} + \frac{\partial^2 v^2}{\partial y^2} \right) + \frac{1}{3} \left(u \frac{\partial^2 v}{\partial x \partial y} + v \frac{\partial^2 u}{\partial x \partial y} \right) \right. \right.$$
$$\left. + \frac{1}{2} \left(\frac{\partial^2 v^2}{\partial x^2} + \frac{\partial^2 u^2}{\partial y^2} \right) + 2 \frac{\partial v}{\partial x} \frac{\partial u}{\partial y} - \frac{4}{3} \frac{\partial u}{\partial x} \frac{\partial v}{\partial y} \right]$$
$$+ \frac{\partial \mu}{\partial x} \left[\frac{2}{3} \frac{\partial u^2}{\partial x} + \frac{1}{2} \frac{\partial v^2}{\partial x} + v \frac{\partial u}{\partial y} - \frac{2}{3} u \frac{\partial v}{\partial y} \right] + \frac{\partial \mu}{\partial y} \left[\frac{2}{3} \frac{\partial v^2}{\partial y} \right.$$
$$\left. \left. + \frac{1}{2} \frac{\partial u^2}{\partial y} + u \frac{\partial v}{\partial x} - \frac{2}{3} v \frac{\partial u}{\partial x} \right] \right\} .$$

Equation (16) constitutes a system of four partial differential equations whose solutions are to be represented in two-dimensional space and in time. Sufficient information must be given both initially and during the course of the solution to ensure that the mathematical

model always approximates the physical model. These bits of information are respectively known as the initial conditions and the boundary conditions.

The initial conditions are usually well established and are unique to each particular problem. However, the boundary conditions can vary considerably from one problem to another and must be chosen for each particular problem so as to provide an adequate description of the type of flow under investigation. Because of the boundary conditions, the form of the difference equations will vary as a function of the placement of the net point in the flow field. Thus, the difference equations used in describing points lying entirely within the field of flow, i.e., field points, will not be the same as the difference equations used in describing points lying either on walls or on planes of symmetry, i.e., boundary points. Therefore, the required number of finite-difference approximations of Equation (16) depends upon the flow-field configuration of each particular problem.

Finite-Difference Technique

Since Equation (16) is reduced to the inviscid flow equations when large Reynold numbers (Re $\rightarrow \infty$) are used, the differencing method employed is that developed by V. V. Rusanov [31] for the general, first-order, nonlinear, partial differential equation

$$\frac{\partial f}{\partial t} + \frac{\partial F^x}{\partial x} + \frac{\partial F^y}{\partial y} = 0 .$$

In this method, "artificial viscosity" terms are used to "smear" the properties in regions of shock discontinuities so that they take on

characteristics similar to those produced by the regular fluid viscosity. In other words, this "artificial viscosity" is used to force the fluid properties to be continuous in the shock region although they may be rapidly changing. Consequently, the shock region can be treated as a general field region in solving the equations.

The addition of the artificial viscosity terms to Equation (16) results in modifying the equation as follows:

$$\frac{\partial f}{\partial t} + \frac{\partial F^x}{\partial x} + \frac{\partial F^y}{\partial y} = \frac{\partial}{\partial x}\left[A(x,y,t)\frac{\partial f}{\partial x}\right] + \frac{\partial}{\partial y}\left[B(x,y,t)\frac{\partial f}{\partial y}\right] + S. \qquad (17)$$

The coefficients $A(x,y,t)$ and $B(x,y,t)$ represent the artificial viscosity terms whose functional values are obtained from a stability analysis. The requirements necessary for the proper selection of these coefficients are those given by J. von Neumann [38]:

1. The conservation equations, with the dissipation terms added, must be such that solutions without discontinuities can be obtained.

2. The thickness of the shock must be of the same order as the mesh spacing $(\Delta x, \Delta y)$ used in the numerical calculations.

3. The effect of the artificial dissipation terms must be negligible outside the shock regions.

4. The Rankine-Hugoniot equations must be applicable across shock layers.

In the difference scheme applied to Equation (17), use is made of a forward difference in time and a central difference in space. The difference net is shown in Figure 3 where the increments of the independent variables $(\Delta x, \Delta y, \Delta t)$ are denoted in the difference scheme as (h_1, h_2, τ).
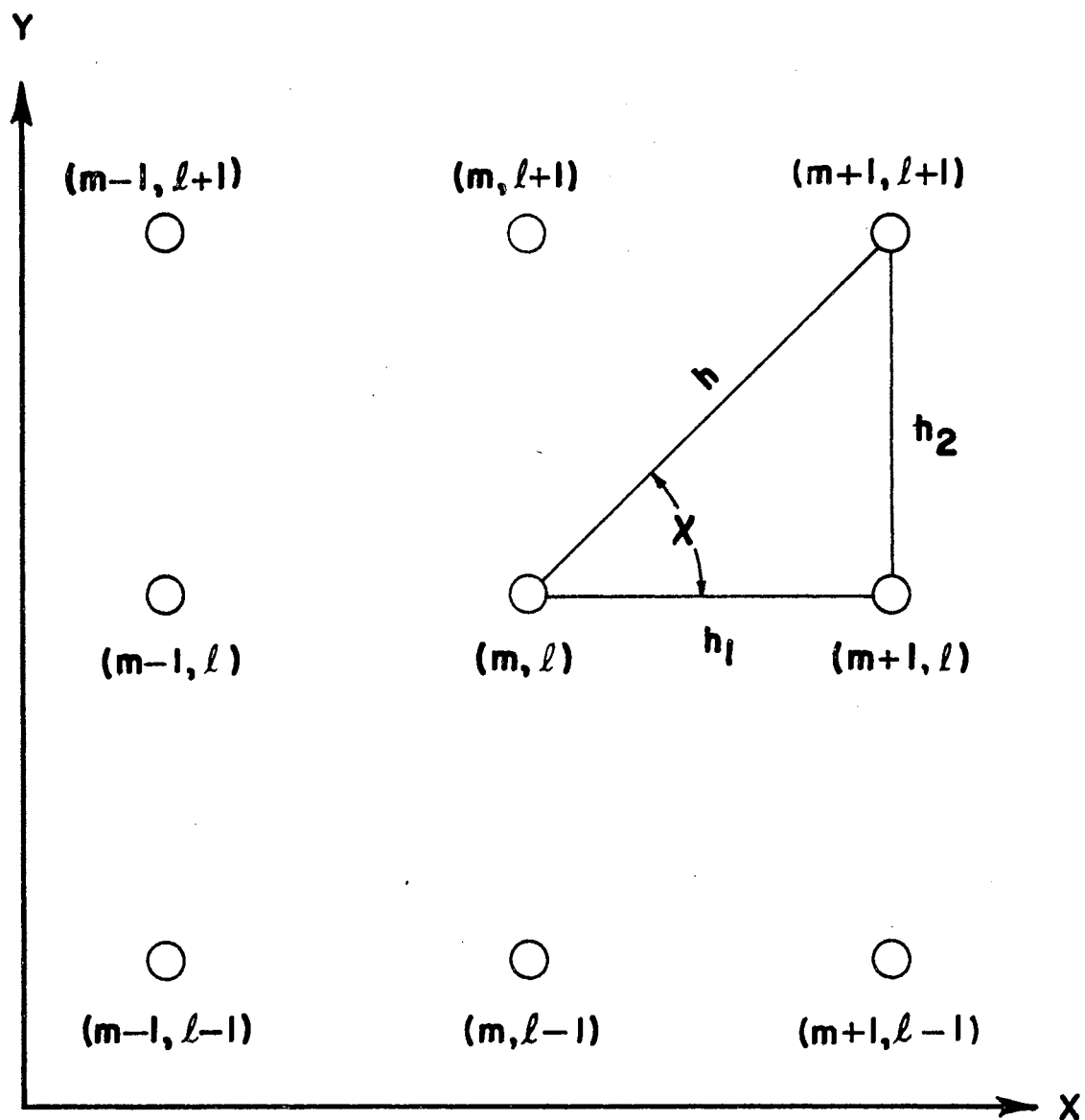
Figure 3. Finite-Difference Net Notation

The subscript (m, ℓ) denotes the "node" or pivotal point at which the derivatives are to be evaluated, i.e., $(x = mh_1, y = \ell h_2)$. The subscripts $(m+1, \ell)$, $(m-1, \ell)$, $(m, \ell+1)$, and $(m, \ell-1)$ denote the location of the neighboring "nodes" relative to the pivotal node (m, ℓ). The superscript n represents the nth time plane for which the fluid properties are to be evaluated. From Figure 3, it is seen that

$$h_1 = h \cos \chi \,,$$

$$h_2 = h \sin \chi \,,$$

and

$$h = (h_1{}^2 + h_2{}^2)^{\frac{1}{2}} \,.$$

By the designation of

$$K_1 = \frac{\tau}{h_1}$$

and

$$K_2 = \frac{\tau}{h_2}$$

one obtains the expressions

$$K = (K_1{}^2 + K_2{}^2)^{\frac{1}{2}} = \frac{(h_1{}^2 + h_2{}^2)^{\frac{1}{2}}}{h_1 h_2} \tau \,,$$

$$K_1 = K \sin \chi \,, \tag{18}$$

$$K_2 = K \cos \chi \,,$$

where τ is the time increment Δt.

By the use of the notation previously described, the derivatives in Equation (17) will be approximated as

$$\frac{\partial f}{\partial t} = \frac{f_{m,\ell}^{n+1} - f_{m,\ell}^{n}}{\tau} \,,$$

$$\frac{\partial F^x}{\partial x} = \frac{F^x_{m+1,\ell} - F^x_{m-1,\ell}}{2h_1},$$

$$\frac{\partial F^y}{\partial y} = \frac{F^y_{m,\ell+1} - F^x_{m,\ell-1}}{2h_2},$$

$$\frac{\partial}{\partial x}\left(A\frac{\partial f}{\partial x}\right) = \frac{1}{h_1}\left[A_{m+\frac{1}{2},\ell}\left(\frac{\partial f}{\partial x}\right)_{m+\frac{1}{2},\ell} - A_{m-\frac{1}{2},\ell}\left(\frac{\partial f}{\partial x}\right)_{m-\frac{1}{2},\ell}\right]^n$$

$$= \frac{1}{h_1^2}\left[A_{m+\frac{1}{2},\ell}(f_{m+1,\ell} - f_{m,\ell}) - A_{m-\frac{1}{2},\ell}(f_{m,\ell} - f_{m-1,\ell}\right]^n,$$

and

$$\frac{\partial}{\partial y}\left(B\frac{\partial f}{\partial y}\right) = \frac{1}{h_2^2}\left[B_{m,\ell+\frac{1}{2}}(f_{m,\ell+1} - f_{m,\ell}) - B_{m,\ell-\frac{1}{2}}(f_{m,\ell} - f_{m,\ell-1})\right]^n.$$

The difference approximation of Equation (17) is then written as

$$f^{n+1}_{m,\ell} = f^n_{n,\ell} + \tau S - \frac{\tau}{2h_1}(F^x_{m+1,\ell} - F^x_{m-1,\ell})^n - \frac{\tau}{2h_2}(F^y_{m,\ell+1}$$

$$-F^y_{m,\ell-1})^n + \frac{\tau}{h_1^2}\left[A_{m+\frac{1}{2},\ell}(f_{m+1,\ell} - f_{m,\ell}) - A_{m-\frac{1}{2},\ell}(f_{m,\ell}\right.$$

$$\left.-f_{m-1,\ell})\right]^n + \frac{\tau}{h_2^2}\left[B_{m,\ell+\frac{1}{2}}(f_{m,\ell+1} - f_{m,\ell})\right.$$

$$\left.- B_{m,\ell-\frac{1}{2}}(f_{m,\ell} - f_{m,\ell-1})\right]^n.$$

From the definitions

$$A^n_{m,\ell} = \frac{h_1^2}{2}\alpha^n_{m,\ell},$$

$$B^n_{m,\ell} = \frac{h_2^2}{2}\beta^n_{m,\ell},$$

$$\Phi^x_{m+\frac{1}{2},\ell} = \alpha^n_{m+\frac{1}{2},\ell}(f_{m+1,\ell} - f_{m,\ell})^n, \qquad (20)$$

$$\Phi^x_{m-\frac{1}{2}, \ell} = \alpha^n_{m-\frac{1}{2}, \ell} (f_{m, \ell} - f_{m-1, \ell})^n ,$$

$$\Phi^y_{m, \ell+\frac{1}{2}} = \beta^n_{m, \ell+\frac{1}{2}} (f_{m, \ell+1} - f_{m, \ell})^n ,$$

$$\Phi^y_{m, \ell-\frac{1}{2}} = \beta^n_{m, \ell-\frac{1}{2}} (f_{m, \ell} - f_{m, \ell-1})^n ,$$

the final difference approximation of Equation (19) then becomes

$$f^{n+1}_{m, \ell} = f^n_{m, \ell} + \tau S^n - \frac{K_1}{2} (F^x_{m+1, \ell} - F^x_{m-1, \ell})^n - \frac{K_2}{2} (F^y_{m, \ell+1}$$

$$\tag{21}$$

$$-F^y_{m, \ell-1})^n + \frac{1}{2} (\Phi^x_{m+\frac{1}{2}, \ell} - \Phi^x_{m-\frac{1}{2}, \ell} + \Phi^y_{m, \ell+\frac{1}{2}} - \Phi^y_{m, \ell-\frac{1}{2}})^n .$$

Rusanov [31] obtained the expressions for $\alpha^n_{m, \ell}$ and $\beta^n_{m, \ell}$ by using the linear stability analysis, i.e.,

$$\alpha^n_{m, \ell} = \omega K(w + c)^n_{m, \ell} \sin^2 \chi$$

and

$$\tag{22}$$

$$\beta^n_{m, \ell} = \omega K(w + c)^n_{m, \ell} \cos^2 \chi$$

where

$$w = (u^2 + v^2)^{\frac{1}{2}}$$

and ω is a damping parameter determined from the stability analysis. The parameter ω is related to K and $(w + c)^n_{m, \ell}$ by the inequality

$$K^2 \left[(w + c)^n_{m, \ell} \right]^2 \leq \omega K(w + c)^n_{m, \ell} \leq 1 \tag{23}$$

which must be satisfied for all (m, ℓ). The quantity $\sigma^n_{m, \ell} = K(w + c)^n_{m, \ell}$ is the Courant number at the nodal point (m, ℓ) in the nth time plane. The maximum Courant number present in the field at time n can be designated as

$$\sigma_0 = \max \sigma_{m,\ell}^n$$

so that the stability condition $\Big($Equation (23)$\Big)$ is satisfied for all n

if

$$\sigma_0 \leq 1 \tag{24a}$$

and

$$\sigma_0 \leq \omega \leq \frac{1}{\sigma_0} \ . \tag{24b}$$

The numerical value of σ_0 and ω may be established prior to any

calculations. Once the calculations have commenced, the value of K

for each time plane can be determined from the relation

$$K = \frac{\sigma_0}{\max(w + c)_{m,\ell}^n} \ . \tag{25}$$

The value of τ for each time plane can then be determined by use of

Equation (18). This operation and holding the parameters σ_0 and ω con-

stant throughout the calculations are sufficient to satisfy the stability

criteria.

Tyler [10] has shown the linear stability analysis used by Rusanov

[31] in defining an acceptable set of inviscid conservation equations.

Walker [11] attempted to extend the stability analysis for the more com-

plicated equations describing the turbulent jet mixing region where the

turbulent shear stresses are much greater than those that occur in

laminar flow. The results obtained by Walker [11] for the limiting case

of negligible turbulent stresses were identical to those presented by

Rusanov [31]. However, in applying the method to a numerical analysis,

Walker [11] found that the inequality $\Big($Equation (24b)$\Big)$ could be greatly

relaxed, i.e., much smaller ω values could be used because of the stabilizing effect of the turbulent shear stresses.

The basic stability requirement used in this analysis is that developed by Rusanov [31] since Equation (16), as mentioned previously, can only be used to define phenomena related to an inviscid condition as the Reynolds number becomes very large. However, the stability analysis presented by Rusanov [31] is very brief and several major steps and basic assumptions have been omitted. The interested reader should refer to the works of Tyler [10] and Walker [11] for the complete stability analysis.

The final finite-difference approximation $\left(\text{Equation (21)}\right)$ is a general equation which, in its present form, is not applicable throughout the field of study. As mentioned previously, the required number of finite-difference approximations of Equation (16), and consequently Equation (21), depends upon the flow-field configuration of each particular problem.

In order to obtain the variations of Equation (21) necessary for the present investigation, a basic lattice was constructed to describe the flow-field configuration (Figure 4). The field contained a total of 1,920 nodal points in 40 rows and 48 columns. The sharp leading edge of the flat plate was chosen one-half mesh spacing from its nearest neighbor, as indicated in the figure. It will also be noted that the first row of nodal points ($\ell=1$) does not lie on the line y = 0. The open circles denote the regular mesh points while the full circles represent auxiliary points which are normally considered as part of the boundary conditions.
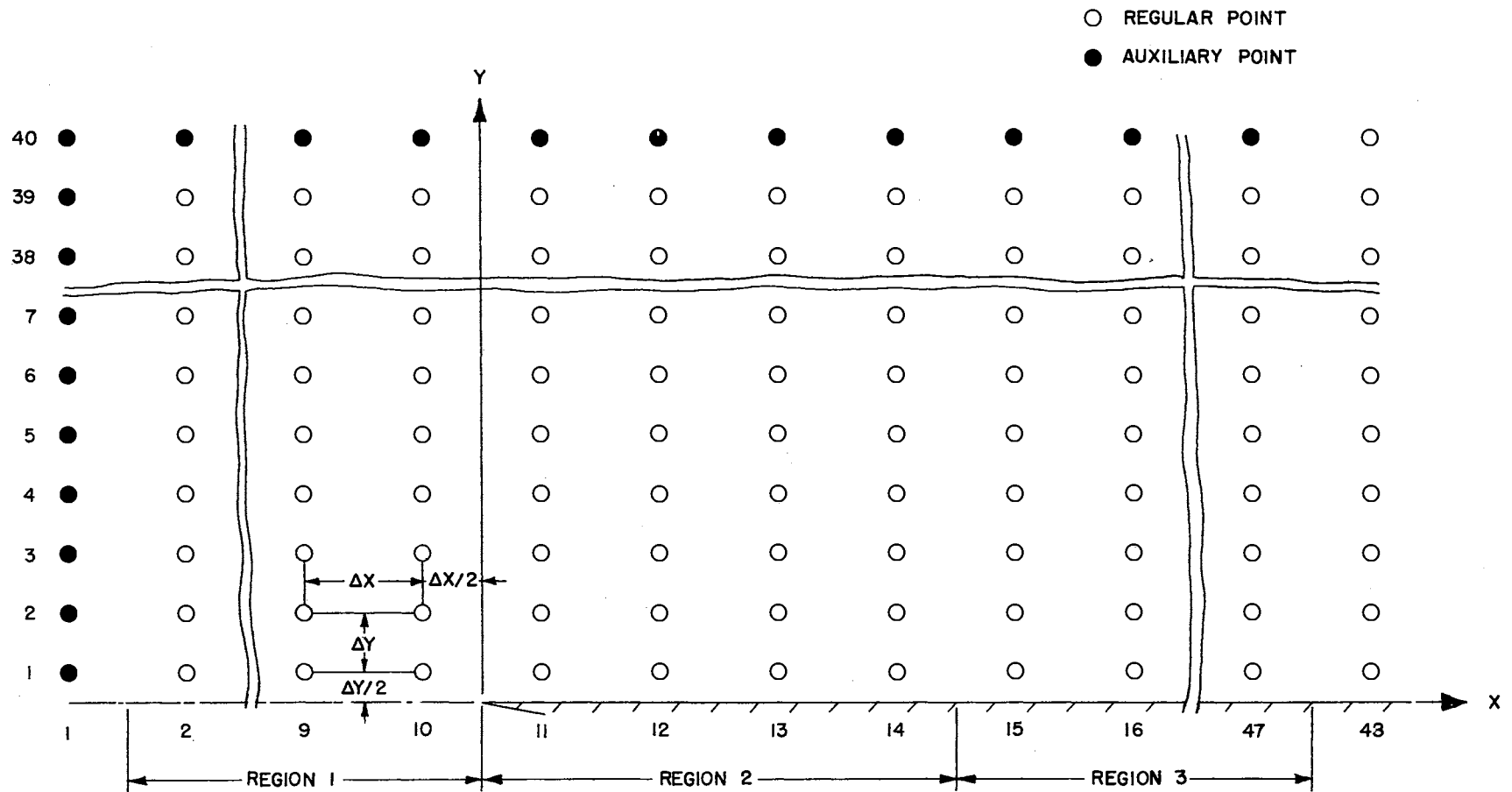
Figure 4. The Basic Lattice for the Calculation of Viscous Flow Near the
Sharp Leading Edge of a Flat Plate

The extreme left boundary (m=1) represents the free-stream conditions. All fluid properties along this column remain constant throughout the calculating process and are therefore considered as initial and boundary conditions. Although the physical location of the left boundary is arbitrary, it is advisable to place the boundary a considerable distance upstream from the leading edge because a finite-difference technique cannot be used to define a discrete attached shock. However, the difference technique can be used to establish gradients over several mesh widths and thus provide a representation of a detached shock. Therefore, the left boundary should be located a sufficient distance upstream from the plate leading edge so that the fluid properties remain unaltered by the phenomenon occurring near the leading edge.

The upper boundary (ℓ=40) presents no difficulty because the field is large enough so that the leading-edge shock is completely contained within the flow field. On the basis of this condition, it can be implied that the fluid properties along the upper boundary remain unaltered and therefore represent the free-stream initial and boundary conditions.

The extreme right column (m=48) is considered a "floating" boundary where the fluid properties are allowed to change with time. Kurzrock and Mates [29] and Thommen [28] evaluated the fluid properties along this boundary (column) for each time plane by extrapolating from the calculated upstream properties. When an oblique shock crosses this boundary, certain difficulties can be encountered in using an extrapolation technique since the resulting gradients can be quite large

and erroneous and therefore produce undesired perturbations upstream. Such undesirable results have been obtained by Eaton [39]. To alleviate these problems, in this investigation all x-direction gradients along this boundary (column) were assigned a value of zero. This is the method successfully used by Jackomis [40], Tyler [10] and Walker [11]. In order to meet this requirement, the properties were redefined at the end of each time plane by the use of Equation (26):

$$\rho_{48,\ell}^{n+1} = \rho_{47,\ell}^{n+1} \,,$$

$$P_{48,\ell}^{n+1} = P_{47,\ell}^{n+1} \,,$$

$$u_{48,\ell}^{n+1} = u_{47,\ell}^{n+1} \,,$$

$$v_{48,\ell}^{n+1} = v_{47,\ell}^{n+1} \,. \tag{26}$$

The actual numerical calculations are now limited to those nodal points lying completely within the flow field, i.e., the field points, and those points along the row $\ell = 1$, for $1 < m < 48$. Additional comments on the field point calculations are not required since it is obvious that Equation (21) is applicable for such points. Along the row $\ell = 1$ three different types of boundary conditions are imposed which require three additional modifications to the field point difference Equation (21). A discussion of each flow region, designated regions 1, 2, and 3, along the row $\ell = 1$ follows, and a brief description of the application of the boundary conditions is presented. For brevity, Tables I and II contain a list of all the finite-difference approximations necessary for the field point calculations. Tables III through

TABLE I

FINITE-DIFFERENCE APPROXIMATIONS OF FIELD POINT
PARTIAL DIFFERENTIAL TERMS

Term	Difference Approximation
$\partial u/\partial x$	$(u_{m+1,\ell} - u_{m-1,\ell})/2\Delta x$
$\partial u/\partial y$	$(u_{m,\ell+1} - u_{m,\ell-1})/2\Delta y$
$\partial v/\partial x$	$(v_{m+1,\ell} - v_{m-1,\ell})/2\Delta x$
$\partial v/\partial y$	$(v_{m,\ell+1} - v_{m,\ell-1})/2\Delta y$
$\partial u^2/\partial x$	$(u^2_{m+1,\ell} - u^2_{m-1,\ell})/2\Delta x$
$\partial u^2/\partial y$	$(u^2_{m,\ell+1} - u^2_{m,\ell-1})/2\Delta y$
$\partial v^2/\partial x$	$(v^2_{m+1,\ell} - v^2_{m-1,\ell})/2\Delta x$
$\partial v^2/\partial y$	$(v^2_{m,\ell+1} - v^2_{m,\ell-1})/2\Delta y$
$\partial^2 u/\partial x^2$	$(u_{m+1,\ell} - 2u_{m,\ell} + u_{m-1,\ell})/(\Delta x)^2$
$\partial^2 u/\partial y^2$	$(u_{m,\ell+1} - 2u_{m,\ell} + u_{m,\ell-1})/(\Delta y)^2$
$\partial^2 v/\partial x^2$	$(v_{m+1,\ell} - 2v_{m,\ell} + v_{m-1,\ell})/(\Delta x)^2$
$\partial^2 v/\partial y^2$	$(v_{m,\ell+1} - 2v_{m,\ell} + v_{m,\ell-1})/(\Delta y)^2$
$\partial^2 T/\partial x^2$	$(T_{m+1,\ell} - 2T_{m,\ell} + T_{m+1,\ell})/(\Delta x)^2$
$\partial^2 T/\partial y^2$	$(T_{m,\ell+1} - 2T_{m,\ell} + T_{m,\ell-1})/(\Delta y)^2$
$\partial^2 u^2/\partial x^2$	$(u^2_{m+1,\ell} - 2u^2_{m,\ell} + u^2_{m-1,\ell})/(\Delta x)^2$
$\partial^2 u^2/\partial y^2$	$(u^2_{m,\ell+1} - 2u^2_{m,\ell} + u^2_{m,\ell-1})/(\Delta y)^2$
$\partial^2 v^2/\partial x^2$	$(v^2_{m+1,\ell} - 2v^2_{m,\ell} + v^2_{m-1,\ell})/(\Delta x)^2$
$\partial^2 v^2/\partial y^2$	$(v^2_{m,\ell+1} - 2v^2_{m,\ell} + v^2_{m,\ell-1})/(\Delta y)^2$
$\partial^2 u/\partial x\partial y$	$(u_{m+1,\ell+1} - u_{m-1,\ell+1} - u_{m+1,\ell-1} + u_{m-1,\ell-1})/4\Delta x\Delta y$
$\partial^2 v/\partial x\partial y$	$(v_{m+1,\ell+1} - v_{m-1,\ell+1} - v_{m+1,\ell-1} + v_{m-1,\ell-1})/4\Delta x\Delta y$

TABLE II

FINITE-DIFFERENCE APPROXIMATIONS OF FIELD POINT CONSERVATIVE TERMS

Conservation Equation	Conservative Term	Difference Approximation
Continuity	$F^x_{m+1,\ell} - F^x_{m-1,\ell}$	$\rho_{m+1,\ell}\, u_{m+1,\ell} - \rho_{m-1,\ell}\, u_{m-1,\ell}$
Continuity	$F^y_{m,\ell+1} - F^y_{m,\ell-1}$	$\rho_{m,\ell+1}\, v_{m,\ell+1} - \rho_{m,\ell-1}\, v_{m,\ell-1}$
X-Momentum	$F^x_{m+1,\ell} - F^x_{m-1,\ell}$	$\rho_{m+1,\ell}\, u^2_{m+1,\ell} + P_{m+1,\ell} - \rho_{m-1,\ell}\, u^2_{m-1,\ell} - P_{m-1,\ell}$
X-Momentum	$F^y_{m,\ell+1} - F^y_{m,\ell-1}$	$\rho_{m,\ell+1}\, u_{m,\ell+1}\, v_{m,\ell+1} - \rho_{m,\ell-1}\, u_{m,\ell-1}\, v_{m,\ell-1}$
Y-Momentum	$F_{m+1,\ell} - F_{m-1,\ell}$	$\rho_{m+1,\ell}\, u_{m+1,\ell}\, v_{m+1,\ell} - \rho_{m-1,\ell}\, u_{m-1,\ell}\, v_{m-1,\ell}$
Y-Momentum	$F^y_{m,\ell+1} - F^y_{m,\ell-1}$	$\rho_{m,\ell+1}\, v^2_{m,\ell+1} - \rho_{m,\ell-1}\, v^2_{m,\ell-1}$
Energy	$F^x_{m+1,\ell} - F^x_{m-1,\ell}$	$(e_{m+1,\ell} + P_{m-1,\ell})u_{m+1,\ell} - (e_{m-1,\ell} + P_{m-1,\ell})u_{m-1,\ell}$
Energy	$F^y_{m,\ell+1} - F^y_{m,\ell-1}$	$(e_{m,\ell+1} + P_{m,\ell+1})v_{m,\ell-1} - (e_{m,\ell-1} + P_{m,\ell-1})v_{m,\ell-1}$

VIII contain a list of the finite-difference approximations necessary for the three different types of boundary conditions imposed along the row $\ell = 1$ in the case of a flow configuration similar to the one used in this investigation.

Difference Equations Used in the Analysis of Region 1

If the nodal points along the row $\ell = 1$ had been placed along the line $y = 0$, the problem in region 1 could have been reduced to the problem related to the centerline (streamline) ahead of an infinitely thin flat plate. In such a flow (Figure 5), all curvature terms in the y direction are forced to zero. An additional boundary condition of zero mass flow across the centerline allows the four relationships of interest to be defined as follows:

$$P_{m, \ell+1} = P_{m, \ell-1} \,,$$

$$\rho_{m, \ell+1} = \rho_{m, \ell-1} \,,$$

$$u_{m, \ell+1} = u_{m, \ell-1} \,,$$

$$v_{m, \ell+1} = -v_{m, \ell-1} \,. \tag{27}$$

When these relationships (Equation (27)) are applied to region 1 (Figure 5), it is obvious that

$$P_{m, \ell-1} = P_{m, \ell} \,,$$

$$\rho_{m, \ell-1} = \rho_{m, \ell} \,,$$

$$u_{m, \ell-1} = u_{m, \ell} \,, \tag{28}$$

and

$$v_{m, \ell-1} = -v_{m, \ell} \,.$$

$(m, \ell+1)$

$\circ$

$(m-1, \ell)$　　　(m, ℓ)　　　$(m+1, \ell)$

$\circ$　　　　　$\circ$　↓　　　$\circ$

$\Delta y/2$

―――――――――――――――――― ₵ ―――――

$\circ$

$(m, \ell-1)$

REGION I FLOW

$(m, \ell+1)$

$\circ$―

Δy

$(m-1, \ell)$　　　(m, ℓ)　　　$(m+1, \ell)$

――$\circ$―――――――$\circ$―― ₵ ――$\circ$――

$\circ$

$(m, \ell-1)$
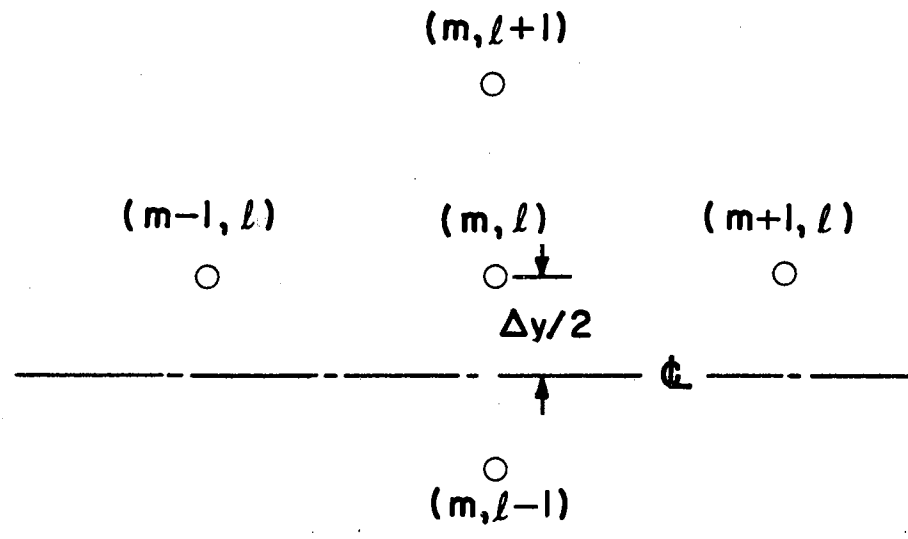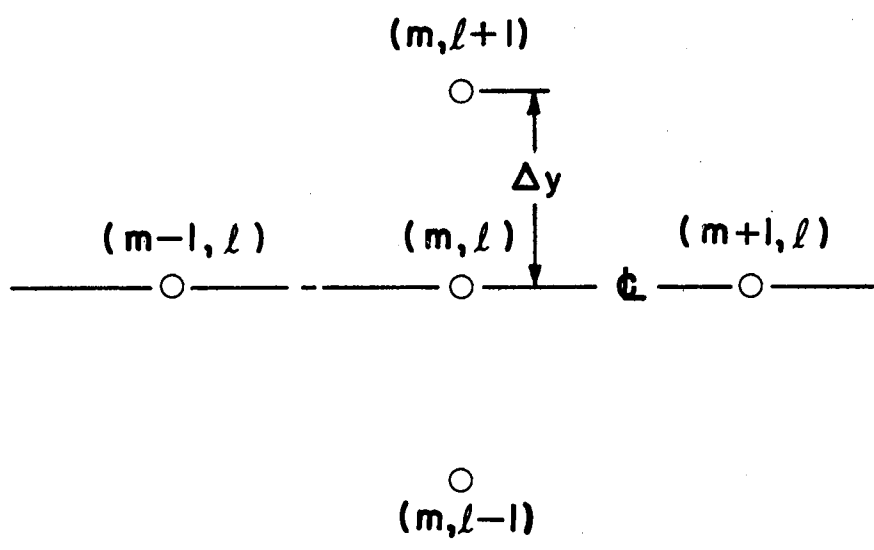
CENTERLINE FLOW

Figure 5. Comparison Between Region 1 Flow and Centerline Flow

Since all nodal points $(m, \ell-1)$ in this region are out of the region of
calculation, it is convenient to rewrite the field-point difference
equation (Equation (21)) by using the relationships (Equation (28)).
Thus all properties at $(m, \ell-1)$ can be written in terms of their equiva-
lent values at (m, ℓ). The new difference equation developed in this
fashion is straightforward. Tables III and IV contain a list of all
the finite-difference approximations necessary to calculate the fluid
properties in this region.

Difference Equations Used in the Analysis of Region 2

Region 2 is a most critical region since it is impossible to know
exactly the behavior of the flow properties in this region. The un-
certainty encountered in this region and the questionable validity of
the continuum equations for the solution of problems encountered near
the stagnation point were the main reasons the leading edge was chosen
one-half mesh width from its nearest neighbor. The selection of this
position eliminated the stagnation point problem since all velocities
along the row $\ell = 1$ are finite and nonzero. To represent the flow
more accurately in this region, slip flow was used in a very simple
and somewhat crude manner, i.e., a simple schedule was used (Figure 6)
to provide maximum slip at $m = 11$. A decreasing amount of slip was
applied at each downstream nodal point until the no-slip condition was
reached at $m = 15$. The use of this approach prevented the occurrence
of any large decrease in velocity at the first nodal point ($m = 11$) and
subsequent abrupt decreases downstream. From Figure 6 it can be seen
that the velocity profile near the plate surface is assumed to be linear.

TABLE III

**FINITE-DIFFERENCE APPROXIMATIONS OF REGION 1
PARTIAL DIFFERENTIAL TERMS**

Term	Difference Approximation
$\partial u/\partial x$	Same as Field Point (Table I)
$\partial u/\partial y$	$(u_{m,\ell+1} - u_{m,\ell})/2\Delta y$
$\partial v/\partial x$	Same as Field Point (Table I)
$\partial v/\partial y$	$(v_{m,\ell+1} + v_{m,\ell})/2\Delta y$
$\partial u^2/\partial x$	Same as Field Point (Table I)
$\partial u^2/\partial y$	$(u^2_{m,\ell+1} - u^2_{m,\ell})/2\Delta y$
$\partial v^2/\partial x$	Same as Field Point (Table I)
$\partial v^2/\partial y$	$(v^2_{m,\ell+1} - v^2_{m,\ell})/2\Delta y$
$\partial^2 u/\partial x^2$	Same as Field Point (Table I)
$\partial^2 u/\partial y^2$	$(u_{m,\ell+1} - u_{m,\ell})/(\Delta y)^2$
$\partial^2 v/\partial x^2$	Same as Field Point (Table I)
$\partial^2 v/\partial y^2$	$(v_{m,\ell+1} - 3v_{m,\ell})/(\Delta y)^2$
$\partial^2 T/\partial x^2$	Same as Field Point (Table I)
$\partial^2 T/\partial y^2$	$(T_{m,\ell+1} - T_{m,\ell})/(\Delta y)^2$
$\partial^2 u^2/\partial x^2$	Same as Field Point (Table I)
$\partial^2 u^2/\partial y^2$	$(u^2_{m,\ell+1} - u^2_{m,\ell})/(\Delta y)^2$
$\partial^2 v^2/\partial x^2$	Same as Field Point (Table I)
$\partial^2 v^2/\partial y^2$	$(v^2_{m,\ell+1} - v^2_{m,\ell})/(\Delta y)^2$
$\partial^2 u/\partial x \partial y$	$(u_{m+1,\ell+1} - u_{m,\ell+1} - u_{m+1,\ell} + u_{m,\ell})/\Delta x \Delta y$
$\partial^2 v/\partial x \partial y$	$(v_{m+1,\ell+1} - v_{m,\ell+1} - v_{m+1,\ell} + v_{m,\ell})/\Delta x \Delta y$

TABLE IV

FINITE-DIFFERENCE APPROXIMATIONS OF REGION 1 CONSERVATIVE TERMS

Conservation Equation	Conservative Term	Difference Approximation
Continuity	$F^x_{m+1,\ell} - F^x_{m-1,\ell}$	Same as Field Point (Table II)
Continuity	$F^y_{m,\ell+1} - F^y_{m,\ell-1}$	$\rho_{m,\ell+1}\, v_{m,\ell+1} + \rho_{m,\ell}\, v_{m,\ell}$
X-Momentum	$F^x_{m+1,\ell} - F^x_{m-1,\ell}$	Same as Field Point (Table II)
X-Momentum	$F^y_{m,\ell+1} - F^y_{m,\ell-1}$	$\rho_{m,\ell+1}\, u_{m,\ell+1}\, v_{m,\ell+1} + \rho_{m,\ell}\, u_{m,\ell}\, v_{m,\ell}$
Y-Momentum	$F^x_{m+1,\ell} - F^x_{m-1,\ell}$	Same as Field Point (Table II)
Y-Momentum	$F^y_{m,\ell+1} - F^y_{m,\ell-1}$	$\rho_{m,\ell+1}\, v^2_{m,\ell+1} + P_{m,\ell+1} - \rho_{m,\ell}\, v^2_{m,\ell} - P_{m,\ell}$
Energy	$F^x_{m+1,\ell} - F^x_{m-1,\ell}$	Same as Field Point (Table II)
Energy	$F^y_{m,\ell+1} - F^y_{m,\ell-1}$	$(e_{m,\ell+1} + P_{m,\ell+1})v_{m,\ell+1} + (e_{m,\ell} + P_{m,\ell})v_{m,\ell}$

U(11,2)   U(12,2)   U(13,2)   U(14,2)

(11,2)   (12,2)   (13,2)   (14,2)

0.8U(11,2)   0.6U(12,2)   0.5U(13,2)   0.4U(14,2)

(11,1)   (12,1)   (13,1)   (14,1)

(SURFACE)   (SURFACE)   (SURFACE)   (SURFACE)

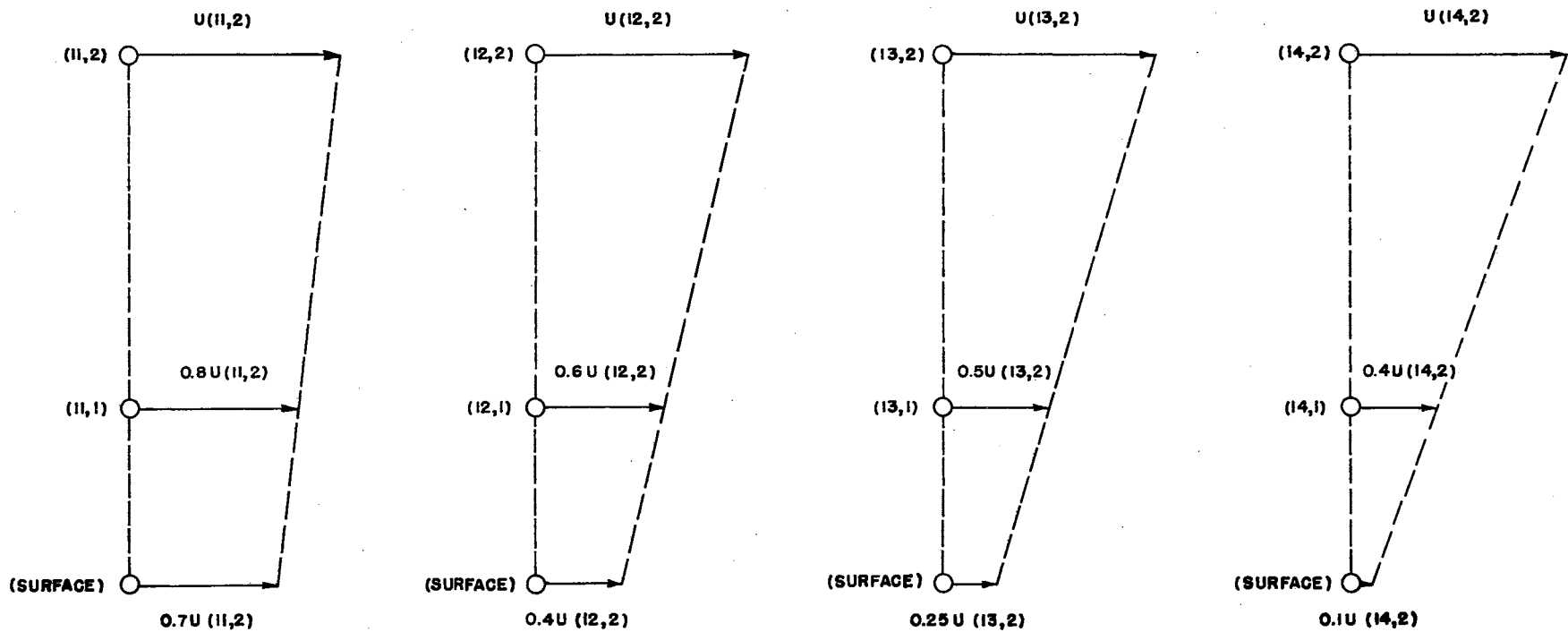0.7U(11,2)   0.4U(12,2)   0.25U(13,2)   0.1U(14,2)

Figure 6.   Slip Flow Approximation Near the Leading Edge of a Flat Plate

Once the x-component of velocity at $\ell = 2$ has been calculated, then the x-component of velocity at $\ell = 1$ is known in terms of the assumed slip flow condition. Consequently, there is no necessity of solving the x-momentum equation.

Although the slip flow condition is allowed, the zero mass transfer condition through the surface is enforced. It is assumed that the nodal spacing in the y-direction (Δy) is small enough so that the velocity profiles in this region can be represented in linear form. The y-component of velocity v can be approximated as

$$v_{m,1} = \frac{1}{3} v_{m,2} \tag{29}$$

which, by linear extrapolation, enforces the boundary condition

$$v \big|_{y=0} = 0.$$

Consequently, the y-momentum equation is unnecessary since v is approximated.

No easy method of approximating the density and pressure is known; therefore, these values must be determined by using a modified version of Equation (21). Here again, approximations must be made since no information is available on the gradients in this region. The method used in obtaining these approximations is such that all curvature terms are forced to zero; consequently, the gradients are linear and are functions of the properties at (m, ℓ) and $(m, \ell+1)$. Since the slip condition is allowed, the properties at $(m, \ell-1)$ are defined by use of the following relationships:

$$P_{m,\ell-1} = 2P_{m,\ell} - P_{m,\ell+1} \quad ,$$

$$\rho_{m,\ell-1} = 2\rho_{m,\ell} - \rho_{m,\ell+1} \quad ,$$

$$u_{m,\ell-1} = 2u_{m,\ell} - u_{m,\ell+1} \quad , \tag{30}$$

$$v_{m,\ell-1} = -v_{m,\ell} \quad .$$

After Equation (21) has been modified by insertion of the above relation-ships, it can be used to determine the new values of density and pressure in this region. Tables V and VI contain lists of all the required finite-difference approximations necessary for these calculations.

Difference Equations Used in the Analysis of Region 3

Region 3 represents the usual boundary layer region where the no-slip condition is applied. As mentioned previously, it is assumed that Δy is sufficiently small so that the velocity profiles in the region near the plate surface can be considered as being linear. Thus the condition represented by Equation (29) is assumed in this region as well as the conditions represented by Equation (31), i.e.,

$$u_{m,1} = \frac{1}{3} u_{m,2} \quad ,$$

$$v_{m,1} = \frac{1}{3} v_{m,2} \quad . \tag{31}$$

As in the solution presented in Region 2, only the continuity and energy equations must be solved since the velocity components are assumed.

The x-component of velocity gradient in the y-direction is not known, but it must be determined for each time plane. To preserve this gradient at y = 0 and apply the gradients in the finite difference

TABLE V

**FINITE-DIFFERENCE APPROXIMATIONS OF REGION 2
PARTIAL DIFFERENTIAL TERMS**

Term	Difference Approximation
$\partial u/\partial x$	Same as Field Point (Table I)
$\partial u/\partial y$	$(u_{m,\ell+1} - u_{m,\ell})/\Delta y$
$\partial v/\partial x$	Same as Field Point (Table I)
$\partial v/\partial y$	$(v_{m,\ell+1} + v_{m,\ell})/2\Delta y$
$\partial u^2/\partial x$	Same as Field Point (Table I)
$\partial u^2/\partial y$	$2(u_{m,\ell}u_{m,\ell+1} - u^2_{m,\ell})/\Delta y$
$\partial v^2/\partial x$	Same as Field Point (Table I)
$\partial v^2/\partial y$	$(v^2_{m,\ell+1} - v^2_{m,\ell})/2\Delta y$
$\partial^2 u/\partial x^2$	Same as Field Point (Table I)
$\partial^2 u/\partial y^2$	0.0
$\partial^2 v/\partial x^2$	Same as Field Point (Table I)
$\partial^2 v/\partial y^2$	0.0
$\partial^2 T/\partial x^2$	Same as Field Point (Table I)
$\partial^2 T/\partial y^2$	0.0
$\partial^2 u^2/\partial x^2$	Same as Field Point (Table I)
$\partial^2 u^2/\partial y^2$	$(2u^2_{m,\ell+1} - 4u_{m,\ell}\,u_{m,\ell+1} + 2u^2_{m,\ell})/(\Delta y)^2$
$\partial^2 v^2/\partial x^2$	Same as Field Point (Table I)
$\partial^2 v^2/\partial y^2$	$(v^2_{m,\ell+1} - v^2_{m,\ell})/(\Delta y)^2$
$\partial^2 u/\partial x\partial y$	$(u_{m+1,\ell+1} - u_{m,\ell+1} - u_{m+1,\ell} + u_{m,\ell})/\Delta x\Delta y$
$\partial^2 v/\partial x\partial y$	$(v_{m+1,\ell+1} - v_{m,\ell+1} - v_{m+1,\ell} + v_{m,\ell})/\Delta x\Delta y$

TABLE VI

FINITE-DIFFERENCE APPROXIMATIONS OF REGION 2 CONSERVATIVE TERMS

Conservation Equation	Conservative Term	Difference Approximation
Continuity	$F^x_{m+1,\ell} - F^x_{m-1,\ell}$	Same as Field Point (Table II)
Continuity	$F^y_{m,\ell+1} - F^y_{m,\ell-1}$	$\rho_{m,\ell+1}\, v_{m,\ell+1} + (2\rho_{m,\ell} - \rho_{m,\ell+1})v_{m,\ell}$
X-Momentum	$F^x_{m+1,\ell} - F^x_{m-1,\ell}$	Not Needed
X-Momentum	$F^y_{m,\ell+1} - F^y_{m,\ell-1}$	Not Needed
Y-Momentum	$F^x_{m+1,\ell} - F^x_{m-1,\ell}$	Not Needed
Y-Momentum	$F^y_{m,\ell+1} - F^y_{m,\ell-1}$	Not Needed
Energy	$F^x_{m+1,\ell} - F^x_{m-1,\ell}$	Same as Field Point (Table II)
Energy	$F^y_{m,\ell+1} - F^y_{m,\ell-1}$	$(e_{m,\ell+1} + p_{m,\ell+1})v_{m,\ell+1} + \tfrac{1}{2}(2\rho_{m,\ell} - \rho_{m,\ell+1})$ $[(2u_{m,\ell} - u_{m,\ell+1})^2 + v^2_{m,\ell}]v_{m,\ell}$

calculations, it is necessary to require the condition

$$u_{m,\ell-1} = - u_{m,\ell} \ . \tag{32}$$

Again, to obtain the zero mass flux through the plate surface, the following identity is required:

$$v_{m,\ell-1} = - v_{m,\ell} \ . \tag{33}$$

The adiabatic wall condition is applied in this region in order to satisfy the boundary condition:

$$\frac{\partial T}{\partial y} \Big|_{y=0} = 0 \ .$$

In the nondimensional form, the temperature is determined by the equation of state,

$$T_{m,\ell} = \frac{P_{m,\ell}}{\rho_{m,\ell}} \ .$$

The image technique used by Burstein [41] is applied to the properties p and ρ so that

$$P_{m,\ell-1} = P_{m,\ell} \tag{34a}$$

and

$$\rho_{m,\ell-1} = \rho_{m,\ell} \tag{34b}$$

After Equation (21) has been modified by inserting the conditions represented by Equations (32), (33), (34a), and (34b), it can be used for the analysis of region 3. All the necessary finite-difference approximations necessary for solving the continuity and energy equations in this region are presented in Tables VII and VIII. The assumptions, the technique, and the equations described in this chapter are those used to obtain a solution of the problem considered in this study.

TABLE VII

FINITE-DIFFERENCE APPROXIMATIONS OF REGION 3
PARTIAL DIFFERENTIAL TERMS

Term	Difference Approximation
$\partial u/\partial x$	Same as Field Point (Table I)
$\partial u/\partial y$	$(u_{m,\ell+1} + u_{m,\ell})/2\Delta y$
$\partial v/\partial x$	Same as Field Point (Table I)
$\partial v/\partial y$	$(v_{m,\ell+1} + v_{m,\ell})/2\Delta y$
$\partial u^2/\partial x$	Same as Field Point (Table I)
$\partial u^2/\partial y$	$(u^2_{m,\ell+1} - u^2_{m,\ell})/2\Delta y$
$\partial v^2/\partial x$	Same as Field Point (Table I)
$\partial v^2/\partial y$	$(v^2_{m,\ell+1} - v^2_{m,\ell})/2\Delta y$
$\partial^2 u/\partial x^2$	Same as Field Point (Table I)
$\partial^2 u/\partial y^2$	0.0
$\partial^2 v/\partial x^2$	Same as Field Point (Table I)
$\partial^2 v/\partial y^2$	0.0
$\partial^2 T/\partial x^2$	Same as Field Point (Table I)
$\partial^2 T/\partial y^2$	$(T_{m,\ell+1} - T_{m,\ell})/(\Delta y)^2$
$\partial^2 u^2/\partial x^2$	Same as Field Point (Table I)
$\partial^2 u^2/\partial y^2$	$(u^2_{m,\ell+1} - u^2_{m,\ell})/(\Delta y)\partial$
$\partial^2 v^2/\partial x^2$	Same as Field Point (Table I)
$\partial^2 v^2/\partial y^2$	$(v^2_{m,\ell+1} - v^2_{m,\ell})/(\Delta y)^2$
$\partial^2 u/\partial x\partial y$	$(u_{m+1,\ell+1} - u_{m,\ell+1} - u_{m+1,\ell} + u_{m,\ell})/\Delta x\Delta y$
$\partial^2 v/\partial x\partial y$	$(v_{m+1,\ell+1} - v_{m,\ell+1} - v_{m+1,\ell} + v_{m,\ell})/\Delta x\Delta y$

TABLE VIII

FINITE-DIFFERENCE APPROXIMATIONS OF REGION 3 CONSERVATIVE TERMS

Conservation Equation	Conservative Term	Difference Approximation
Continuity	$F^x_{m+1,\ell} - F^x_{m-1,\ell}$	Same as Field Point (Table II)
Continuity	$F^y_{m,\ell+1} - F^y_{m,\ell-1}$	$\rho_{m,\ell+1}\, v_{m,\ell+1} + \rho_{m,\ell}\, v_{m,\ell}$
X-Momentum	$F^x_{m+1,\ell} - F^x_{m-1,\ell}$	Not Needed
X-Momentum	$F^y_{m,\ell+1} - F^y_{m,\ell-1}$	Not Needed
Y-Momentum	$F^x_{m+1,\ell} - F^x_{m-1,\ell}$	Not Needed
Y-Momentum	$F^y_{m,\ell+1} - F^y_{m,\ell-1}$	Not Needed
Energy	$F^x_{m+1,\ell} - F^x_{m-1,\ell}$	Same as Field Point (Table II)
Energy	$F^y_{m,\ell+1} - F^y_{m,\ell-1}$	$(e_{m,\ell+1} + p_{m,\ell+1})v_{m,\ell+1} + (e_{m,\ell} + p_{m,\ell})v_{m,\ell}$

54

CHAPTER V

PRESENTATION OF RESULTS

Equation (17) represents the system of nonlinear, partial differential equations which were used to determine the characteristics of the general flow field near the sharp leading-edge of a flat plate. The finite-difference approximations and assumptions used in this effort are described in Chapter IV.

The complete study included two cases of interest. Case I involved the development of the leading-edge shock wave and the laminar boundary layer. Case 2 was an extension of Case 1, achieved by introducing an externally produced oblique shock which was incident just aft of the leading-edge of the flat plate.

Results Obtained in Case 1 Study

The basic lattice used is that shown in Figure 4. The field contains 1600 nodal points of interest in 40 rows and 40 columns. The plate was accelerated instantaneously to a constant velocity of Mach 3.0. The free-stream fluid properties were the atmospheric properties existing at a flight altitude of 100,000 feet. This particular flight condition was chosen for three reasons:

1. A laminar boundary layer can be expected even during the process of separation and reattachment.

2. The boundary layer can be expected to grow rapidly near the leading edge and introduce the possibility of an interaction between the leading-edge shock wave and the laminar boundary layer.

3. The stability of the numerical technique is strongly dependent on the Reynolds number (observe Equations (13), (14), and (15)). Thus numerical stability and the requirement for less artificial dissipation can be more easily obtained by use of a low Reynolds number.

The nondimensional properties used as initial input and fixed boundary conditions were

$$u_o = 3.5496 \qquad \Delta x = 0.001666$$

$$v_o = 0.0 \qquad \Delta y = 0.000833$$

$$p_o = 1.0 \qquad R_e = 3.06(10^5)$$

$$\rho_o = 1.0 \qquad P_r = 0.72$$

$$\sigma_o = 0.5 \qquad \mu = (T)^{.76}$$

$$\omega = 0.3 \qquad L = 1 \text{ ft}$$

The small size of the mesh was necessary to obtain a good representation of the boundary layer. In other words, if the boundary layer growth on a given airfoil is to be determined, the boundary layer can be expected to be thin compared to the physical dimensions of the airfoil. In the analysis of a thin boundary layer, several nodes must be used; consequently, the Δy must also be physically small. To obtain a good resolution of the shock and to satisfy the von Neumann requirement, the magnitude of Δx has to be of the same order as Δy. The requirement for a small Δx and Δy and the limited storage capacity of the digital

computer resulted in a restriction of the size of the flow field that could be used. Consequently, only a small region near the leading edge could be analyzed.

The constant static pressure ratio lines which occur in the flow field are shown in Figure 7. The leading-edge shock wave is completely contained within two mesh widths, and the shock appears to be attached at the leading edge. The shock angle in this region is approximately 42 degrees. The constant pressure ratio lines indicate that the shock is highly curved in this region, and such a curvature of the shock in this region indicates a viscous interaction which is normally neglected in thin boundary layer analysis. Such observations are not abnormal, however, in wind tunnel tests conducted in the past. Reference 5 contains a shadowgraph taken during wind tunnel tests where the test conditions were similar to those used in this investigation. Examination of this shadowgraph clearly indicates a curved shock near the leading edge.

As the fluid particles pass through the highly curved shock near the leading edge, an unusual pressure distribution just downstream can be expected. The numerical calculations in this investigation bear out this anticipation. This local high-pressure region is shown in Figure 7. Downstream from the high pressure region, the pressure is observed to decay rapidly. Following along with this reduction in pressure, a favorable pressure gradient is introduced in conjunction with the diminution in the strength of the shock. A shock wave angle of 24 degrees was measured near the downstream vertical boundary ($m = 40$). The curvature of the shock near this boundary indicates that the shock

strength would continue to decrease gradually if the field of calculation could be extended. The calculated shock angle of 24 degrees which occurs in the free stream is in good agreement with the measured 23 degrees observed in Reference 5. It is worth noting that, if the concept of thin boundary layer theory had been used, a leading-edge Mach wave of 19.6 degrees would be predicted. It should also be noted that (1) such theory does not include a consideration of the pressure variations downstream from the leading edge and (2) these variations could significantly alter the boundary layer growth characteristics in this region. In other words, the possibility of similarity is questionable.

The point of maximum pressure ratio was 4.45, calculated at the coordinate (0.03, 0.005). The physical location of this high pressure region is not conducive to testing; therefore, the accuracy of the calculated maximum pressure is unknown. However, the accuracy of the numerical technique can be fairly easily checked in terms of satisfying the Rankine-Hugoniot relations. As an example, use of the numerical technique results in prediction of a shock angle of 42 degrees and a pressure ratio across the shock of 4.45. For the same Mach number and shock angle, use of the Rankine-Hugoniot relations results in a prediction of a pressure ratio of 4.52. Therefore, the pressure ratios are in agreement within 2 percent.

The calculated pressure ratio variation along the row immediately above the plate surface (y = 0.005 inch) is shown in Figure 8. A pressure increase through the shock wave is clearly indicated. The decrease in pressure in the direction downstream of the shock wave

follows the pattern obtained by Kurzrock and Mates [29] in hypersonic flow. This trend is also observed in Thommen's [28] results for the case of low Reynolds number flow. An undershoot in pressure occurs just upstream of the shock wave and is preceded by rapidly damped oscillations. This phenomenon has been observed by Thommen [28] and Eaton [39]. Kurzrock and Mates observed no such phenomenon since their calculations were initiated at the plate leading edge where the properties are specified as boundary conditions and remain constant throughout the calculations. The magnitude of the pressure undershoot appears to depend on the viscosity (artificial, real, or a combination of both) and the mesh dimension ratio $\frac{\Delta x}{\Delta y}$. Eaton [39] had to use a large value of ω to prevent the pressure from becoming negative. Thommen [28] reduced the mesh dimension ratio to unity and completely eliminated the undershoot problem, but the flow problem considered by Thommen [28] involved the consideration of a very low Reynolds number; consequently, the presence of a good real-viscosity influence was assured in this region.

The calculated skin-friction coefficient, $C_f\sqrt{R_{e_{x,o}}}$, is also shown in Figure 8 for the no-slip flow region downstream from the leading-edge of the plate. Analysis of the phenomenon indicates that the boundary layer has not reached its normal growth pattern, i.e., the skin-friction coefficient is rapidly growing as a function of downstream distance rather than reaching a maximum value and remaining constant regardless of downstream distance thereafter. Further discussion of the boundary layer growth pattern will be subsequently presented in this section.

The trend toward increase in the skin-friction coefficient as a function of distance indicates that, if the field of calculation were extended an additional one-half inch, the coefficient would approach the value of 0.61 given by Shapiro [42] for the case of similar flow conditions. However, the limited storage capacity of the computer did not permit such extended calculations. The behavior of the calculated skin-friction coefficient follows the trend shown by Kurzrock and Mates [29] for the case hypersonic flow, i.e., an initial rapid increase as a function of downstream distance.

The calculated pressure ratio distributions are shown in Figure 9 at various downstream locations. The peak pressure ratio obtained in each curve provides an indication of the presence of the shock wave. At x = 0.09 inch, the shock is still strong and therefore introduces a large pressure gradient, $\frac{dp}{dy}$, in the boundary layer. Farther down-stream, at x = 0.390 inch, the shock was weakened considerably; conse-quently, the resulting pressure gradient, $\frac{dp}{dy}$, is greatly reduced, but it has not reached the zero value normally expected in boundary layer theory. The surface pressures are shown to decrease as a function of distance, and a continuing reduction is indicated as a function of down-stream distance (Figure 9).

The nondimensional tangential velocity profiles near the leading edge are shown in Figure 10. The initial velocity profiles (Curves A and B) indicate that the leading-edge shock does not interact with the boundary layer within the first two calculation points (x $\leqq$ 0.03 inch). This lack of interaction is perhaps due to the initially large shock angle in this region. Velocity overshoots are also observed near the

leading edge. The viscous interaction is more pronounced in curves C, D, and E, as indicated by the location of the point of inflection in the velocity profiles. The edge of the boundary layer cannot be defined in this region since the inflection points are associated with the reduction in velocity of the fluid particles as they pass through the established shock wave. The only conclusion that can be stated about the boundary layer in this region is that it has not developed sufficiently to be adequately defined.

Additional nondimensional velocity profiles and corresponding nondimensional temperature profiles at various x locations are shown in Figures 11 through 15. The velocity and temperature profiles at $x = 0.09$ inch again indicate that the boundary layer has not yet fully developed. The surface temperature is high as a result of the rapid decrease in velocity observed in the region $x < 0.09$ inch. For example, the maximum temperature ratio was observed to be 4.27 at $x = 0.07$ inch. At $x = 0.09$ inch, the temperature ratio has decreased to 3.35, but it has not yet reached the expected constant adiabatic wall temperature.

The data in Figures 12 through 15 indicate that the boundary layer is completely developed, i.e., a velocity at the edge of the boundary layer can be defined for each curve. It is also observed that the boundary layer edge velocity increases with downstream distance. This trend indicates a weakening shock wave and the corollary fact that the velocity of the inviscid flow field between the shock wave and the boundary layer is gradually approaching the free-stream velocity. At the same time, the thickness of the inviscid flow field is growing as a function of distance from the leading edge, and the boundary layer growth rate is decreasing.

The velocity distribution plotted in terms of the similarity parameter, η, is shown in Figure 16 for the station location x = 0.490 inch. The velocity at the outer edge of the boundary layer is again seen to be less than that of the free-stream velocity. A preliminary check at the station location x = 0.390 inch indicated that similarity had not yet been obtained.

There is a strong similarity in the behavior of the boundary layer thickness distribution calculated as a function of the downstream distance from the leading edge and that observed in the shadowgraph shown in Reference 5. During the later stages of this investigation, it became evident that an exact agreement with other theoretical methods would be very unlikely because of four factors:

1. The use of the artificial dissipation term (ω) would make the viscous effects become more influential and thus make the boundary layer grow at a faster rate than that predicted by the use of other theoretical methods.

2. The decision to allow slip flow near the plate leading edge automatically resulted in the introduction of a high temperature region (temperature jump) downstream from the leading-edge shock. The associated fluid viscosity would also be very influential in this region (i.e., it would result in a rapid rate of initial boundary layer growth).

3. The proper convergence of the finite-difference technique in the region very near the plate leading edge is strongly dependent on the incremental distance Δy (i.e., Δy should be sufficiently small in order to establish the boundary

layer thickness one node downstream from the leading edge).
The computer storage capacity limits the size of Δy if the
region of study is to be of any significant size and the von
Neumann requirement is to be satisfied. Thus if Δy is not
sufficiently small, as was the case in this study, proper
convergence cannot be expected near the plate leading edge.
A rapid initial boundary layer growth rate can be expected
near the leading edge and this, unfortunately, will in-
fluence the boundary layer thickness distribution at all
streamwise locations downstream.

4. The locally high pressure region immediately downstream from
the leading-edge shock should have some influence on the
initial growth rate of the boundary layer.

Use of the above factors resulted in a wedge type of boundary layer
growth near the plate leading edge similar to that proposed by Oguchi
[43] for hypersonic flow. This type of boundary layer behavior near
the leading edge is also indicated in the shadowgraphs in Reference 5.
This rapid rate of initial boundary layer growth ($\delta \propto x$) must produce a
thick boundary layer far downstream from the plate leading edge. The
calculated boundary layer thickness at x = 0.490 inch is two times the
thickness predicted by use of the method of Van Driest [44]. However,
a comparison of the growth rate downstream from x = 0.090 inch (the
downstream limit of the wedge type of boundary layer) indicates that
the rate of the boundary layer growth is approximately the same as
that predicted by use of the Van Driest method [44].

As shown in Figures 12 through 15, the surface temperature ratio
has stabilized to a value of 2.90. Therefore, the wall temperature is

greater than the adiabatic wall temperature. In this investigation, the recovery factor is found to be 1.055 rather than the usual square root of the Prandtl number assumed in adiabatic laminar flat plate flow. A marked similarity does exist between the temperature profile and velocity profile at each x location, i.e., the thermal boundary layer and the viscous boundary layer are coincident.

In order to test the conservation of mass, the mass flux was integrated from the plate surface to the upper boundary at the position x = 0.490 inch. The results of this calculation are shown in Figure 17 and the error observed in the mass flux was found to be 0.08 percent.

The loss in total pressure will normally be large in the viscous boundary layer. Calculations based on local fluid properties at the station x = 0.490 inch indicate a minimum total pressure recovery ratio of 0.0357 at the plate surface (Figure 18). From the figure, the total pressure recovery is observed to take place in a normal manner. In the inviscid region between the edge of the boundary layer and the weakened shock wave, the total pressure is changing slightly as a result of the smearing process used in the numerical solution. The incident angle of the shock at this location is estimated to be 24 degrees. Inviscid theory and thin-shock approximations can be used to predict a total pressure ratio across the shock as being 0.995. If the calculated total pressure ratios in the inviscid flow region are averaged, a value of 0.9458 is obtained. If this value is compared with the inviscid total pressure recovery, then the method of calculations is in error by approximately 5 percent. The error can most probably be attributed to the smearing of the shock in this region.

Results Obtained in the Case 2 Study

The basic lattice used in this portion of the investigation is that shown in Figure 4. The free-stream properties were the same as those used in Case 1. A strong external incident shock wave was introduced on the upper boundary ($\ell = 40$) at $x = 0.010$ inch ($m = 11$). The shock strength was equivalent to the turning of the inviscid freestream ($M_o = 3.0$) through a 25-degree turning angle. The static pressure ratio across the incident shock was 4.925. The nondimensionalized fluid properties downstream of the incident shock were

$p = 4.925$

$\rho = 2.795$

$u = 2.4347$

$v = 1.1354$

The incident shock wave was assumed to be formed within one mesh width (Δx) on the upper surface between $m = 10$ and $m = 11$. The fluid properties upstream of $m = 11$ on the upper boundary were those of the freestream while those properties from the nodal points (11, 40) to (27, 40) were those given above. Points (28, 40) to (48, 40) were extrapolated from below to permit reflected influences to penetrate the upper boundary.

The calculated pressure field is shown in Figure 19 as a series of constant pressure ratio lines. Figure 19 contains several interesting features which should be discussed and analyzed in some detail. These include

1. The leading-edge shock wave

2. The incident shock wave

3. The incident shock as it transforms into a bifurcated shock
   with the two branches extending into the viscous layer

4. A local high-pressure region immediately downstream from the
   bifurcated shock

5. Expansion waves in the flow field downstream from the shock-
   impingement point

6. The formation of a compression shock downstream from the
   shock-impingement point.

In Chapter II it was mentioned that the interaction phenomenon is
only a local phenomenon and has no influence on the fluid flow upstream
of the interaction region. A comparison of Figures 19 and 7 revealed
that the leading-edge shock waves are identical. All fluid properties
near the leading edge are identical, and a check of the nondimensional
velocity at m = 15 (x = 0.09 inch) indicates that the profiles are
identical.

On the basis of inviscid theory, the calculated angle of the in-
cident shock wave was found to be 44.15 degrees. Measurements based
on the finite-difference method of analysis indicate that the incident
shock angle is 43.5 degrees. The data in Figure 19 also show fair
resolution of the incident shock in the inviscid flow region. These
data also provide a good representation of the shock-shock interaction
region. In this region, analysis of the constant pressure ratio lines
indicates that the incident shock continues downward toward the plate
surface. However, the shock strength increases (note the closeness of
the isobars), and the shock is approaching a normal position with re-
spect to the plate surface. As the incident shock approaches the normal

position, the constant pressure ratio lines form two distinct legs which clearly indicate that the incident shock has become a bifurcated shock. The front leg extends forward and downward until it approaches the plate surface. Because of the subsonic portion of the flow in the boundary layer, the leg cannot penetrate down to the surface. The constant pressure lines in the subsonic portion then become approximately normal to the plate surface. The rear leg extends downstream and downward a much shorter distance than the forward leg. This difference is attributed to the existence of the flow separation region and its low-velocity recirculatory motion which cannot support the pressure gradients. Thus the pressure lines are approximately normal in this low-velocity region and the rear leg loses its identity.

The existence of the bifurcated shock is not unexpected. Fage and Sargent [45] have reported on this phenomenon. They have defined the branches of the bifurcated shock as continuous compression regions. This definition constitutes an adequate description of the phenomenon defined by using the numerical technique.

As the stem of the bifurcated shock approaches a normal position, a high-pressure bubble is formed immediately downstream of the stem. This is a local region, and the pressure of such a region can only be assessed in a speculative fashion since the flow pattern is quite complicated. However, the data in Figure 19 clearly indicate a curvature of the shock stem. The strength of the shock is changing, and at one point, the shock strength approaches that of a normal shock. This local effect produces the high-pressure bubble, but there is a following gradual collapse because of the expansion waves existing on the under side of the high-pressure bubble.

The maximum calculated pressure ratio in the bubble was 12.7. In terms of inviscid flow theory and normal shock relations, a pressure ratio of 10.33 would be predicted on the basis of the free-stream Mach number of 3.0. Results of this comparison indicate that the calculated pressure ratio is apparently high by 22.9 percent. However, a leading-edge shock has to exist upstream so that the pressure ahead of the stem is not that of the free stream. The pressure ratio has to be larger than the free-stream pressure ratio of unity and the local Mach number smaller than that of the free-stream Mach number. To demonstrate the need for this requirement, properties were selected at a point immediately upstream of the stem. At this point, the pressure ratio was 2.031, and the local Mach number was 2.39. From the normal shock relations, the static pressure ratio across the shock was found to be 6.497. Thus the maximum pressure ratio in the bubble would be 2.031 x 6.497 = 13.2. On the basis of this reasoning, the calculated pressure ratio is low by 3.8 percent.

The constant pressure ratio lines also indicate the presence of a compression shock downstream of the shock-impingement point. This shock is produced by the compression waves first formed in the boundary layer. Within the boundary layer, these waves are almost normal (Figure 19) and then bend quite rapidly and become close together; this latter action is an indication of an increasing pressure gradient. At the end of the field of calculation, the compression shock has almost coalesced with the weakened leading-edge shock to form a single shock wave.

The computed results shown in Figure 19 are beneficial in determining a flow model which describes the shock phenomena associated with this investigation. The model is shown in Figure 20. Unlike the flow model shown in Figure 2, the boundary layer is not shown since it is difficult to estimate, with any degree of confidence, the exact location of the outer edge. Instead, tangential velocity profiles in the separation flow region are shown in Figure 21.

It is also of interest to observe the fluid particle flow directions in the separated flow region. The velocity vectors are plotted for a portion of the field which includes the separated flow region. This plot is shown in Figure 22. The recirculatory region is clearly observed and is seen to contain very low velocity fluid. The separation point is at $m = 20$ ($x = 0.190$) and the reattachment point is at $m = 34$ ($x = 0.470$). The velocity vectors indicate a large amount of mass entrainment above the separated region (note the rapid turning of the velocity vectors in the upper left-hand corner). Farther downstream, the velocity vectors indicate that the flow has smoothed out and reattachment has occurred. At this point, the velocity vectors indicate that a small amount of mass flux is still being fed into the boundary layer; thus the downstream boundary layer is still being compressed and has not attained its ultimate form.

The static pressure ratio distribution along the row $y = 0.005$ inch is shown in Figure 23. The initial increase in the pressure ratio near the leading edge is followed by a decrease identical to that shown in Figure 8. However, the influence of the adverse pressure gradient is felt at $x = 0.11$ inch from the leading edge; consequently, the

pressure ratio reaches a minimum and then begins to rise once more. A plateau pressure is approached downstream of separation and is followed by another rapid increase in pressure in the reattachment region. The pressure ratio is seen to level out only at the far downstream boundary at a value of 13.16. This pressure is close to that obtained in the local high-pressure region discussed previously.

The incident shock strength is such that a Mach reflection must occur. This reflection eliminates the possibility of comparing the downstream surface static pressure with the inviscid case of an incident and reflection shock. If the free-stream flow is allowed to pass through a normal shock, then, on the basis of inviscid flow theory, the downstream pressure ratio will be 10.33. Such a comparison would indicate a 22.9 percent difference. However, the flow field at the extreme right boundary has not completely reached steady equilibrium. It is expected that, if the field of calculation had been extended, a peak maximum pressure ratio would have been reached and a subsequent reduction in pressure would follow the peak. This phenomenon is normally observed in testing which involves regions far removed from the stagnation region.

The density distribution is shown in Figure 24 in the form of constant-density ratio lines. The trends are observed to parallel the constant-pressure ratio lines in Figure 18, except in the region near the plate surface. In the separated flow region, the density ratio and the pressure ratio are seen to vary in a similar fashion. This similarity is to be expected since the separated region contains low-energy air at an almost constant temperature. Upstream of separation and

downstream of reattachment, the density ratio tends to flatten out and appear parallel to the wall. Results of interferometric studies involving weak shocks [42] show the identical behavior when flow separation is not present.

The results demonstrate the ultimate potential of the finite-difference technique used in this investigation. Convergence of the governing equations to the proper solution requires a larger number of nodal points than used in this investigation. However, the new generation digital computer with its increased storage capacity will alleviate such a problem.

It is hoped that the results presented in this section will lead to a re-examination of past assumptions related to the efficiency and accuracy of thin boundary layer theory in applications near the plate leading edge.

CHAPTER VI

CONCLUSIONS AND RECOMMENDATIONS

Conclusions

The primary objective of this investigation was to develop a method whereby the shock-laminar boundary layer interaction phenomenon could be described by using one set of general finite difference equations. The laminar viscous effects were well represented, even though "artificial viscosity" terms, required for numerical stability, were present. The analysis included three interaction phenomena: the leading-edge shock with the boundary layer; the leading-edge shock with the incident shock; and the incident shock with the laminar boundary layer. The precise accuracy of the method of analysis cannot be determined because test data are not available in the region of interest. However, the numerical results appear reasonable, and they represent an acceptable prediction of the behavior of the fluid flow and shock forms as they are normally observed in regions other than that near the leading edge.

A principal difficulty which was overcome was the treatment of the leading edge problem. The stagnation region has long been a difficult region to analyze, particularly when the method of finite differences is used. The selection of a slip-flow schedule near the leading edge and the location of the first row of nodal points ($\frac{\Delta y}{2}$ above the plate

surface) completely eliminated the stagnation point and the related problems in this region.

Results of the numerical computations indicate an interaction phenomenon between the leading-edge shock and the viscous layer. This phenomenon is normally associated with hypersonic flow. Indications are that the interaction does not occur at the leading edge but rather a short distance downstream. On the basis of hypersonic theory, this shift downstream indicates a weak interaction phenomenon. Another important conclusion is that the method can be used to predict the behavior of the strong incident shock as it intersects the leading-edge shock and proceeds down toward the plate surface. As the incident shock penetrates the boundary layer, it approaches a normal position and then branches to form two distinct shock legs. The appearance of the shock is identical to that of the bifurcated shock often observed in experimental testing. The author knows of no other analytical method which can be used to predict such behavior.

Flow separation and reattachment were also observed in the numerical computations. The fluid circulation is clearly observed since this method of analysis can be used to predict all the fluid properties, including the velocity components. A local high-pressure region occurred behind the stem of the bifurcated shock. Such a region can be expected since the incident shock approaches a normal position locally.

The computations were also valuable in describing the shock phenomenon by means of a flow model for a strong shock. The resulting flow model agrees quite well with the often-used models for weak incident shock-boundary layer interaction with flow separation and reattachment.

Recommendations

The results of this investigation indicate that the method holds great promise for analyzing many complicated viscid-inviscid flow field problems. On the basis of the findings in this investigation, the following recommendations are made:

1. An extensive investigation should be initiated in order to obtain quantitative experimental data near the leading edge of a sharp flat plate. The physical dimensions are such that only analytical methods are available for describing the flow field at the present time. The validity of the thin shock, thin boundary layer approximation are questionable at high supersonic and moderate density conditions where the hypersonic approximations are invalid.

2. The use of the artificial viscosity enhances numerical stability and allows calculations through shock waves. It also influences the convergence to a final solution which may or may not represent the physical phenomenon. A thorough study should be initiated in an effort to determine more concretely the required relationship between the mesh size spacing, the artificial viscosity, and the physical viscosity required for assurance of the proper convergence.

3. The results of this analysis indicate the great potential of the method. It is therefore recommended that the method be applied to problems of a similar nature where experimental data are available. The method should also be extended to other flow configurations, such as wedges, plate-wedge combinations, and axisymmetric bodies.

BIBLIOGRAPHY

1. Lees, L., and Reeves, B. L., "Supersonic Separated and Reattaching Laminar Flow," GALCIT 574, Part 1, 1963.

2. Crocco, L., "A Suggestion for the Numerical Solution of the Steady Navier-Stokes Equations," AIAA, Vol. 3, No. 10, 1963, p. 1824.

3. Hayes, W. D., and Probstein, R. F., Hypersonic Flow Theory, Adademic Press, New York, 1959.

4. Lees, L., "Interaction Between the Laminar Boundary Layer Over a Plate Surface and an Incident Oblique Shock Wave," Princeton University, Aeronautical Engineering Laboratory Report No. 143, 1949.

5. Chapman, D. R., Kuehn, D. M., and Larson, H. K., "Investigation of Separated Flows in Supersonic and Subsonic Streams With Emphasis on the Effects of Transition," NACA Report 1356, 1958.

6. Glick, H. S., "Modified Crocco-Lees Mixing Theory for Supersonic Separated and Reattaching Flows," J. Aero. Sci., Vol. 29, 1962, p. 1238.

7. Mitwally, E. M., "Shock Wave-Boundary Layer Interaction With Tangential Injection," Ph.D. Dissertation, Oklahoma State University, August, 1965.

8. Schlichting, H., Boundary Layer Theory, McGraw-Hill Book Company, Inc., New York, Fourth Edition, 1960.

9. Meksyn, D., New Methods in Laminar Boundary-Layer Theory, Pergamon Press, New York, 1961.

10. Tyler, L. D., "Numerical Solutions of the Flow Field Produced by a Plane Shock Wave Emerging into a Crossflow," Ph.D. Dissertation, Oklahoma State University, May, 1965; Published as Eng. Res. Rpt. SBW-10 by Tyler, L. D., and Zumwalt, G. W., 1965.

11. Walker, W. F., "A Numerical Solution for the Interaction of a Moving Shock Wave With a Turbulent Mixing Region," Ph.D. Dissertation, Oklahoma State University, May, 1966.

12. Walker, W. F., and Tyler, L. D., "Literature Survey on Shock Wave Interactions with Shocks and Bodies," Oklahoma State University Report SBW-7, 1965.

13. Flügge-Lotz, I., and Baxter, D. C., "The Solution of Compressible Laminar Boundary Layer Problems by a Finite Difference Method, Part I: Description of the Method," Technical Report No. 103, Division of Eng. Mech., Stanford University, 1956.

14. Flügge-Lotz, I., "A Difference Method for the Computation of the Laminar Compressible Boundary Layer," 50 Jahre Grenzschicht-forschung, Fr. Vieweg und Sohn, Braunschweig, 1955, p. 393.

15. Baxter, D. C., and Flügge-Lotz, I., "The Solution of Compressible Laminar Boundary Layer Problems by a Finite Difference Method, Part II: Further Discussion of the Method and Computation of Examples," Technical Report No. 110, Division of Eng. Mech., Stanford University, 1957.

16. Flügge-Lotz, I., and Howe, J. T., "The Solution of Compressible Laminar Boundary Layer Problems by a Finite Difference Method, Part 3: The Influence of Suction or Blowing at the Wall," Technical Report No. 111, Division of Eng. Mech., Stanford University, 1957.

17. Flügge-Lotz, I., and Yu, E., "Development of a Finite-Difference Method for Computing a Compressible Laminar Boundary Layer with Interaction," Technical Report No. 127, Division of Eng. Mech., Stanford University, 1960.

18. Kramer, R. F., and Lieberstein, H. M., "Numerical Solution of the Boundary-Layer Equations Without Similarity Assumptions," J. Aero. Sci., Vol. 26, 1959, p. 508.

19. Flügge-Lotz, I., and Blottner, F. G., "Computation of the Compressible Laminar Boundary Layer Flow Including Displacement-Thickness Interaction Using Finite-Difference Methods," Technical Report No. 131, Division of Eng. Mech., Stanford University, 1962.

20. Crank, J., and Nicolson, P., "A Practical Method for Numerical Evaluation of Solutions of Partial Differential Equations of the Heat Conduction Type," Proc. Camb. Phil. Soc., Vol. 43, 1947, p. 50.

21. Low, G. M., "The Compressible Laminar Boundary Layer with Heat Transfer and Small Pressure Gradient," NACA TN 3028, 1953.

22. Li, T-Y, and Nagamatsu, H. T., "Similar Solutions of Compressible Boundary-Layer Equations," J. Aero. Sci., Vol. 22, 1955, p. 607.

23. Wu, J. C., "The Solution of Laminar Boundary-Layer Equations by the Finite-Difference Method," Douglas Aircraft Company, Inc., Report No. SM-37484, 1960.

24. Fannelöp, T., and Flügge-Lotz, I., "The Laminar Compressible Boundary Layer Along a Wave-Shaped Wall," Ing.-Arch. 33, 1963, p. 24-35.

25. Clutter, D. W., and Smith, A. M. O., "Solution of the General Boundary-Layer Equations for Compressible Laminar Flow, Including Transverse Curvature," Douglas Aircraft Co., Report No. LB31088, 15 Feb., 1963.

26. Smith, A. M. O., and Clutter, D. W., "Machine Calculations of Compressible Laminar Boundary Layers," AIAA, Vol. 3, No. 4, 1965, p. 639.

27. Smith, A. M. O., and Jaffe, N. A., "General Method for Solving the Nonequilibrium Boundary-Layer Equations of a Dissociating Gas," AIAA Paper No. 65-129, 1965.

28. Thommen, H. U., "A Method for the Numerical Solution of the Complete Navier-Stokes Equations for Steady Flows," General Dynamics/Convair GDC-ERR-AN733, April, 1965.

29. Kurzrock, J. W., and Mates, R. E., "Exact Numerical Solutions of the Time-Dependent Compressible Navier-Stokes Equations," AIAA Paper No. 66-30, 1966.

30. Cole, J. K., Private Communication.

31. Rusanov, V. V., "The Calculation of the Interaction of Non-Stationary Shock Waves and Obstacles," National Research Council of Canada Library, Ottawa, Canada, Tech. Translation 1027 by D. A. Sinclair, 1962. Translated from: Zhurnal Vychislitelnoi Fiziki, Akademiya Nauk, SSSR 1, Vol. 1, No. 2, 1961, pp. 267-279.

32. Filler, L., and Ludloff, H. F., "Stability Analysis and Integration of the Viscous Equations of Motion," Mathematics of Computation, Vol. 15, 1961, p. 261.

33. Lax, P. D., "Weak Solutions of Nonlinear Hyperbolic Equations and Their Numerical Computation," Comm. Pure and Appl. Math., Vol. 7, No. 1, 1954, p. 159.

34. Gary, J., "On Certain Finite-Difference Schemes for the Equations of Hydrodynamics," AEC Computing and Applied Mathematics Center Report NYO-9188, 1962.

35. Lax, P. D., and Wendroff, B., "Systems of Conservation Laws," Comm. Pure and Appl. Math., Vol. 8, 1960, p. 217.

36. Thommen, H. U., and D'Attores, L., "Calculation of Steady, Three-Dimensional Supersonic Flow-Fields by a Finite-Difference Method," AIAA Paper No. 65-26, 1965.

37. Welch, J. E., Harlow, F. H., Shannon, J. P., and Daly, B. J., "THE MAC METHOD - A Computing Technique for Solving Viscous, Incompressible, Transient Fluid-Flow Problems Involving Free Surfaces," Los Alamos Scientific Laboratory of the University of California Report LA-3425, 1966.

38. von Neumann, J., and Richtmyer, R. D., "A Method for the Numerical Calculation of Hydrodynamic Shocks," J. Appl. Physics, Vol. 21, 1950, p. 232.

39. Eaton, R. R., "A Numerical Solution for the Flow Field of a Super-sonic Cone-Cylinder Entering and Leaving a Blast Sphere Diametrically", to be published as Ph.D. Dissertation, Oklahoma State University.

40. Jackomis, W. N., "Transient Flow Field Analysis of a Plane Blast Wave Intercepting a Stationary Cone at Zero Angle of Attack," Ph.D. Dissertation, Oklahoma State University, May, 1965; Published as Eng. Res. Rpt. SBW-9 by Jackomis, W. N., and Zumwalt, G. W., August, 1965.

41. Burstein, S. Z., "Numerical Methods in Multidimensional Shocked Flows," AIAA, Vol. 2, No. 12, 1964, p. 2111.

42. Shapiro, A. H., The Dynamics and Thermodynamics of Compressible Fluid Flow, Vol. II, The Roland Press Company, New York, 1954.

43. Oguchi, H., "The Sharp Leading Edge Problem in Hypersonic Flow," Rarefied Gas Dynamics (Supplement 1), Academic Press, New York, 1961, p. 501.

44. Van Driest, E. R., "Investigation of Laminar Boundary Layer in Compressible Fluids Using the Crocco Method," NACA TN 2597, 1952.

45. Fage, A., and Sargent, R. F., "Shock Wave and Boundary Layer Phenomena Near a Flat Surface," Proc. Roy. Soc., Ser. A., Vol. 190, 1947, p. 1.

APPENDIX A

PLOTTED COMPUTER RESULTS

The results of the numerical computation required in this study are presented in graphical form in this appendix. All computations were performed on the Oklahoma State University computing center IBM 7040 digital computer. The estimated time required to calculate the new fluid properties at one node (per time plane) was 0.032 seconds. The Case 1 study required 400 time planes (5.7 hours computing time) to approach the steady-state solution. Case 2 required 700 time planes (12 hours of computing time) for the steady-state solution to be reached.
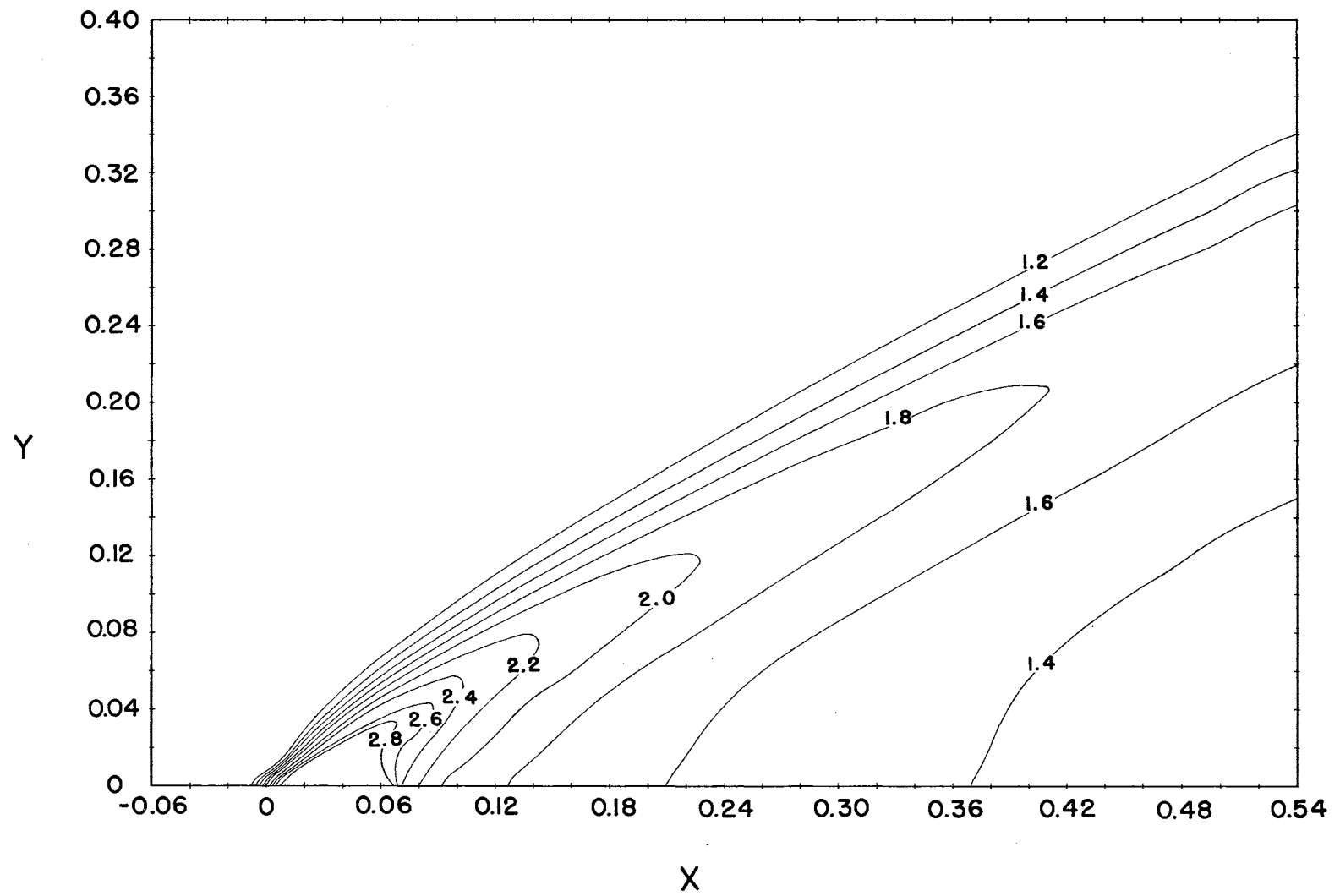
Figure 7. Constant Pressure Lines for Case 1
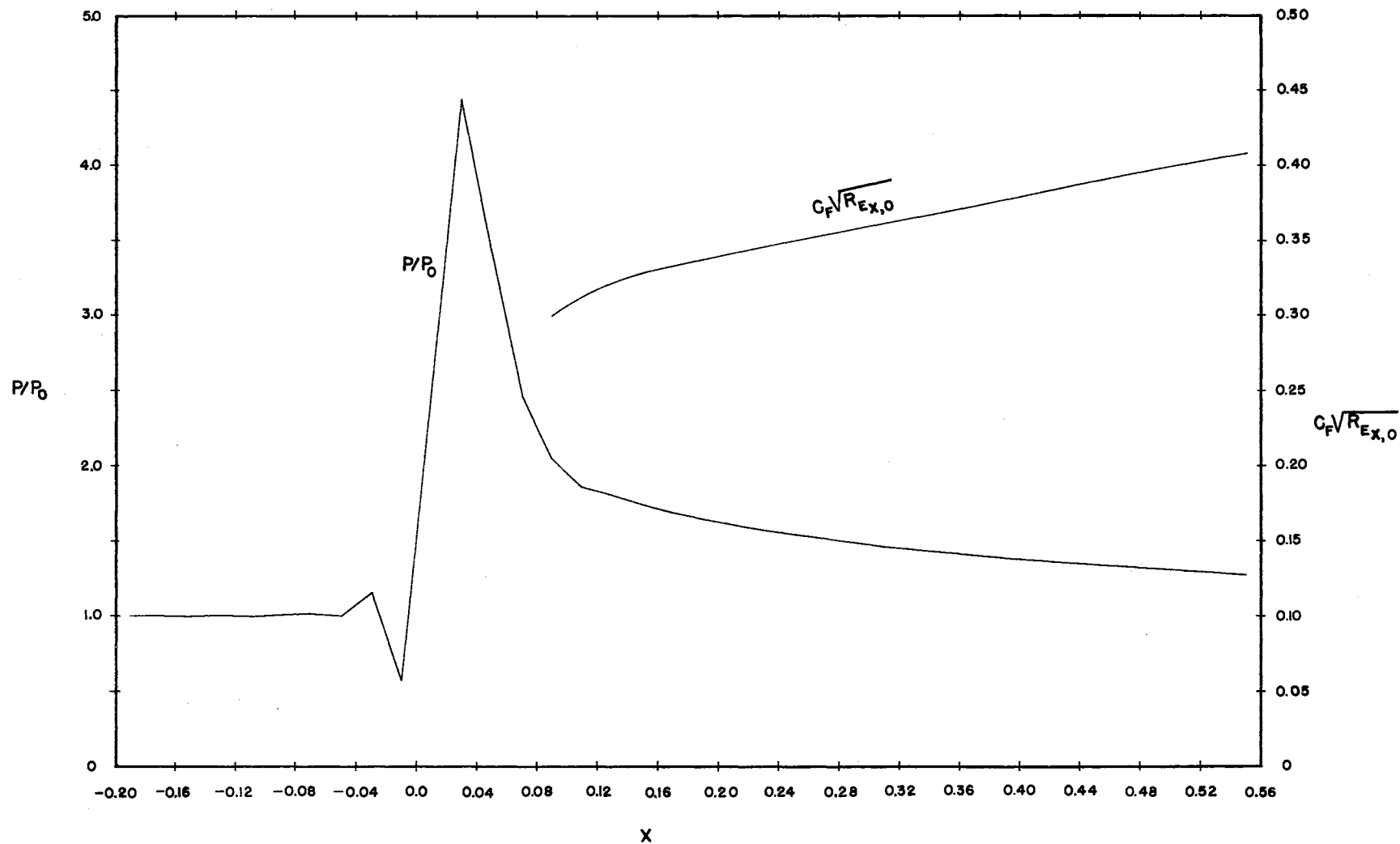
Figure 8. Pressure Distribution Along Row $\ell = 1$ and Plate Skin Friction
Distribution for Case 1
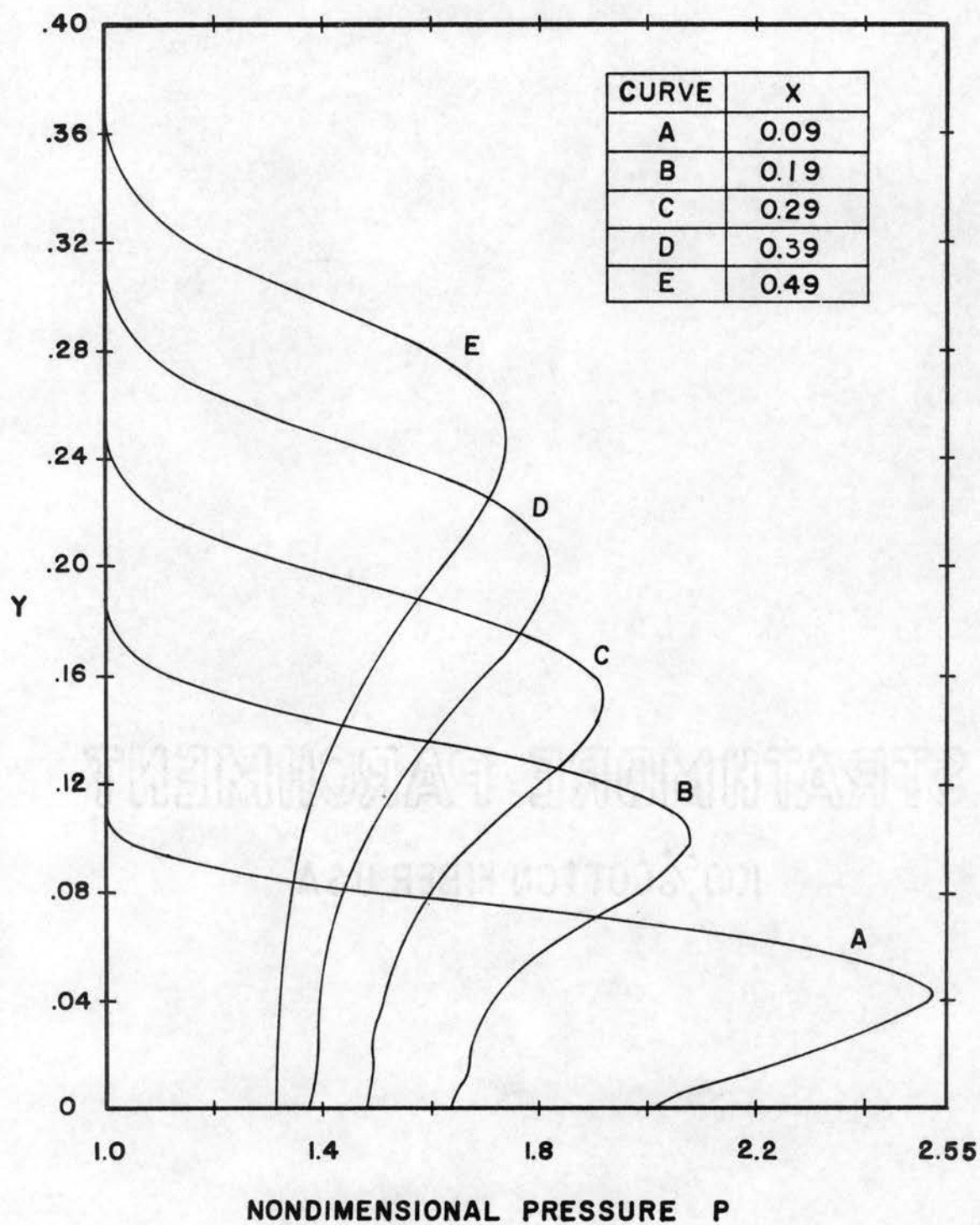
Figure 9. Pressure Profiles at Different Positions X for Case 1
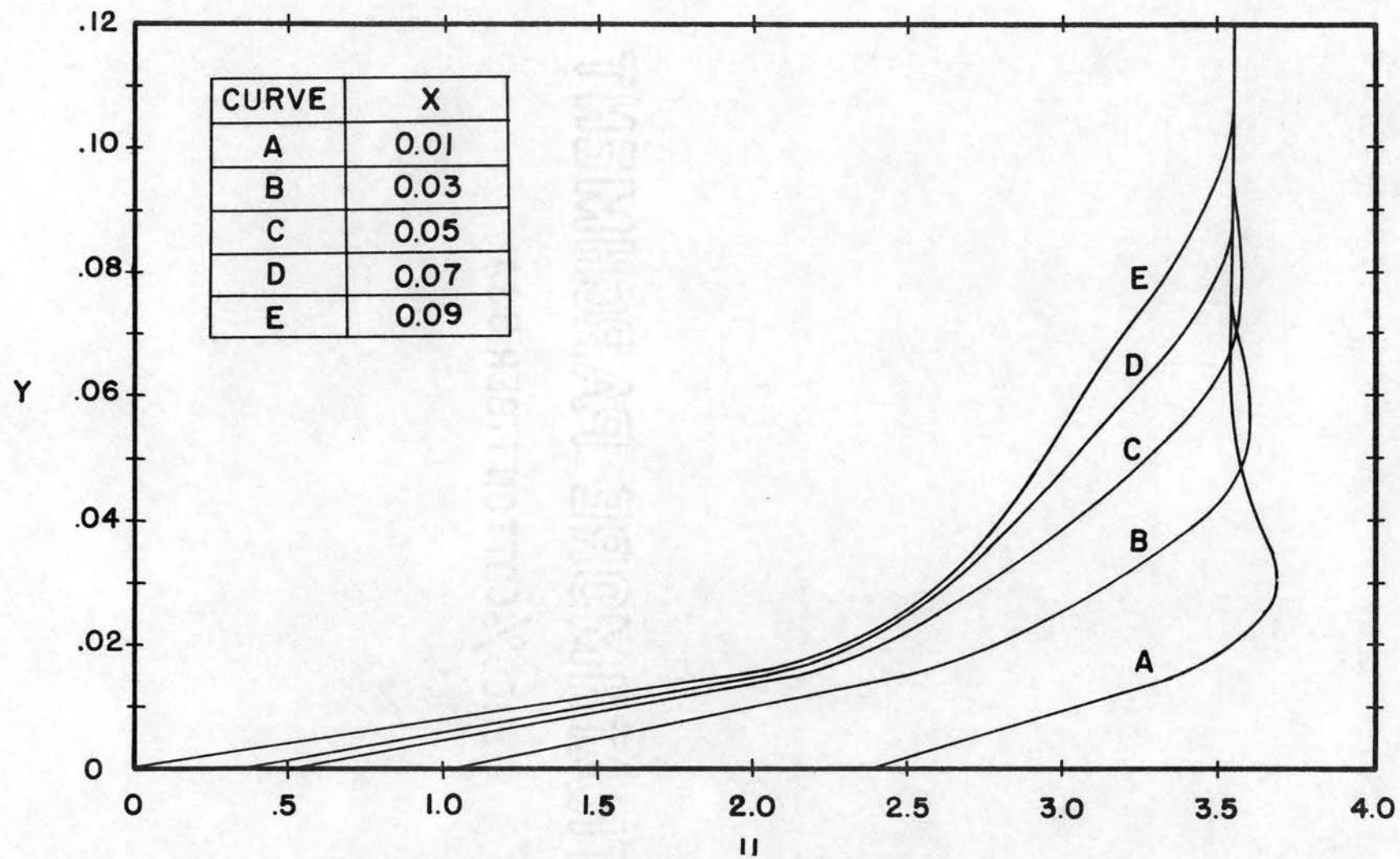
Figure 10. Tangential Velocity Profiles Near Plate Leading Edge for Case 1
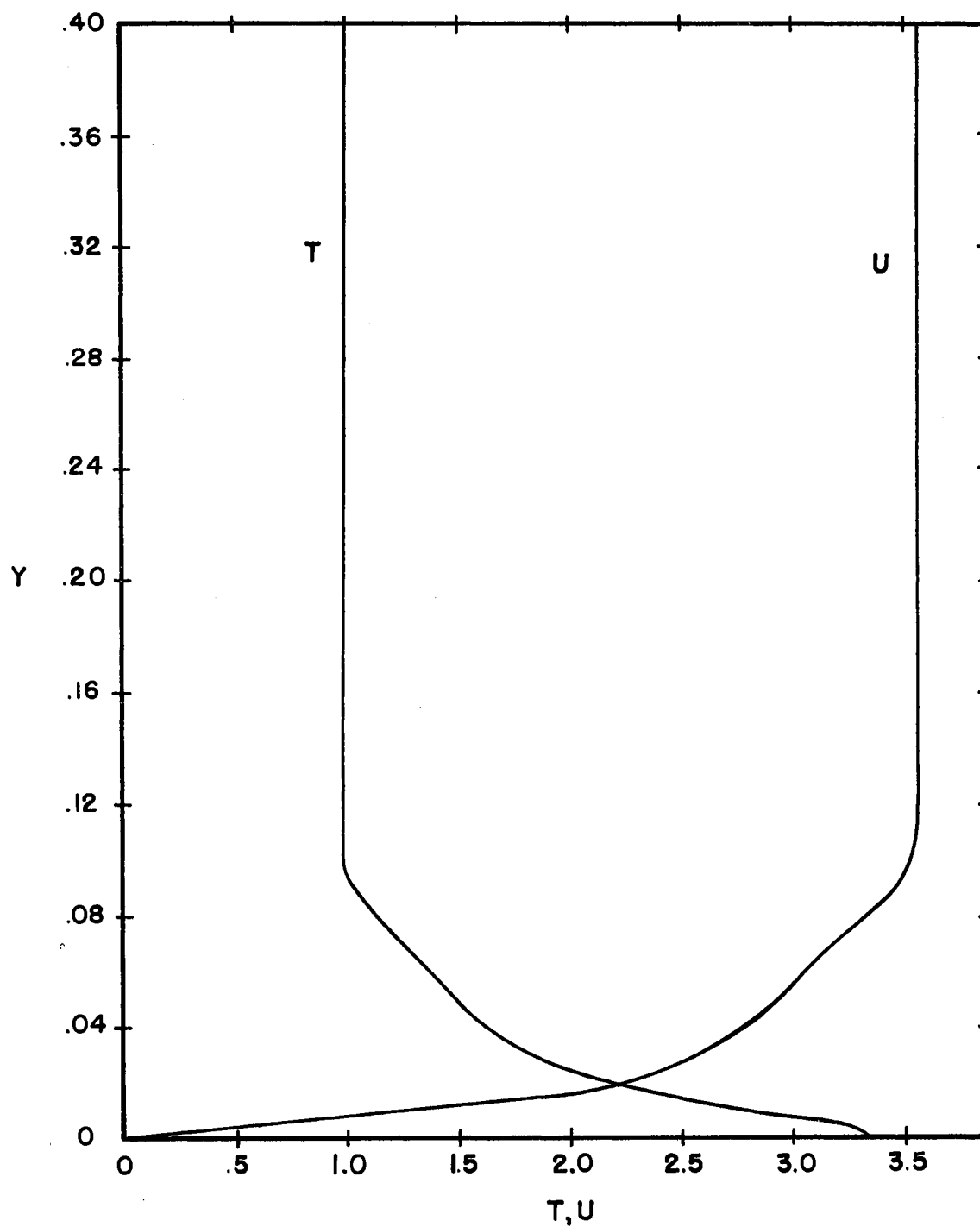
Figure 11. Temperature and Tangential Velocity Profile at X = 0.090
for Case 1
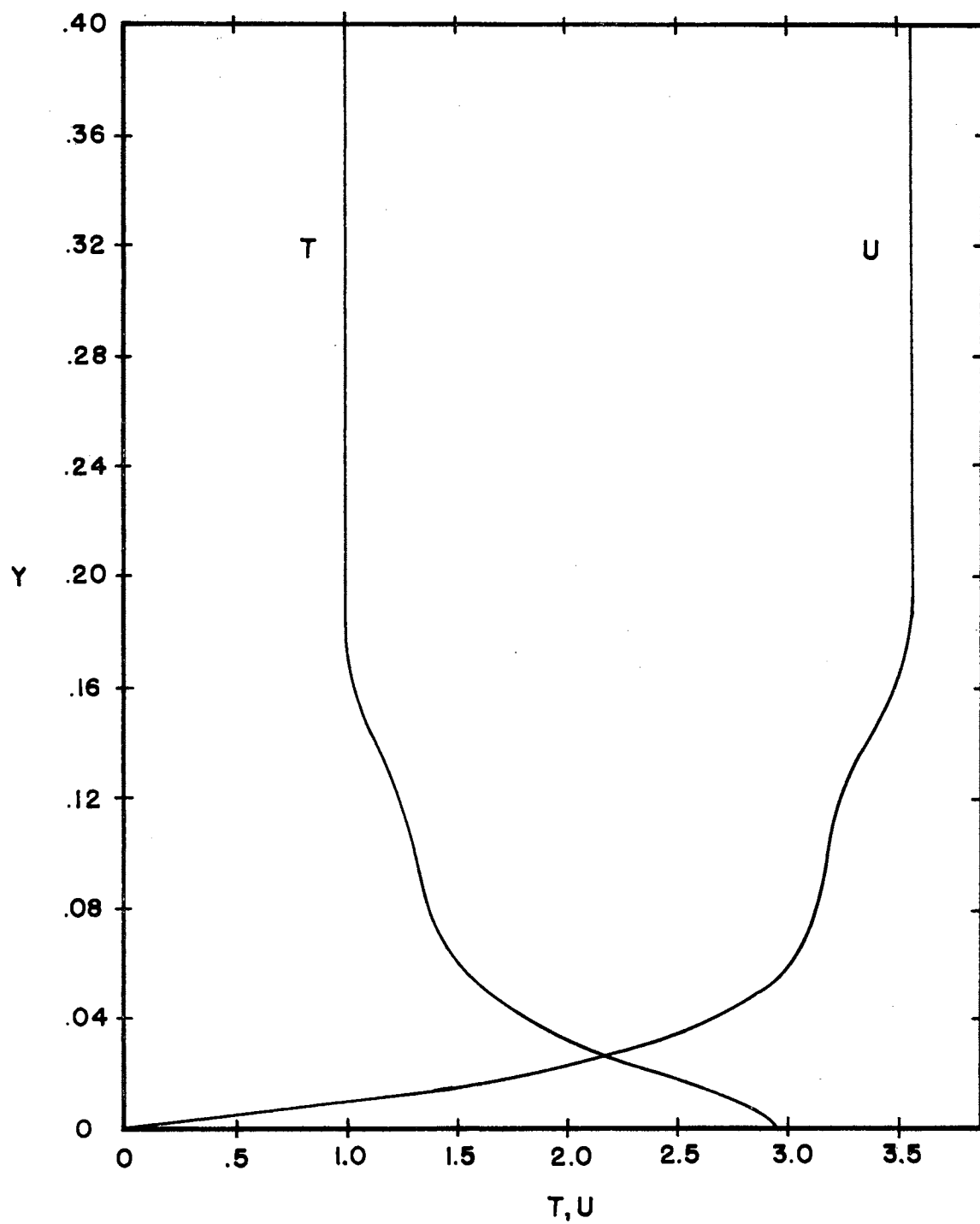
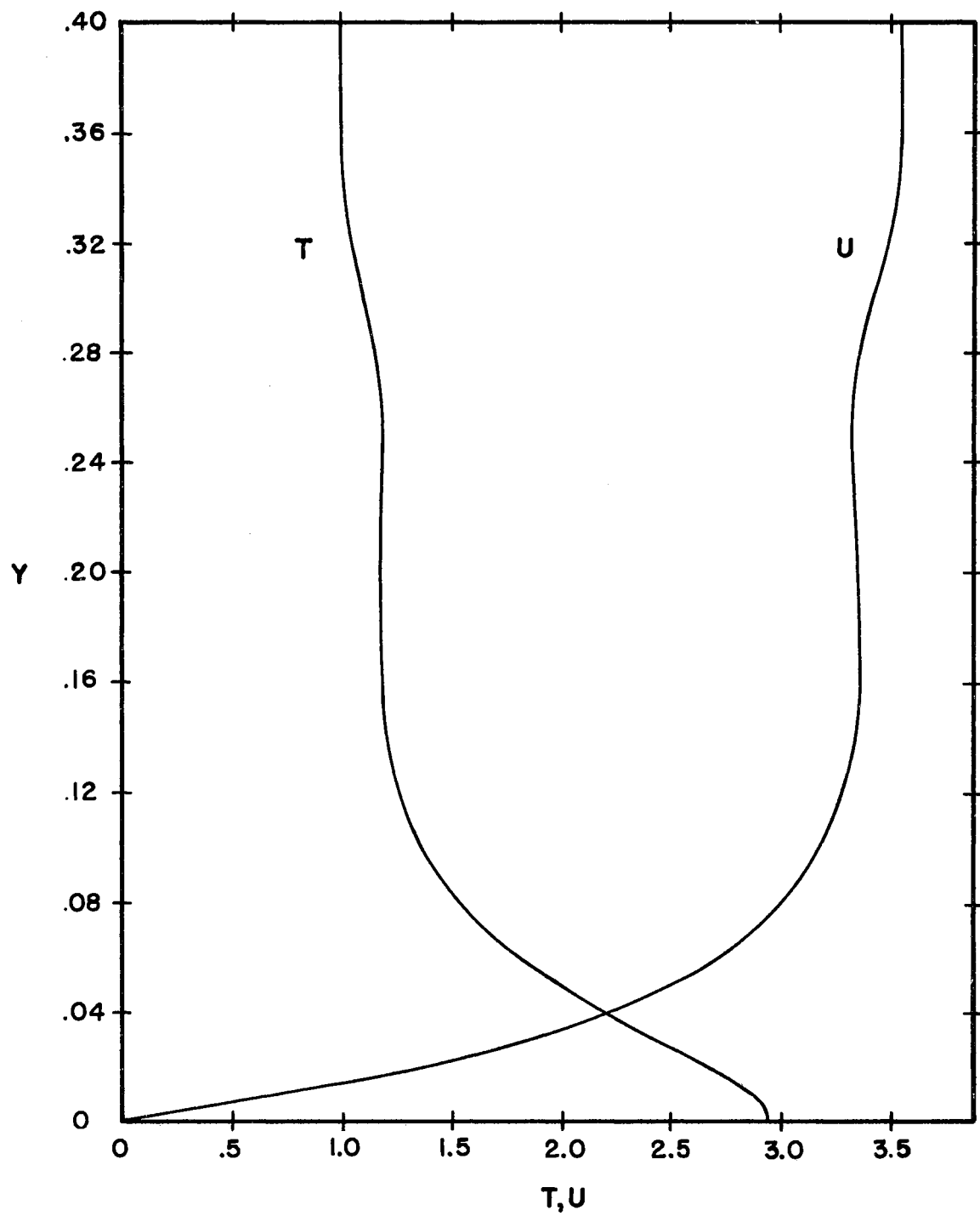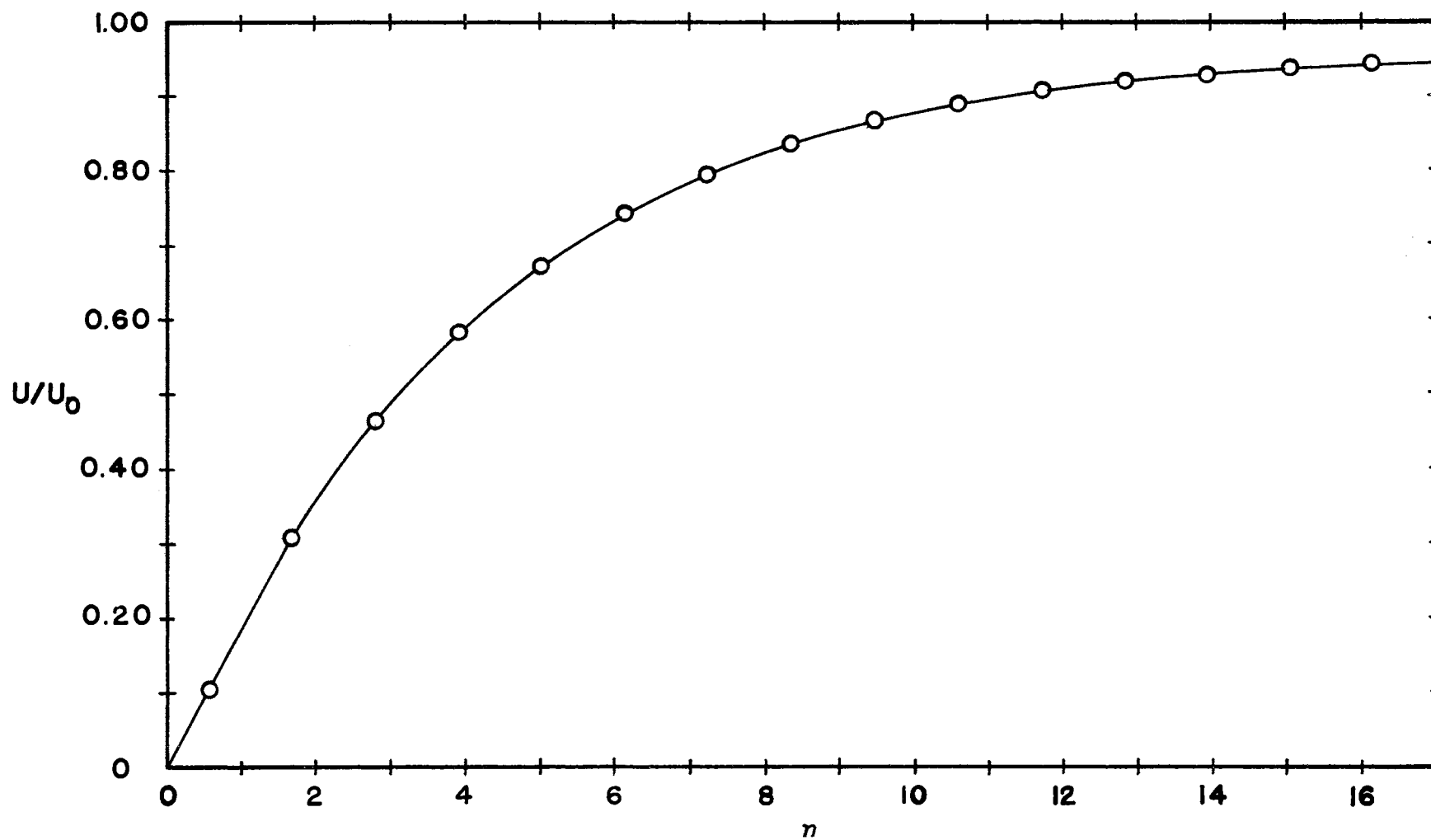Figure 12. Temperature and Tangential Velocity Profile at X = 0.190
for Case 1
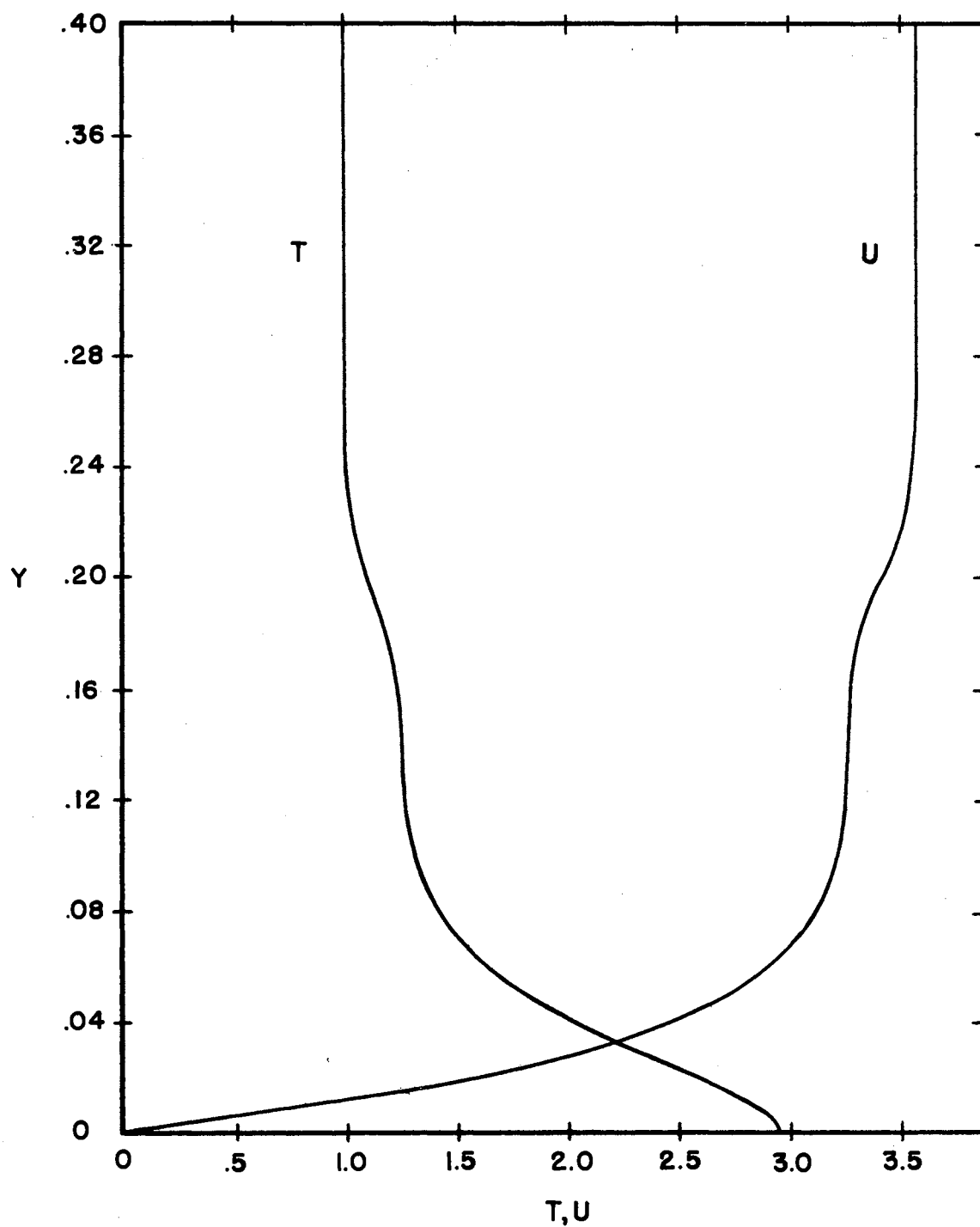
Figure 13. Temperature and Tangential Velocity Profile at X = 0.290
for Case 1
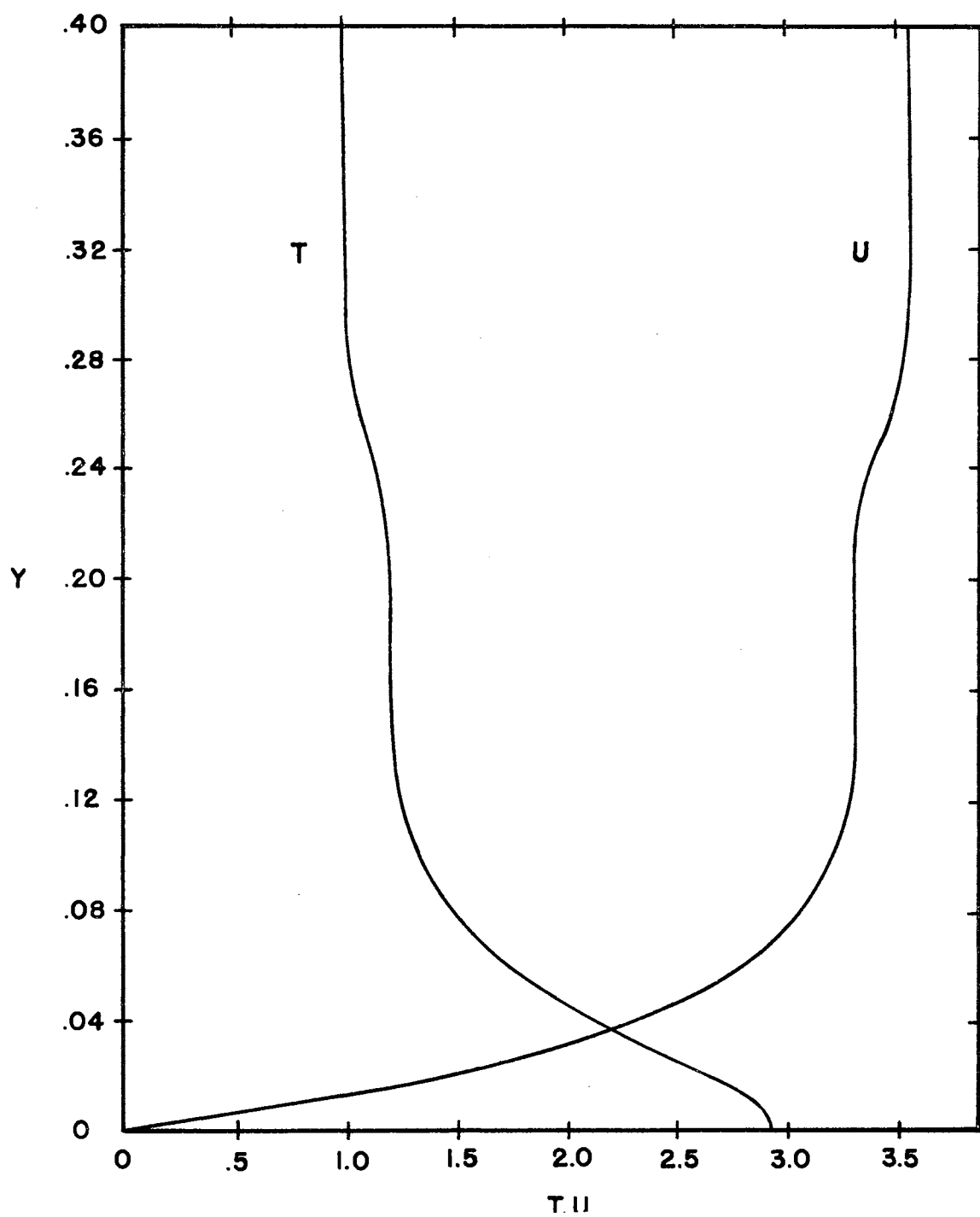
Figure 14.   Temperature and Tangential Velocity Profile at X = 0.390
for Case 1

Figure 15.   Temperature and Tangential Velocity Profile at X = 0.490
for Case 1

Figure 16. Velocity Distribution at X = 0.490 for Case 1
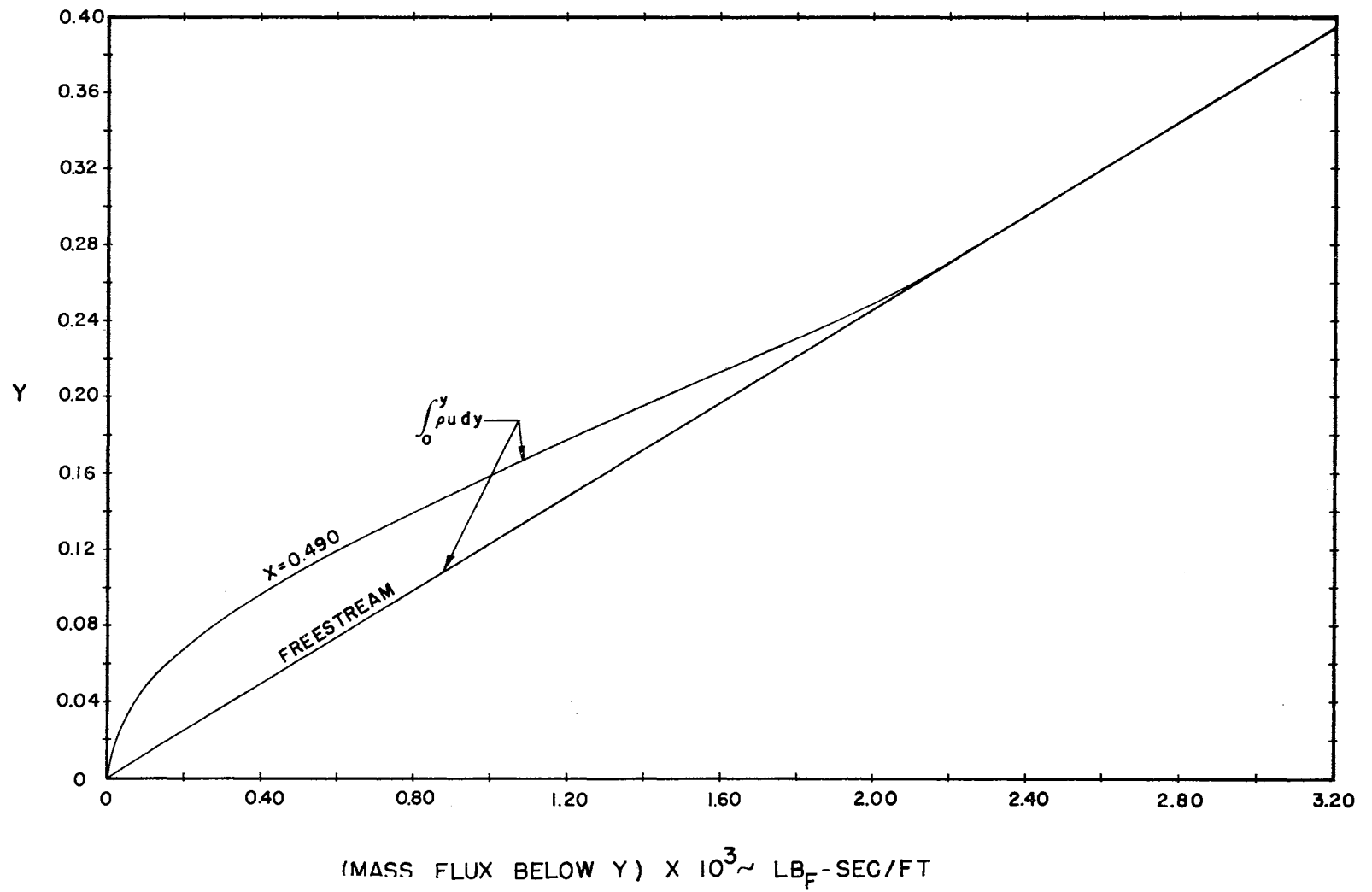
Figure 17. Integrated Mass Flux at X = 0.490 for Case 1
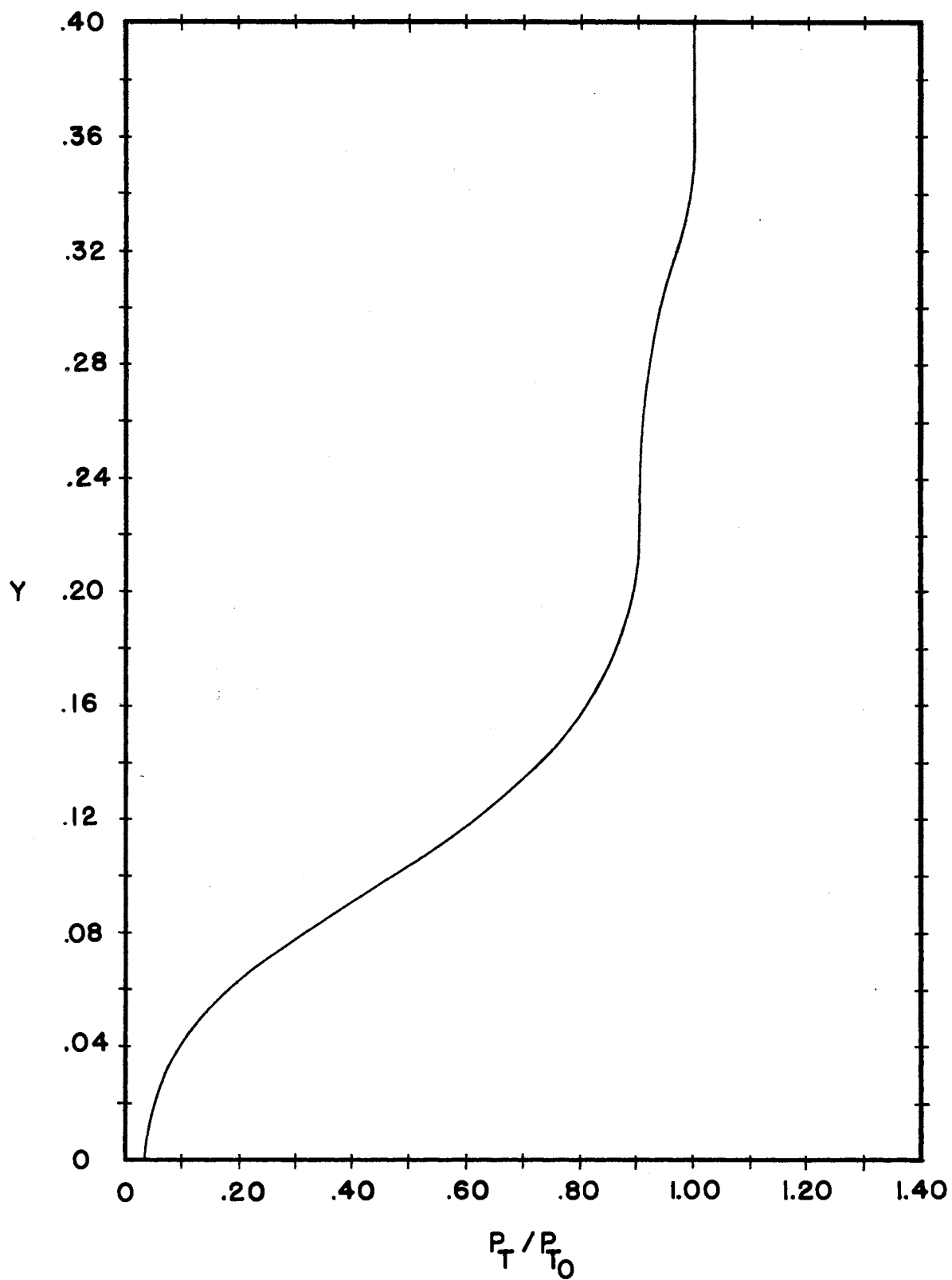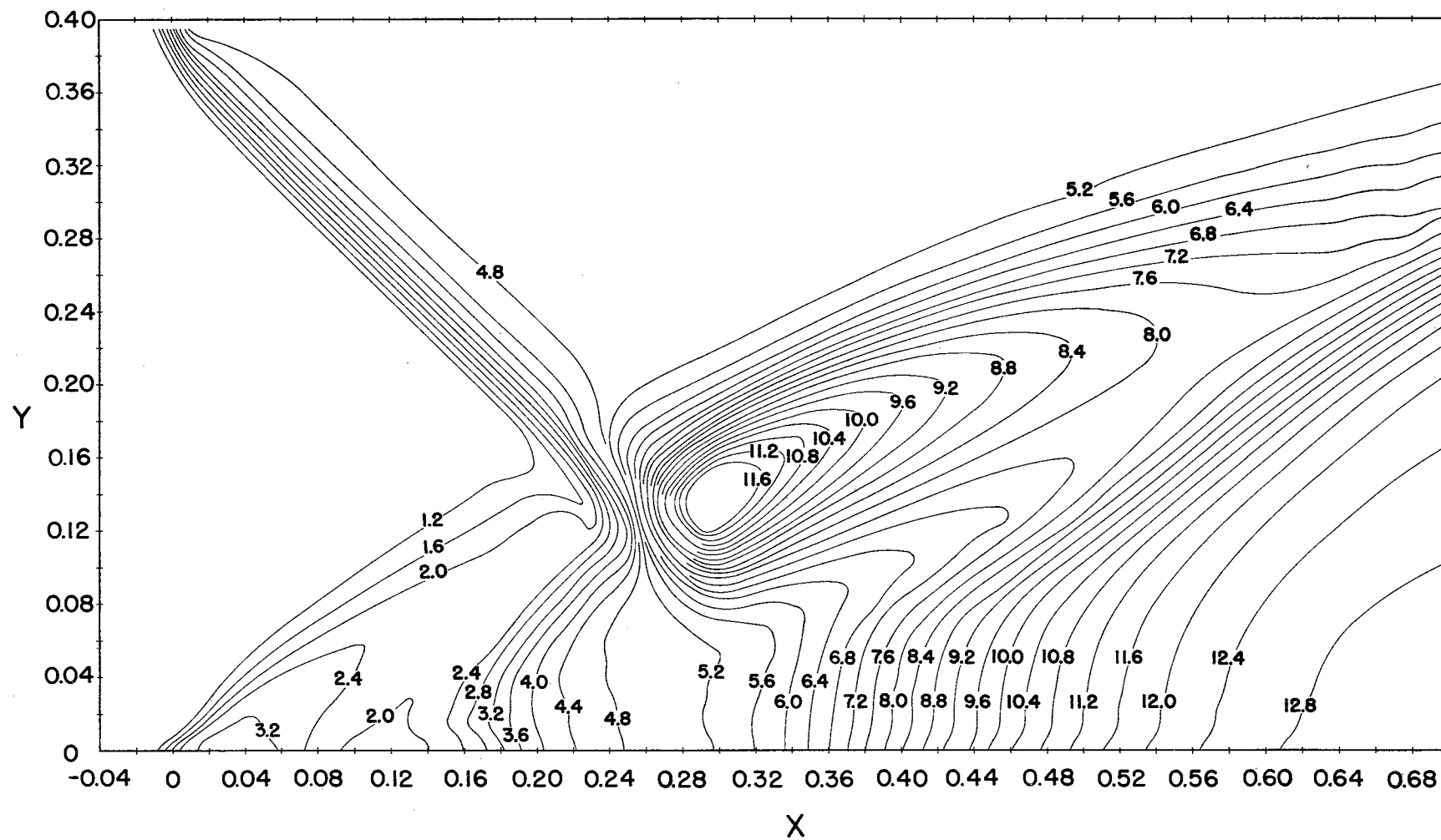
Figure 18. Total Pressure Ratio at X = 0.490 for Case 1

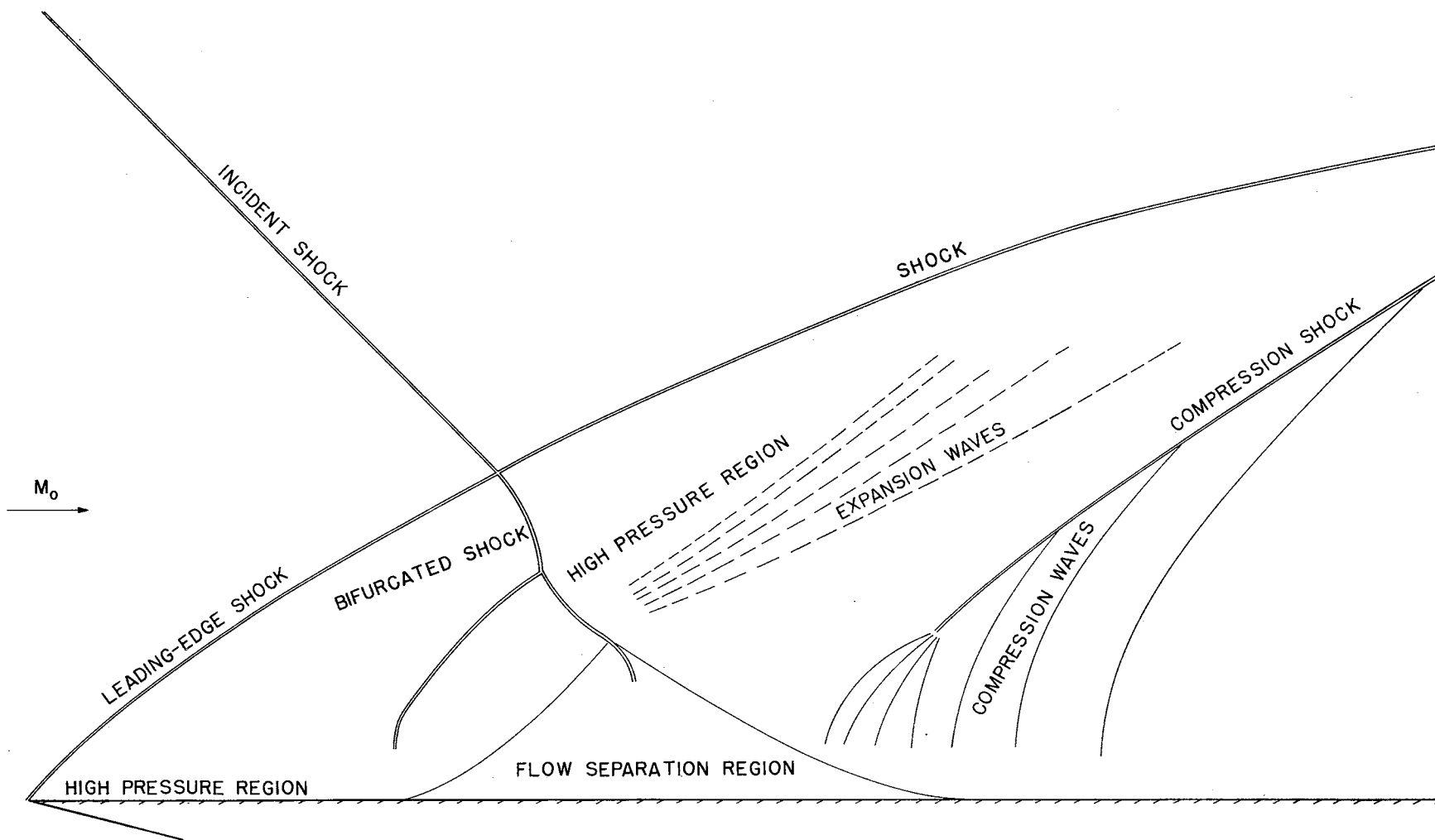Figure 19. Constant Pressure Lines for Case 2

Figure 20. Flow Model for Strong Incident Shock-Laminar Boundary Interaction
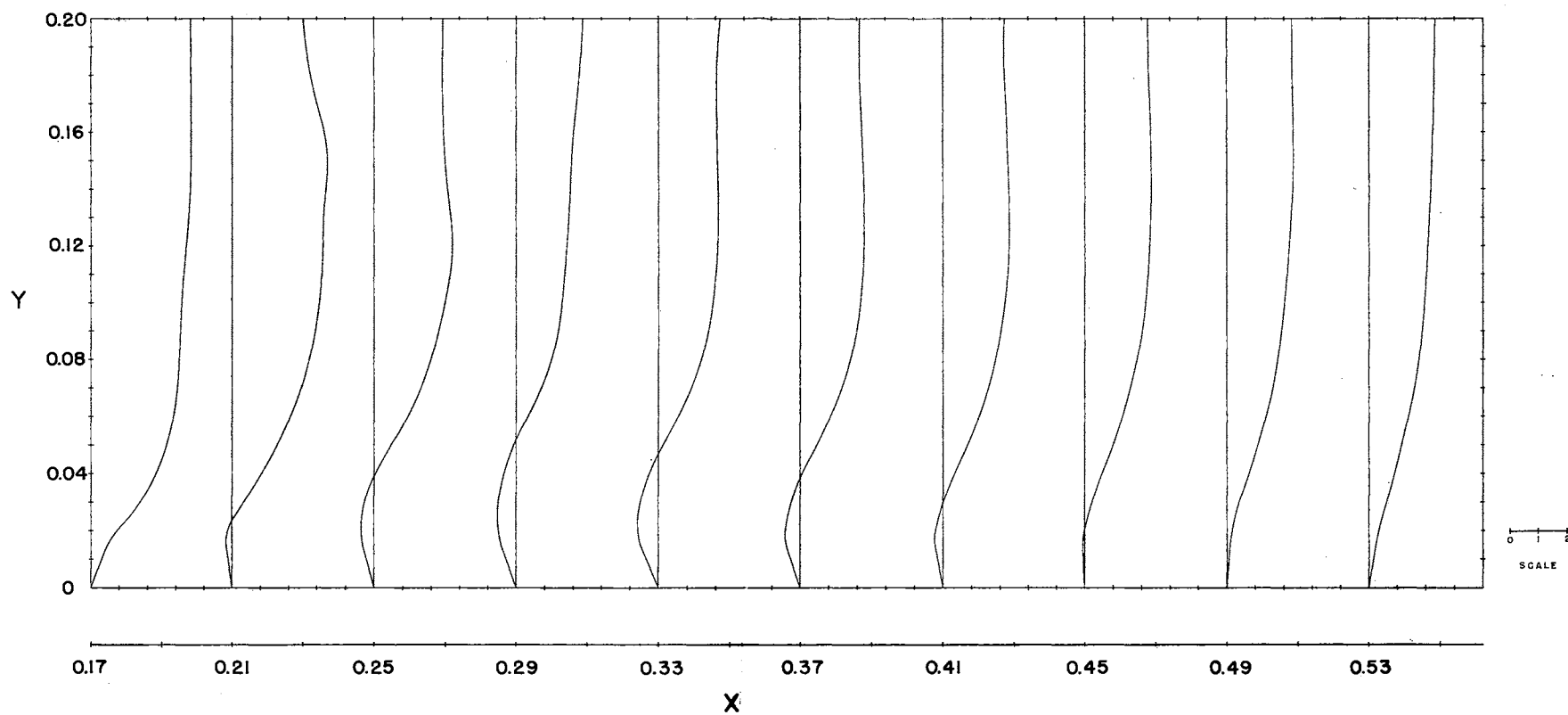Near Leading Edge of Flat Plate

Figure 21. Tangential Velocity Profiles in Flow Separation Region for Case 2
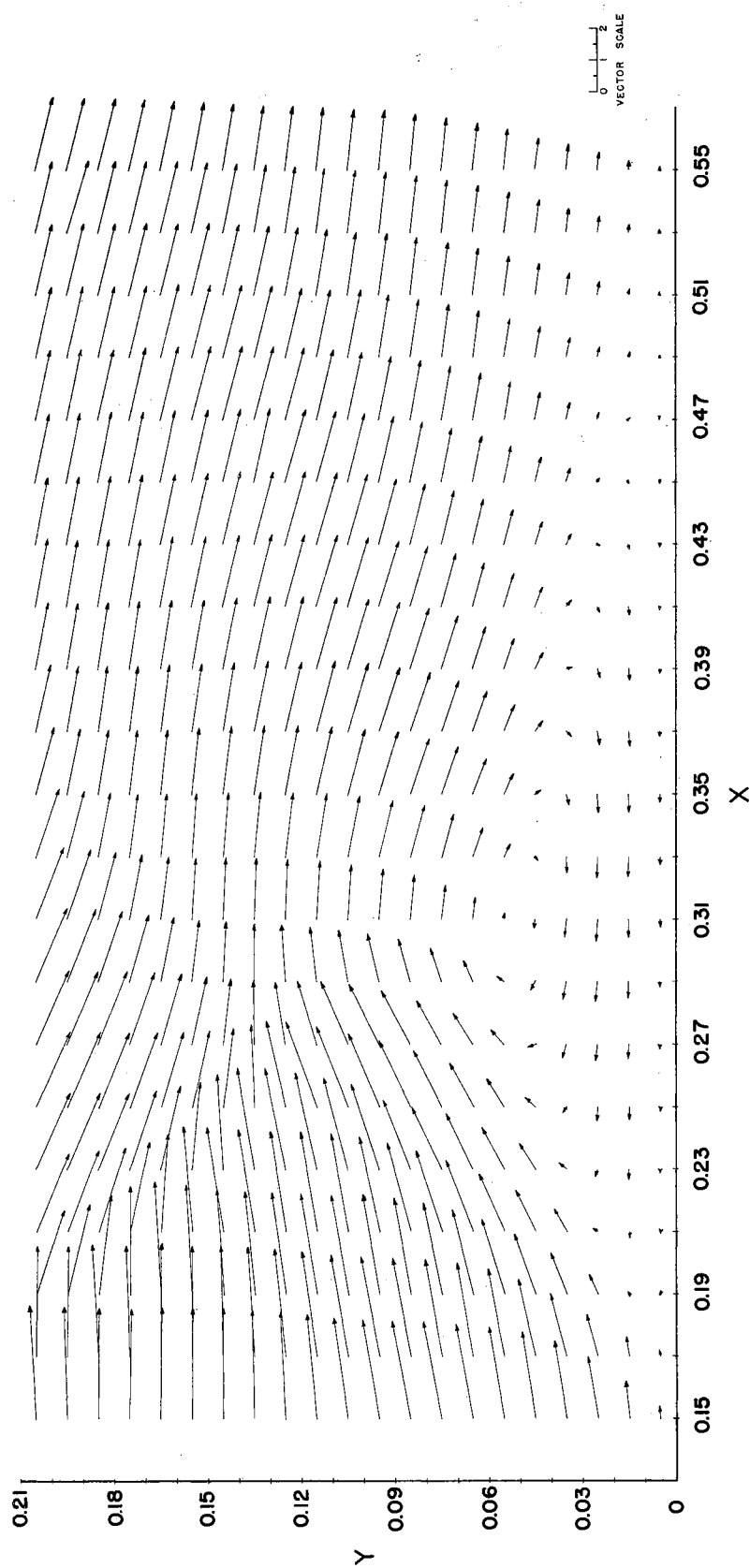
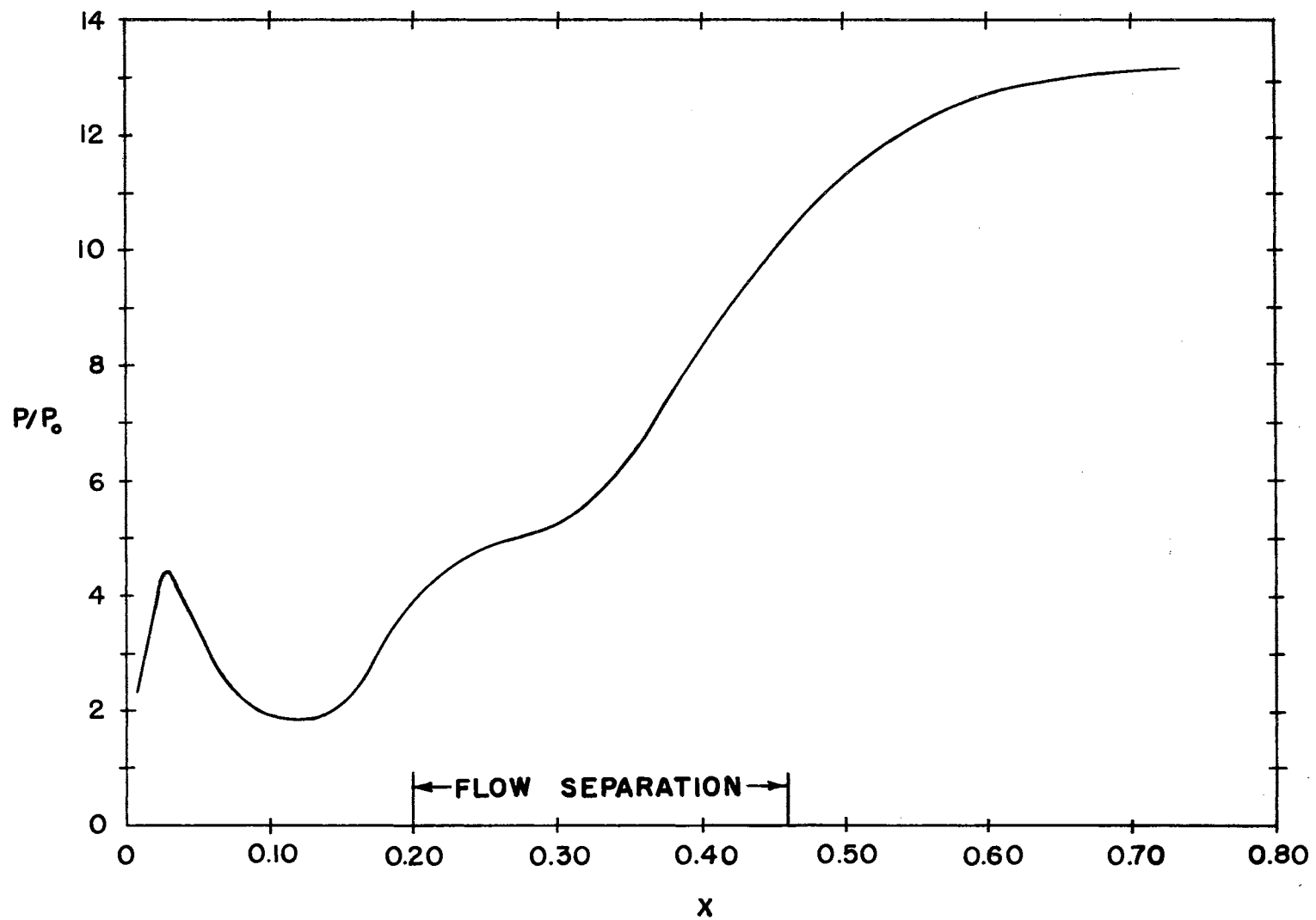Figure 22. Velocity Vector Field in Flow Separation Region for Case 2

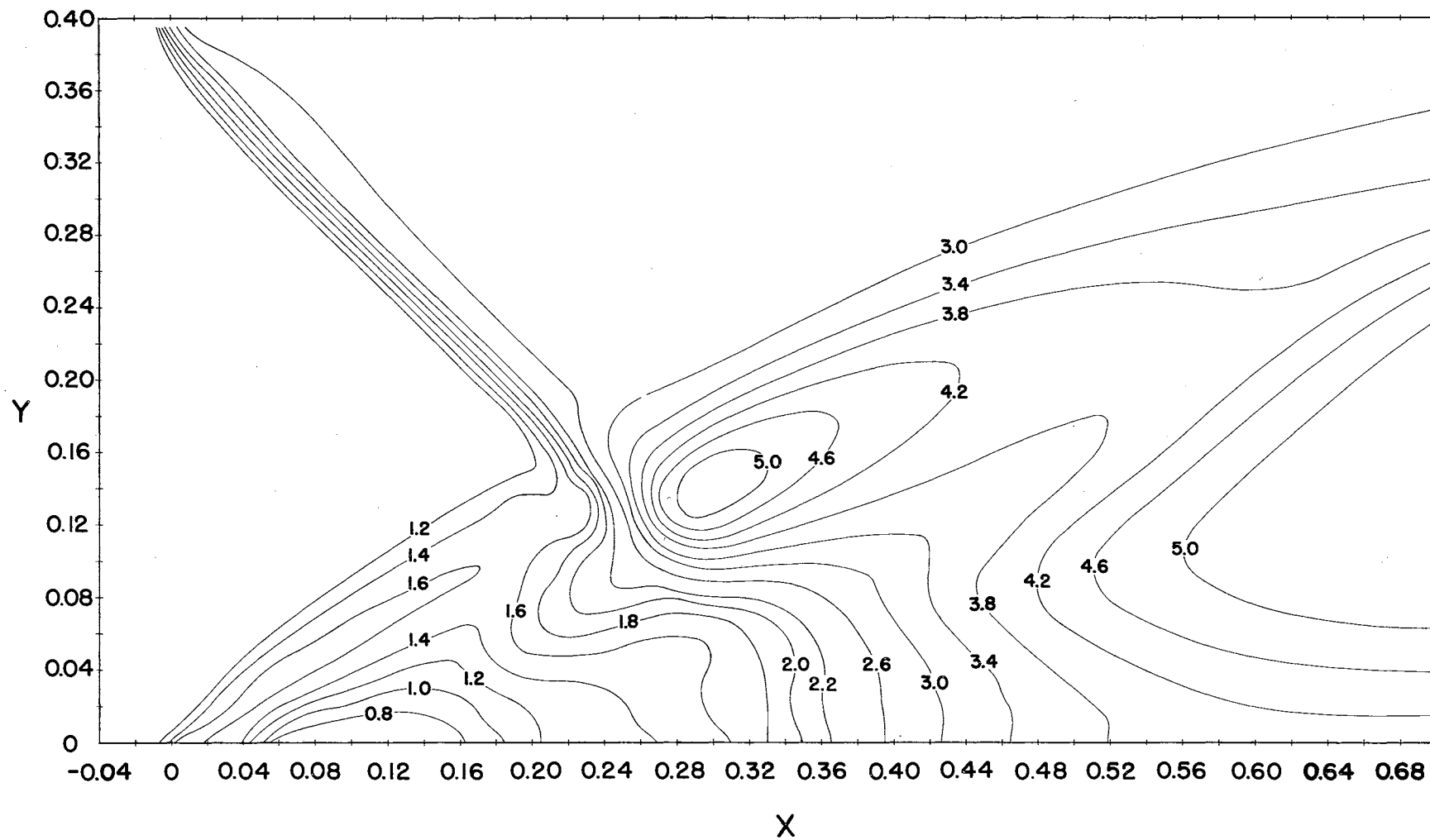Figure 23. Pressure Distribution Along Row $\ell = 1$ for Case 2

Figure 24. Constant Density Lines for Case 2

APPENDIX B

NONDIMENSIONALIZING THE CONSERVATION EQUATIONS

The method used for nondimensionalizing the conservation equations
represents somewhat of a deviation from the standard nondimensionalizing
technique used in boundary layer theory. The reference conditions used
are those conditions which exist in the free stream, and they are de-
noted by the subscript "o". The bar (-) is used to indicate the dimen-
sional quantity, and L is used to refer to a characteristic length.
The nondimensionalized thermodynamic properties, distances, and time
are given in Equations B-1:

$$p = \frac{\bar{p}}{\bar{p}_o} \qquad x = \frac{\bar{x}}{L} \qquad k = \frac{\bar{k}}{\bar{k}_o}$$

$$T = \frac{\bar{T}}{\bar{T}_o} \qquad y = \frac{\bar{y}}{L} \qquad t = \frac{\bar{t}}{L}\sqrt{\frac{\bar{p}_o}{\bar{\rho}_o}} \qquad \text{(B-1)}$$

$$\rho = \frac{\bar{\rho}}{\bar{\rho}_o} \qquad \mu = \frac{\bar{\mu}}{\bar{\mu}_o}$$

The velocities are nondimensionalized by assigning the Mach numbers
the same values in terms of the dimensional quantities as the Mach
numbers in terms of nondimensional values; for example,

$$\bar{M} = \frac{\bar{u}}{\bar{c}} \quad \text{and} \quad M = \frac{u}{c} \ .$$

Since c is the local speed of sound and is defined by

$$c = \sqrt{\frac{\gamma p}{\rho}} \quad \text{and} \quad \bar{c} = \sqrt{\frac{\gamma \bar{p}}{\bar{\rho}}} \quad ,$$

the equality (Equation B-2) can be written as

$$\frac{u}{\sqrt{\frac{\gamma p}{\rho}}} = \frac{\bar{u}}{\sqrt{\frac{\gamma \bar{p}}{\bar{\rho}}}} \quad . \tag{B-2}$$

By the use of the thermodynamic relations (Equations B-1),

$$\sqrt{\frac{\gamma p}{\rho}} = \sqrt{\frac{\bar{p}_0}{\bar{\rho}_0}} \sqrt{\frac{\gamma \bar{p}}{\bar{\rho}}} \quad ;$$

Consequently, Equation B-2 can be rewritten as

$$\frac{\bar{u}}{\sqrt{\frac{\gamma \bar{p}}{\bar{\rho}}}} = \frac{u}{\sqrt{\frac{\bar{p}_0}{\bar{\rho}_0}} \sqrt{\frac{\gamma \bar{p}}{\bar{\rho}}}}$$

or

$$u = \frac{\bar{u}}{\sqrt{\frac{\bar{p}_0}{\bar{\rho}_0}}} \quad .$$

Therefore, the nondimensionalized x-component and y-component of velocity are written as

$$u = \frac{\bar{u}}{\sqrt{\frac{\bar{p}_0}{\bar{\rho}_0}}} \quad \text{and} \quad v = \frac{\bar{v}}{\sqrt{\frac{\bar{p}_0}{\bar{\rho}_0}}} \quad . \tag{B-3}$$

Other useful relationships in the nondimensionalizing of the space and time derivatives are

$$\frac{\partial}{\partial \bar{x}} = \frac{\partial}{\partial x} \frac{\partial x}{\partial \bar{x}} = \frac{1}{L} \frac{\partial}{\partial x} \quad ,$$

$$\frac{\partial}{\partial \bar{y}} = \frac{\partial}{\partial y} \frac{\partial y}{\partial \bar{y}} = \frac{1}{L} \frac{\partial}{\partial y} \quad , \tag{B-4}$$

$$\frac{\partial}{\partial \bar{t}} = \frac{\partial}{\partial t} \frac{\partial t}{\partial \bar{t}} = \frac{1}{L} \sqrt{\frac{\bar{p}_o}{\bar{\rho}_o}} \frac{\partial}{\partial t} \; .$$

Continuity Equation

The application of the relations represented by Equations B-1, B-3, and B-4 to Equation 2 results in

$$\frac{\bar{\rho}_o}{L} \sqrt{\frac{\bar{p}_o}{\bar{\rho}_o}} \frac{\partial \rho}{\partial t} + \frac{\bar{\rho}_o}{L} \sqrt{\frac{\bar{p}_o}{\bar{\rho}_o}} \frac{\partial}{\partial x} (\rho u) + \frac{\bar{\rho}_o}{L} \sqrt{\frac{\bar{p}_o}{\bar{\rho}_o}} \frac{\partial}{\partial y} (\rho v) = 0 \; .$$

The above equation can be simplified to give the desired nondimensionalized continuity equation:

$$\frac{\partial \rho}{\partial t} + \frac{\partial}{\partial x} (\rho u) + \frac{\partial}{\partial y} (\rho v) = 0 \; . \tag{7}$$

Momentum Equations

The shear stresses which occur in the momentum and energy equations are first nondimensionalized by using Equations B-1, B-3, and B-4. The shear stress Equations 6 become

$$\bar{\tau}_{xx} = \frac{\bar{\mu}_o}{L} \sqrt{\frac{\bar{p}_o}{\bar{\rho}_o}} \left[- \mu \left(\frac{4}{3} \frac{\partial u}{\partial x} - \frac{2}{3} \frac{\partial v}{\partial y} \right) \right] ,$$

$$\bar{\tau}_{yy} = \frac{\bar{\mu}_o}{L} \sqrt{\frac{\bar{p}_o}{\bar{\rho}_o}} \left[- \mu \left(\frac{4}{3} \frac{\partial v}{\partial y} - \frac{2}{3} \frac{\partial u}{\partial x} \right) \right] , \tag{B-5}$$

and

$$\bar{\tau}_{xy} = \frac{\bar{\mu}_o}{L} \sqrt{\frac{\bar{p}_o}{\bar{\rho}_o}} \left[- \mu \left(\frac{\partial u}{\partial y} + \frac{\partial v}{\partial x} \right) \right] .$$

The nondimensional shear stresses can be represented as

$$\tau_{xx} = - \mu \left[\frac{4}{3} \frac{\partial u}{\partial x} - \frac{2}{3} \frac{\partial v}{\partial y} \right] ,$$

$$\tau_{yy} = -\mu \left[\frac{4}{3} \frac{\partial v}{\partial y} - \frac{2}{3} \frac{\partial u}{\partial x} \right] ,$$

and

$$\tau_{xy} = -\mu \left[\frac{\partial u}{\partial y} + \frac{\partial v}{\partial x} \right] ,$$

so that Equation B-5 can be written as

$$\bar{\tau}_{xx} = \frac{\bar{\mu}_o}{L} \sqrt{\frac{\bar{p}_o}{\bar{\rho}_o}} \ \tau_{xx} ,$$

$$\bar{\tau}_{yy} = \frac{\bar{\mu}_o}{L} \sqrt{\frac{\bar{p}_o}{\bar{\rho}_o}} \ \tau_{yy} ,$$

$$\text{(B-6)}$$

and

$$\bar{\tau}_{xy} = \frac{\bar{\mu}_o}{L} \sqrt{\frac{\bar{p}_o}{\bar{\rho}_o}} \ \tau_{xy} .$$

X-Momentum Equation

When relations represented by Equations B-1, B-3, B-4, and B-6 are applied to Equation 3,

$$\frac{\bar{p}_o}{L} \frac{\partial}{\partial t} (\rho u) + \frac{1}{L} \frac{\partial}{\partial x} \left[\bar{p}_o \rho \ u + \bar{p}_o p + \frac{\bar{\mu}_o}{L} \sqrt{\frac{\bar{p}_o}{\bar{\rho}_o}} \ \tau_{xx} \right]$$

$$\text{(B-7)}$$

$$+ \frac{1}{L} \frac{\partial}{\partial y} \left[\bar{p}_o \rho \ uv + \frac{\bar{\mu}_o}{L} \sqrt{\frac{\bar{p}_o}{\bar{\rho}_o}} \ \tau_{xy} \right] = 0 .$$

When each term in Equation B-7 is divided by $(\frac{\bar{p}_o}{L})$, the coefficient of the shear stresses appears as

$$\frac{\bar{\mu}_o}{L \ \bar{p}_o} \sqrt{\frac{\bar{p}_o}{\bar{\rho}_o}} \quad \text{or} \quad \frac{\bar{\mu}_o}{L \sqrt{\bar{p}_o \ \bar{\rho}_o}} .$$

When the Reynolds number (Re) is defined as

$$Re = \frac{\bar{U}_o \, L \, \bar{\rho}_o}{\bar{\mu}_o} \quad ,$$

the coefficient of the shear stresses can be reduced to

$$\frac{\bar{\mu}_o}{L\sqrt{\bar{p}_o \, \bar{\rho}_o}} = \frac{\bar{U}_o \sqrt{\gamma}}{Re\sqrt{\frac{\gamma \bar{p}_o}{\bar{\rho}_o}}} = \frac{M_o \sqrt{\gamma}}{Re} \quad .$$

The following identity is used for simplification:

$$\lambda = \frac{M_o \sqrt{\gamma}}{Re} \quad .$$

Consequently, Equation B-7 becomes

$$\frac{\partial}{\partial t} (\rho u) + \frac{\partial}{\partial x} \left[\rho u^2 + p + \lambda \, \tau_{xx} \right]$$

$$+ \frac{\partial}{\partial y} \left[\rho u v + \lambda \, \tau_{xy} \right] = 0 \quad . \tag{8}$$

Y-Momentum Equation

Equation 4 is nondimensionalized in a fashion similar to that used in simplifying Equation 3 so that the final nondimensionalized y-momentum equation is

$$\frac{\partial}{\partial t} (\rho v) + \frac{\partial}{\partial x} \left[\rho u v + \lambda \, \tau_{xy} \right] + \frac{\partial}{\partial y} \left[\rho v^2 + p + \lambda \, \tau_{yy} \right] = 0. \tag{9}$$

Energy Equation

The energy ($\bar{e}$) has been previously defined as the sum of the internal and kinetic energy per unit volume. In equation form,

$$\bar{e} = \bar{\rho}\left[\bar{c}_v \bar{T} + \frac{1}{2}(\bar{u}^2 + \bar{v}^2)\right].$$

In the case of ideal gas, the above equation can be rewritten as

$$\bar{e} = \frac{\bar{p}}{\gamma - 1} + \frac{\bar{\rho}}{2}(\bar{u}^2 + \bar{v}^2) \qquad (B-8)$$

or

$$\bar{e} = \bar{p}_o\, e$$

where

$$e = \frac{p}{\gamma - 1} + \frac{\rho}{2}(u^2 + v^2).$$

Similarly, the nondimensional expression for $(\bar{e} + \bar{p})$ can be written as

$$(\bar{e} + \bar{p}) = \bar{p}_o\,(e + p).$$

The energy equation (Equation 5) can now be nondimensionalized by using the same procedure used in the case of the momentum equations. If the procedure is followed through, each term in the energy equation can be divided by $\dfrac{\bar{p}_o}{L}\sqrt{\dfrac{\bar{p}_o}{\bar{\rho}_o}}$. Once this division is accomplished, the energy equation appears as

$$\frac{\partial e}{\partial t} + \frac{\partial}{\partial x}\left[(e+p)u - \frac{\bar{k}_o\, k\, \bar{T}_o}{L\,\bar{p}_o\sqrt{\dfrac{\bar{p}_o}{\bar{\rho}_o}}}\frac{\partial T}{\partial x} + \lambda\,(u\tau_{xx} + v\tau_{xy})\right]$$

$$+ \frac{\partial}{\partial y}\left[(e+p)v - \frac{\bar{k}_o\, k\, \bar{T}_o}{L\,\bar{p}_o\sqrt{\dfrac{\bar{p}_o}{\bar{\rho}_o}}}\frac{\partial T}{\partial y}\right. \qquad (B-9)$$

$$\left. + \lambda\,(u\tau_{xy} + v\tau_{yy})\right] = 0.$$

The coefficient of the temperature gradient terms can be simplified by introducing the Prandtl number (Pr) which is $Pr = \dfrac{\bar{\mu}_o \bar{c}_p}{\bar{k}_o}$ and by assuming a constant thermal conductivity throughout the field so that $k = 1$. In the final form, the coefficient can be represented as Ω where

$$\Omega = \frac{\bar{k}_o \; \bar{T}_o}{L \; \bar{p}_o \sqrt{\dfrac{\bar{p}_o}{\bar{\rho}_o}}} = \frac{M_o \gamma \sqrt{\gamma}}{Pr \; Re \; (\gamma - 1)} \; . \tag{B-10}$$

When Equation B-10 is substituted into Equation B-9, the final non-dimensionalized energy equation becomes

$$\frac{\partial e}{\partial t} + \frac{\partial}{\partial x} \left[(e + p)u - \Omega \frac{\partial T}{\partial x} + \lambda \; (u \tau_{xx} + v \tau_{xy}) \right]$$

$$+ \frac{\partial}{\partial y} \left[(e + p)v - \Omega \frac{\partial T}{\partial y} + \lambda \; (u \tau_{xy} + v \tau_{yy}) \right] = 0 \; . \tag{10}$$

VITA

Kenneth Ray Royer

Candidate for the Degree of

Doctor of Philosophy

Thesis: A NUMERICAL SOLUTION OF THE SHOCK-LAMINAR BOUNDARY LAYER
INTERACTION PHENOMENON NEAR THE SHARP LEADING-EDGE OF A
FLAT PLATE

Major Field: Mechanical and Aerospace Engineering

Biographical:

Personal Data: Born in De Quincy, Louisiana, August 19, 1927,
the son of Philip and Ruth Adele Royer.

Education: Graduated from De Quincy High School, De Quincy,
Louisiana in May, 1944; received the Bachelor of Science
degree in Mathematics and Science from Southwestern
Louisiana Institute, Lafayette, Louisiana in May, 1951;
received the Bachelor of Science degree in Mechanical
Engineering from Louisiana Polytechnic Institute, Ruston,
Louisiana in January, 1957; received the Master of Science
degree from Louisiana Polytechnic Institute, Ruston,
Louisiana in June, 1961; completed the requirements for
the Doctor of Philosophy degree in May, 1967.

Professional Experience: Design Engineer for the Fort Worth
Division of General Dynamics Corporation, February 1957 to
February, 1959; Senior Aerothermodynamics Engineer for the
Fort Worth Division of General Dynamics Corporation, June,
1960 to September, 1961; Senior Aerodynamics Engineer for
the Fort Worth Division of General Dynamics Corporation,
June, 1963, to October, 1965; Project Propulsion Engineer
for the Fort Worth Division of General Dynamics Corporation,
June, 1966 to the present time.

Professional Organizations: The author is a member of the American
Institute of Aeronautics and Astronautics.